VTRC Virginia Transportation Research Council

We Bring Innovation to Transportation

Nondestructive Inspection Methods for Liquid Deicer Storage Tanks

http://www.virginiadot.org/vtrc/main/online_reports/pdf/23-r9.pdf

AMIR BEHRAVAN, Ph.D., P.E., Postdoctoral Research Associate

THIEN Q. TRAN, Graduate Research Assistant

MATTHEW M. DeJONG, Undergraduate Research Assistant

MOHAMMAD SHADAB SHAIKH, Graduate Research Assistant

MITCHELL DAVIS, Undergraduate Research Assistant

SEAN LI, Undergraduate Research Assistant

ALAN HERNANDEZ, Undergraduate Research Assistant

ALEXANDER S. BRAND, Ph.D., P.E., Assistant Professor

DEPARTMENT OF CIVIL AND ENVIRONMENTAL ENGINEERING
VIRGINIA POLYTECHNIC INSTITUTE AND STATE UNIVERSITY

Final Report VTRC 23-R9

VIRGINIA TRANSPORTATION RESEARCH COUNCIL
530 Edgemont Road, Charlottesville, VA 22903-2454
vtrc.virginiadot.org

Standard Title Page - Report on Federally Funded Project

1. Report No.: FHWA/VTRC 23-R9	2. Government Accession No.:	3. Recipient's Catalog No.:
4. Title and Subtitle: Nondestructive Inspection Methods for Liquid Deicer Storage Tanks		5. Report Date: December 2022
		6. Performing Organization Code:
7. Author(s): Amir Behravan, Ph.D., P.E., Thien Q. Tran, Matthew M. DeJong, Mohammad Shadab Shaikh, Mitchell Davis, Sean Li, Alan Hernandez, and Alexander S. Brand, Ph.D., P.E.		8. Performing Organization Report No.: VTRC 23-R9
9. Performing Organization and Address: Virginia Transportation Research Council 530 Edgemont Road Charlottesville, VA 22903		10. Work Unit No. (TRAIS):
		11. Contract or Grant No.: 117955
12. Sponsoring Agencies' Name and Address: Virginia Department of Transportation 1401 E. Broad Street Richmond, VA 23219 Federal Highway Administration 400 North 8th Street, Room 750 Richmond, VA 23219-4825		13. Type of Report and Period Covered: Final Contract
		14. Sponsoring Agency Code:
15. Supplementary Notes: This is an SPR-B report		

16. Abstract:

High-density polyethylene (HDPE) is widely used for above-ground storage tanks (ASTs). However, there are currently no guidelines for non-destructive testing (NDT) and evaluation (NDE) of HDPE ASTs. Moreover, the feasibility, limitation, and challenges of using non-destructive testing techniques for field inspection of HDPE ASTs have not been studied yet. This study explored the viability of HDPE AST inspection using infrared thermography (IRT) and ultrasonic testing (UT). The results indicate that: 1) ambient environmental parameters can affect IRT accuracy; 2) there is an ideal time during the day to perform IRT; 3) the heating source and infrared camera orientation can affect IRT accuracy; and 4) with proper measures taken, IRT is a promising method for flaw detection in HDPE ASTs. Additionally, UT can be used following IRT for detailed investigation to quantify the defect size and depth. The manuscript concludes with a discussion of limitations and best practices for implementing IRT and UT for HDPE AST inspection in the field.

17 Key Words: Nondestructive tests; infrared thermography; ultrasonic testing	18. Distribution Statement: No restrictions. This document is available to the public through NTIS, Springfield, VA 22161.		
19. Security Classif. (of this report): Unclassified	20. Security Classif. (of this page): Unclassified	21. No. of Pages: 75	22. Price:

Form DOT F 1700.7 (8-72) Reproduction of completed page authorized

FINAL REPORT

NONDESTRUCTIVE INSPECTION METHODS FOR LIQUID DEICER STORAGE TANKS

Amir Behravan, Ph.D., P.E.
Postdoctoral Research Associate

Thien Q. Tran
Graduate Research Assistant

Matthew M. DeJong
Undergraduate Research Assistant

Mohammad Shadab Shaikh
Graduate Research Assistant

Mitchell Davis
Undergraduate Research Assistant

Sean Li
Undergraduate Research Assistant

Alan Hernandez
Undergraduate Research Assistant

Alexander S. Brand, Ph.D., P.E.
Assistant Professor

Department of Civil and Environmental Engineering
Virginia Polytechnic Institute and State University

VTRC Project Manager
Lewis N. Lloyd, Virginia Transportation Research Council

In Cooperation with the U.S. Department of Transportation
Federal Highway Administration

Virginia Transportation Research Council
(A partnership of the Virginia Department of Transportation
and the University of Virginia since 1948)

Charlottesville, Virginia

December 2022
VTRC 23-R9

DISCLAIMER

The project that is the subject of this report was done under contract for the Virginia Department of Transportation, Virginia Transportation Research Council. The contents of this report reflect the views of the authors, who are responsible for the facts and the accuracy of the data presented herein. The contents do not necessarily reflect the official views or policies of the Virginia Department of Transportation, the Commonwealth Transportation Board, or the Federal Highway Administration. This report does not constitute a standard, specification, or regulation. Any inclusion of manufacturer names, trade names, or trademarks is for identification purposes only and is not to be considered an endorsement.

Each contract report is peer reviewed and accepted for publication by staff of the Virginia Transportation Research Council with expertise in related technical areas. Final editing and proofreading of the report are performed by the contractor.

ABSTRACT

High-density polyethylene (HDPE) is widely used for above-ground storage tanks (ASTs). However, there are currently no guidelines for non-destructive testing (NDT) and evaluation (NDE) of HDPE ASTs. Moreover, the feasibility, limitation, and challenges of using non-destructive testing techniques for field inspection of HDPE ASTs have not been studied yet. This study explored the viability of HDPE AST inspection using infrared thermography (IRT) and ultrasonic testing (UT). The results indicate that: 1) ambient environmental parameters can affect IRT accuracy; 2) there is an ideal time during the day to perform IRT; 3) the heating source and infrared camera orientation can affect IRT accuracy; and 4) with proper measures taken, IRT is a promising method for flaw detection in HDPE ASTs. Additionally, UT can be used following IRT for detailed investigation to quantify the defect size and depth. The manuscript concludes with a discussion of limitations and best practices for implementing IRT and UT for HDPE AST inspection in the field.

TABLE OF CONTENTS

FINAL REPORT

NONDESTRUCTIVE INSPECTION METHODS FOR LIQUID DEICER STORAGE TANKS

Amir Behravan, Ph.D., P.E.
Postdoctoral Research Associate

Thien Q. Tran
Graduate Research Assistant

Matthew M. DeJong
Undergraduate Research Assistant

Mohammad Shadab Shaikh
Graduate Research Assistant

Mitchell Davis
Undergraduate Research Assistant

Sean Li
Undergraduate Research Assistant

Alan Hernandez
Undergraduate Research Assistant

Alexander S. Brand, Ph.D., P.E.
Assistant Professor

Department of Civil and Environmental Engineering
Virginia Polytechnic Institute and State University

INTRODUCTION

The Virginia Department of Transportation (VDOT) controls approximately 400 above-ground storage tanks (ASTs) for liquid deicing chemicals to support the winter maintenance program. Tanks range in capacity from 5,000 gals to 10,000 gals and are made of either single- or double-walled high-density polyethylene (HDPE) (see Figure 1). Routine visual inspections are conducted to identify signs of aging and damage as indicators of potential defects that might impact functionality and integrity. Current methods use visual inspection and penetrating dyes to inspect for signs of cracking, crazing, and other damage or deterioration.[1] However, these current methods do not effectively identify additional mechanisms of failure, such as ultraviolet light-induced degradation, increased hoop stress, or manufacturing defects, especially if the defects are subsurface or too small to be seen during visual inspection (e.g., Figure 2). Therefore, to improve VDOT's ability to identify potential defects and determine whether a tank is fit for continued service, additional non-destructive evaluation (NDE) techniques need to be considered.

As reported by many HDPE producers, HDPE exhibits outstanding performance when in contact with various chemical solutions (i.e., no damage after 30 days of exposure). However, the performance criteria are not defined (e.g., appearance change, color change, mass change, volume change, etc.). Therefore, more systematic research is required to study the signs of HDPE ASTs degradation to prevent HDPE ASTs premature failure. The consequences of HDPE ASTs failure are economic (e.g., loss of product, the cost for cleanup and / or remediation), environmental (e.g., soil erosion, surface and groundwater contamination, or impacts on ecological health), potential for worker injury, and potential tort and regulatory liability.[2-7] Accordingly, the development of a reliable Non-Destructive Test (NDT) method to evaluate HDPE tank integrity prior to a release is an important need for the industry.

Figure 1. Examples of single-walled (left) and double-walled (right) high-density polyethylene above ground storage tanks managed by VDOT

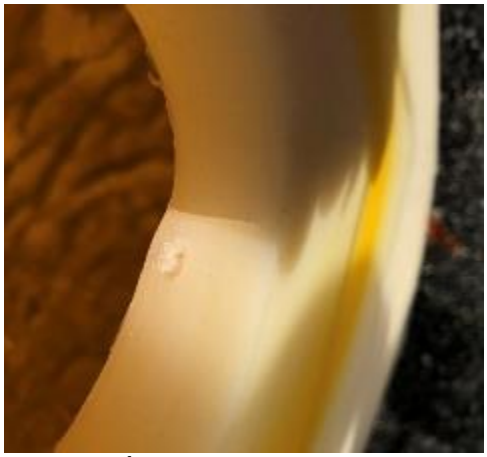

Figure 2. A subsurface small void (about 1/8th of an inch in width parallel to the tank wall) in the wall of a VDOT double-walled high-density polyethylene above ground storage tank

Based on the review of potential NDE methods, summarized in the literature review section, this study focused only on infrared thermography (IRT) and ultrasonic testing (UT)

methods. While acoustic emission (AE) is effective for leak detection, it cannot provide the necessary data on defects and cracks for this study. Moreover, while ground-penetrating radar (GPR) is very useful in NDE of other infrastructures, the frequency needed to be applicable to HDPE ASTs is very high such that the application is questionable for this study.

The problem is that currently, there are no industry standards that specify when an AST should be taken out of service. Accordingly, there is room for study to create a set of test procedures and protocols for assessing and determining when to remove a tank from service. Additionally, there are no clear guidelines that the State Departments of Transportation (DOTs) must adhere to to evaluate the condition of the tanks they own and manage. Due to this, most DOTs only perform a periodic visual examination of the tanks.

PURPOSE AND SCOPE

This study aimed to develop and implement an NDE of HDPE ASTs using IRT and UT methods. The scope of the project was to develop a laboratory-scale NDE methodology that could be scaled to field investigations of representative ASTs used for liquid deicer storage at VDOT facilities. This study had four objectives:

1. Examine HDPE properties affecting the life span of an AST. Some of those properties influence the effectiveness of the evaluation techniques, which need to be identified before beginning laboratory work;
2. Investigate the efficiency of IRT and UT for defect detection in HDPE materials;
3. Establish a field setup for implementing IRT and UT for AST inspection; and,
4. Develop recommendations for NDT inspections/assessments and fit for continued use determination of ASTs.

METHODS

The research program was divided into five main tasks that aimed to understand the existing methodologies, analyze the NDE methods in a laboratory setting, experiment with ASTs in the field, and develop an implementation plan for VDOT.

1. *Literature review and survey of state DOT practices*. This task explored the existing NDE methods used on HDPE components, including but not limited to ASTs. As part of this task, a questionnaire was sent to State DOTs to evaluate how other agencies evaluate HDPE ASTs in their inventory.

2. *Laboratory investigation*. This task created a laboratory-scale HDPE tank with known defects to validate the IRT and UT methods to validate the methods in the laboratory to generate threshold values.

3. *Field investigation*. This task applied the knowledge gained from the laboratory investigation to study HDPE ASTs around Virginia.

4. *Development of guidelines*. This task applied the knowledge gained from the laboratory and field studies to establish guidelines on applying IRT and UT to HDPE AST inspections.

Literature Review and Survey of State DOT Practices

A literature review was conducted to evaluate what NDE methods can be or had been employed to study HDPE ASTs, polymer tanks in general, and HDPE in particular. Search engines including Google Scholar and Science Direct were utilized for this purpose, as well as, direct searches of State DOT websites and the Transportation Research Record. There is very little data present in the literature on applications of NDE methods to HDPE components. The literature review section of this report summarizes the authors' study of existing research on this topic.

A questionnaire was prepared to survey the techniques and regulations that State DOTs follow to evaluate their ASTs. Questions were formulated based on information collected from the literature and feedback from members of the TRP and VTRC. A copy of the complete questionnaire and the received responses are available from the authors. This questionnaire focused on four primary areas of investigation as listed below:

- A determination of how many brine tanks are currently in service across the U.S., including their capacity range, age range, and the most common material type;
- How State DOTs maintain their ASTs in different seasons;
- What area(s) of an AST is (are) the most likely area(s) for a tank failure; and,
- What provisions and regulations do State DOTs follow to evaluate the condition of their tanks, and how do they decide when to remove a tank from service?

Laboratory Investigation

Infrared Thermography (IRT)

All objects (e.g., solid, liquid) emit infrared radiation in many wavelengths; however, each wavelength corresponds to a specific temperature.[8] IRT is an NDE technique that employs an infrared (IR) camera to capture the infrared radiation emitted from a given surface, transforming it into electrical signals equivalent to the surface's temperature profile. These signals are displayed in a colorful thermal image known as a thermogram; each color corresponds to a temperature according to the defined scale.[8,9] IRT is a popular NDE technique known for its portability, affordability, ease of use, large area of inspection, and ability to locate a range of surface and subsurface defects.

A thermal gradient over the thickness of the object under study is required to run successful IRT tests. There is difficulty in manipulating the temperature of HDPE to induce the required thermal gradient on the thickness due to its low thermal diffusivity. To accommodate the low thermal diffusivity of HDPE in the laboratory investigation, six 500 W halogen lamps with a total power of 3000 W at a distance of 15.75 in (0.4 m) were used to heat the object (*e.g.*, the tank in this study) for three minutes. This heating setup is called step heating, in which the heating lasts for a predetermined time and then allowing the object to cool naturally for a predetermined time. The power and heating time considered for the lab testing were determined through a set of trial and error experiments and included a consideration of the practical aspects of the test's utility in the field for evaluating the real ASTs. In this study, concentrating the heating power on a small region, over a short distance of 15.75 in (0.4 m) and with a three-minute duration, offers enough of a temperature gradient over the thickness of the specimen to be inspected. This way, more excitation power can be delivered in a shorter period of time, resulting in more effective heating. In this study, the most effective empirical procedure was determined to be as follows: 1) the IR camera was positioned 4.9 ft (1.5 m) away from the object; 2) the target object was heated by the external heating source for three minutes; and 3) immediately after removing the heating source, the change in temperature of the object during the cooling phase was monitored for three minutes (capturing images every 10 secs). The distance between the camera and the object was defined by a preliminary investigation that studied the correlation between the distance, the area under study, and the smallest observable defect size at the best condition. For this purpose, some partial-depth holes with different diameters were created on an HDPE plate, and then the defects were exposed so that they faced the heating source and IR camera. This is the best condition in which all defects could be observed without concerning the low thermal diffusivity of HDPE and thermal attenuation during the experiment. The IR camera was set at different distances, as seen in Figure 3; a distance of 4.9 in (1.5 m) is the greatest distance before the minimum observable defect size increases by about 0.04 in (1 mm). Since this research was trying to study the feasibility of using the IRT technique on real ASTs and for the field investigation, the thermal images have been reported without any additional image processing.

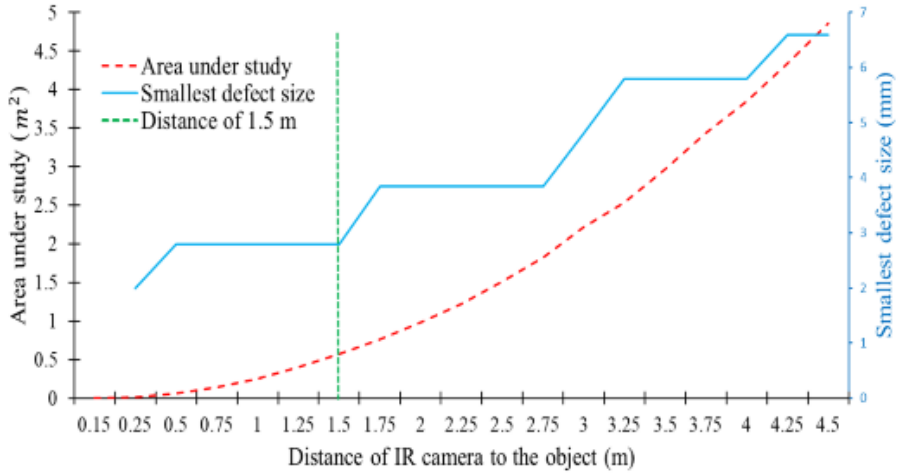

Figure 3. Correlation between the infrared camera distance to the object and the area under study and the smallest observable defect size (note: 1 m = 3.28 ft, 1 mm = 0.039 in, and 1 m^2 = 10.76 ft^2)

During the preliminary investigations on a full-scale HDPE AST, this study tried to use the same experimental setup established in the laboratory and utilized six 500 W halogen lamps with a total power of 3000 W at a distance of 15.75 in (0.4 m) to induce a thermal gradient on the object surface. The findings showed that the lab experiment's heating power was insufficient to induce an adequate thermal gradient on the full-scale HDPE AST wall in the field. Therefore, changing the heating source was the first correction for transferring the IRT from the lab to the field. The preliminary investigations showed that utilizing two stacked 1500 W IR heaters with a total power of 3000 W at a distance of 15.75 in (0.4 m) is effective for defect detection in the field.

Due to the semi-infinite size of the real HDPE AST compared to the lab-scale water tank, the IRT technique with step heating (even with 10 minutes of continuous heating) was not efficient for field investigation. Short-step heating (less than 10 secs) was not enough to induce an adequate thermal gradient and obtain observable contrast between the defects and the intact areas; however, long-step heating reduced the contrast between the defect edge and the original solid area. Therefore, according to the preliminary investigations, the second correction should be applied to the heating method. Thus, step-heating and thermal wave imaging were combined for this study. The heat was deposited on the surface by following alternative heating and cooling phases to induce waveform heat. The grouping of one heating and one cooling cycle is called one cycle. Different heating and cooling duration combinations were considered for this study (Table 1) to investigate the optimum heating-cooling cycles. Six cycles were completed for each combination of heating-cooling durations (e.g., 20 s heating with 60 s cooling), and the IRT was conducted during each cooling phase. Except for the first two cooling phase durations of each heating time group that were constant for all combinations (e.g., 10 s and 20 s), the increment of cooling phase duration was a factor of the heating time duration. This arrangement in selecting cooling phase duration was chosen for practical implementation and faster field investigation. Having a factor of heating phase duration for the cooling phase allows a tank investigator to heat multiple areas when the first spot is in the cooling phase before returning to the first area for heating and conducting the next cycle. For instance, in the combination of 20 s heating and 140 s cooling, labeled as "20-140", the investigator can heat seven areas (7×20 s = 140 s) when the first spot is in the cooling phase and then return to the first spot to start the second cycle of measurement. This heating-cooling cycle allows the heat to penetrate the sample in the form of waves without reducing the contrast between the defects and the sound area. Therefore, the authors believe that applying a waveform heat distribution on the HDPE AST causes the heat to penetrate deeper, increases the contrast between the defect edges, and consequently reveals more subsurface defects. For this reason, the optimum heating-cooling durations need more investigation, which is one goal of this study to correct the setup established in the lab. The IRT evaluation and measurement for each heating-cooling combination were completed twice; one was performed in the morning and in the afternoon. The reason behind performing two repetitions per combination has been explained in section Results from the Full-Scale HDPE AST Experiment (Task 3) under Temperature Measurements.

A Fluke TiX580 thermal imager (IR camera), with the features shown in Table 2, was used for this research. In this research, the goal of using an IR camera was to detect subsurface anomalies and not for accurate temperature measurements. Since the appearance of the defects

depends on the existing thermal gradient across the object's thickness and since the object temperature (O.T) was not controlled only for the lab testing, the IR camera's temperature range was narrowed manually and set to the range [O.T –9 °F, O.T +18 °F] ([O.T –5 °C, O.T +10 °C]). The reasons for this were to: 1) reduce the time needed for defects to appear in the thermal images and 2) detect anomalies with the highest contrast. The other settings of the IR camera is shown in Table 3.

Investigators in the field are interested in evaluating as many tanks as they can in one day without further analysis. Therefore, contrary to the lab testing, to expedite the field investigation, the temperature span on the camera was set on automatic without the need to set it manually to narrow down the temperature range for better defect detection. No further image processing was performed, and the smallest detected defect size was obtained directly from the raw images. This was done to facilitate the evaluation process and speed it up for field implementation. During the field testing, the distance between the camera and the object varied from 2.6 ft (0.8 m) to 3.6 ft (1.1 m).

Table 1. Heating and cooling duration combinations considered for each cycle during an infrared thermography measurement

Heating time (s)	Cooling time (s)						
20	10	20	40	60	80	100	120
30	10	20	30	60	90	120	-
40	10	20	40	80	120	-	-
60	10	20	60	120	-	-	-

Table 2. Infrared camera properties reported by the manufacturer

Detector resolution	640 x 480 (307,200 pixels)
Field of view	34 °H x 24 °V
Temperature measurement range	–4 °F to 1832 °F (–20 °C to 1000 °C)
Accuracy	±3.6 °F (±2 °C) or 2% (whichever is greater)
Thermal sensitivity (NETD)	≤0.09 °F (0.05 °C) at 86 °F (30 °C) target temp (50 mK)
Frame rate	60 Hz
Infrared spectral band	7.5 μm to 14 μm (long wave)

Table 3. Settings of the infrared camera used for the study in the laboratory

Emissivity	0.78
Background	73 °F (23 °C)
Transmission	100%
Range	-4 °F to 212 °F (-20 °C to 100 °C)
Temperature level span	[O.T -9 °F, O.T +18 °F] [O.T -5 °C, O.T +10 °C]
Palette	Blue-Red [Ultra contrast]
Auto capture	18 images every 10 secs

Ultrasonic Testing (UT)

The IRT technique described above helps identify superficial subsurface defects with their approximate size and location. However, this technique cannot give information about the depth of the defect or the location of the abnormality over the thickness of the object and if there are several stacked defects on the same spot. Therefore, after IRT identifies the potential abnormal areas, a more detailed investigation is needed. For the laboratory investigation, conventional pulse-echo ultrasonic testing (PEUT) and phased array ultrasonic testing (PAUT) have been considered because these tests need access to only one side of the investigated specimen and allow for the inspection of ASTs that are filled with liquid. For the field testing, only PAUT was considered.

By calibrating the measuring equipment to the primary wave ("P-wave") velocity of the AST material with knowledge of the wall thickness, both PEUT and PAUT can locate hidden abnormalities. One disadvantage of the application of UT to HDPE is the potential for significant acoustic attenuation and dispersion due to the viscoelasticity of HDPE, with energy losses reported at 18 dB/inch (7 dB/cm) and as large as 38 dB/inch (15 dB/cm).[10-12] Therefore, based on the AST wall thickness and defect sizes, a range of ultrasonic frequencies needs to be considered; for instance, while higher frequencies will likely yield a better resolution, the signal will diminish due to increased scattering.[13] Another challenge with PEUT is that when the defect size is smaller than the probe size, waves will propagate through both the irregularly damaged area and intact area; therefore, more peaks will appear in the response signals, making it challenging to identify the correct peak for the defect to characterize its geometry and its location over the thickness.

In this research, a Proceq Flaw Detector 100 ultrasonic instrument was used in combination with a 5 MHz mono probe from Sonatest for PEUT tests and a 2.25 MHz phased array water wedge probe from SensorScan for PAUT tests (Figure 4). Water wedges have been used in other studies of HDPE material[14-16] primarily because the relatively slow acoustic velocity of HDPE would result in negative refraction from other commonly-used PAUT wedge materials. Wave velocity calibration was done with the mono probe before starting each measurement. The settings used for the calibration are summarized in Table 4.

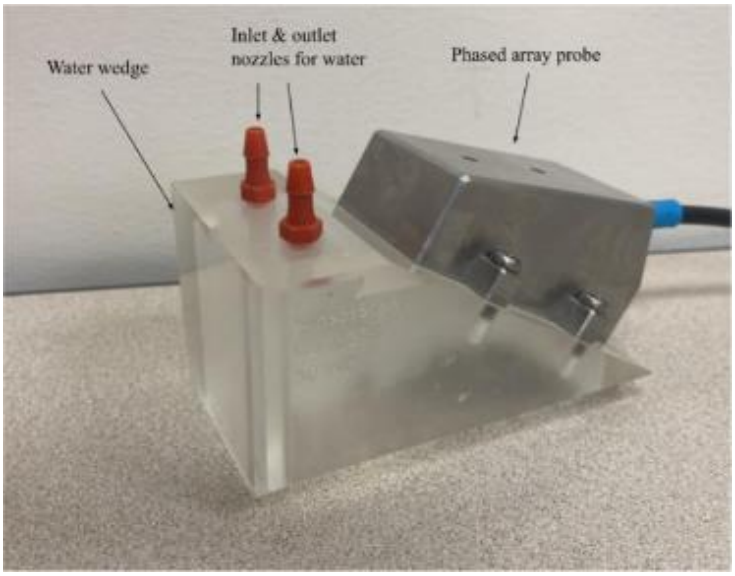

Figure 4. Water wedge probe for phased array ultrasonic testing

Table 4. Settings used for wave velocity calibration with mono probe ultrasonic testing

Voltage mono	100 V
Mono pulse damping	50 ohms
Pulse type	Spike
Probe diameter	0.5 in (12.7 mm)
Reference amplitude	80.0%
Range Path	3.9 in (100 mm)
Travel mode	Half path
Acquired frequency	100 MHz

Laboratory-Scale Experiments

There were specific concerns regarding the HDPE properties that impact the IRT and UT testing effectiveness on the laboratory-scale tank, which is the main focus of this work. The authors have studied those properties and are reported in Behravan et al.[17] Moreover, HDPE performance, when in contact with brine solution, needs closer attention for a better assessment of the HDPE AST performance in the field, which has been investigated in another study.[17]

While the eventual objective of this project is to develop recommendations for field investigation of ASTs, the Task 2 of the present study focused on a laboratory study to control additional variables. In the field, ASTs experience different thermal gradients on the sun-facing vs. shade-facing sides of the tank, as well as variability in the gradients as a function of brine solution temperature and volume in the AST. Therefore, to better control specific variables, a small-scale water tank was created in the laboratory with interchangeable plates of varying thickness and defect content. Figure 5 shows the 24 in × 24 in × 12 in (610 mm × 610 mm × 305 mm) tank used for this purpose. One side of the tank was removed, allowing for HDPE plates of thicknesses 0.25 in (6.4 mm), 0.5 in (12.7 mm), 0.75 in (19.1 mm), 1 in (25.4 mm), and 2 in

(50.8 mm) to be installed for experiments. These plates had specifically manufactured defects (*e.g.* side holes (S.H), scratches (s), and partial holes) to allow for calibration of the IRT and UT methods; the defect map and defect sizes created on the plates are shown in Figure 6 and Table 5.

For each plate installed on the water tank, the IRT experiment was repeated 20 times on different days under different environmental conditions to get a wide range of temperature differences between the water and tank exterior. The condition information for each measurement is available from the authors. Some parameters impacted the measures, such as the specimen size, water temperature in the tank, relative humidity (RH), etc. A preliminary study was conducted to understand the impact of specimen size on the heat transfer properties by applying the IRT technique on two plates with dimensions 12 in × 12 in × 0.5 in (305 mm × 305 mm × 12.7 mm) and 24 in × 24 in × 12 in (610 mm × 610 mm × 305 mm). Both plates were heated for ten minutes. The temperature change of the center of both plates was recorded and plotted. To study the impact of water and its temperature on the measurements, the water temperature was changed manually via a water heater. This approach simulates the water and tank temperature differences during the day from 12:00 AM to 11:59 PM in a real AST. Since this study's IRT experiments were completed outside the lab, there was no control over the RH; therefore, the impact of RH on the measurement is not the focus of this study.

(a) (b)

Figure 5. (a) High density polyethylene (HDPE) water tank with a removed wall and (b) HDPE water tank with an installed HDPE plate with known subsurface and interior defects

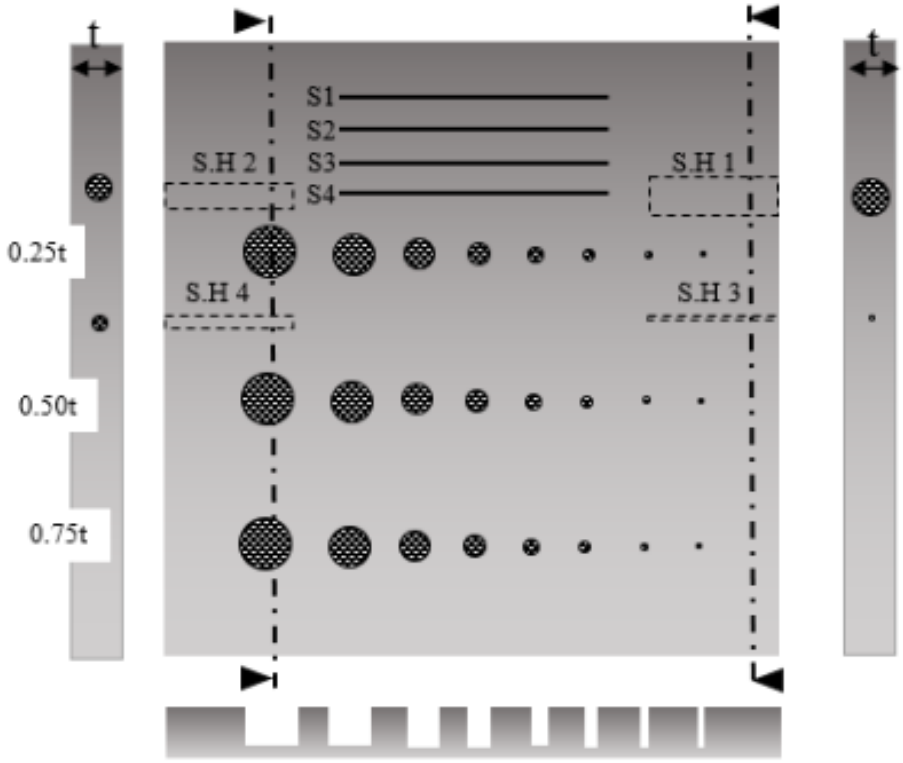

Figure 6. Graphical representation of the defects created on the HDPE plates installed as a wall on the water tank in Figure 5 (note: *"S.H"* represents the *"side hole*" and "S" represents the "scratch")

Table 5. Characters of the created defects on the HDPE plates

Defect name	Description	Depth from interior side [inch (mm)]	Diameter(s) [inch (mm)]*
S1	Scratch	0.04 (1)	N/A
S2	Scratch	0.08 (2)	N/A
S3	Scratch	0.12 (3)	N/A
S4	Scratch	0.20 (5)	N/A
S.H 1	Side hole	0.125t	0.75 t
S.H 2	Side hole	0.25t	0.50 t
S.H 3	Side hole	varies	0.1 t (1/16 inch drill bit was used for all plates)
S.H 4	Side hole	0.375t	0.25 t
R1	Partial hole	0.25t	Diameters from left to right: 1, 0.79, 0.59, 0.39, 0.28, 0.20, 0.11, 0.06 (25.40, 19.99, 15.01, 9.98, 7.01, 5.00, 2.79, and 1.59)
R2	Partial hole	0.50t	Diameters from left to right: 1, 0.79, 0.59, 0.39, 0.28, 0.20, 0.11, 0.06 (25.40, 19.99, 15.01, 9.98, 7.01, 5.00, 2.79, and 1.59)
R3	Partial hole	0.75t	Diameters from left to right: 1, 0.79, 0.59, 0.39, 0.28, 0.20, 0.11, 0.06 (25.40, 19.99, 15.01, 9.98, 7.01, 5.00, 2.79, and 1.59)

*t: Thickness of the HDPE plate

Full Scale Experiments and Field Investigation

Full-scale experiments were performed on a decommissioned single-walled 6,000-gal HDPE AST provided by VDOT (Figure 7). The bottom 4.1 ft (1.25 m) of the tank had a thickness of 0.75 in (19.1 mm), and the remaining height had a thickness of 0.5 in (12.7 mm).

The Task 2 results showed that the temperature inside and outside the tank plays a significant role in successful IRT measurements. Type-T thermocouples connected to a data logger were employed to collect the temperatures from the tank exterior, the liquid inside the tank, and the ambient air. The thermocouples were installed on the tank wall at different elevations (top, middle, and bottom) and on east and west-facing sides close to where the defects exist. Thermocouples were installed on the AST wall using small pieces of HDPE (Figure 7) held with hot glue to ensure that only the HDPE's temperature was collected. One thermocouple was submerged in the water inside the tank, and one thermometer was kept next to the tank in the shade to collect the ambient air temperature. The data logger collected temperatures every minute and reported the average of the temperatures every 30 minutes.

To couple the laboratory experiments from Task 2 and validation experiments with the full-scale HDPE AST in Task 3, defects were manufactured in the AST. Defects with different sizes and depths were created inside the AST to simulate subsurface defects initiating from inside the AST and developing towards the AST's exterior surface. The defects were created on the east and west sides of the AST to study the best timeframe for evaluation regarding a specific side of the AST being in the sun or the shade. After the defects were created inside the AST, the tank was filled with water.

One set of the defects was created on the east side in the thinner part of the AST, and the other set was created on the west side in the thicker part of the AST. The configuration of the defects on both sides is shown in Figure 8. Only five columns of defects were formed on the east side, compared to six columns on the west. The characteristics of the defects are summarized in Table 6 and Table 7. In these tables, "R" refers to the row and "C" refers to the column of the created defects. The defects are named according to their location in rows and columns. For example, the R2C4 defect refers to the defect located in Row 2 and Column 4. The size of the tank, dangerous consequences of the AST failure, and the concentration of the defects in a small area presented challenges in the study. It was risky to create four sets of defects on the AST to study the impact of wall thickness and the location of the defects on the measurements separately. Therefore, one set of defects was made on the thin part, and the other set was created on the thick part of the tank wall.

In Table 6 and Table 7, the aspect ratio (AR) is equal to the ratio of the defect diameter (d) to the defect depth (D) (AR = d/D), and D/t is the ratio of the defect depth to the wall thickness (t). The defect depth has been measured from the external surface.

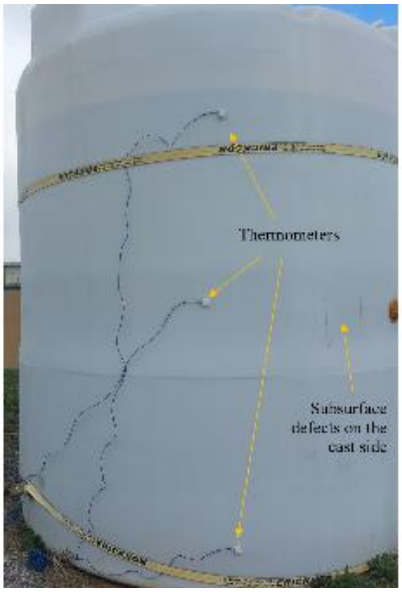

Figure 7. The configuration of the tank under study and the arrangement of the installed thermometers

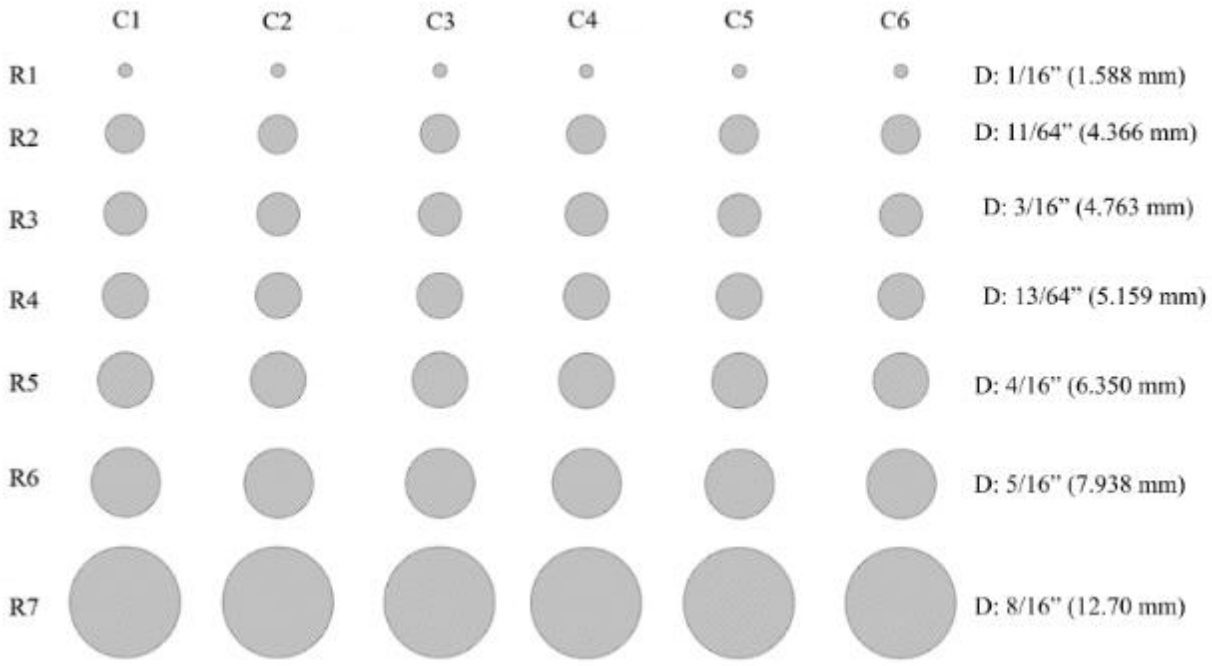

Figure 8. Example of the defects map created inside the tank wall (defects on the west side)

Table 6. Characters of the defects created on the east side of the laboratory 6000-gallon storage tank (t=0.5 in, t=12.7 mm)

Defects	Diameter (in)	C1			C2			C3			C4			C5			C6		
		Depth[1]	AR [2]	D/t [3]	Depth	AR	D/t	Depth	AR	D/t	Depth	AR	D/t	Depth	AR	D/t	Depth	AR	D/t
R1	0.063	N/A	N/A	N/A	N/A	N/A	N/A	N/A	N/A	N/A	N/A	N/A	N/A	N/A	N/A	N/A	N/A	N/A	N/A
R2	0.172	0.104	1.64	0.21	0.252	0.68	0.51	0.325	0.53	0.65	0.387	0.44	0.77	0.452	0.38	0.90	N/A	N/A	N/A
R3	0.188	0.100	1.88	0.20	0.295	0.64	0.59	0.372	0.50	0.74	0.433	0.430	0.87	0.461	0.41	0.92	N/A	N/A	N/A
R4	0.203	0.152	1.34	0.30	0.048	4.23	0.10	0.248	0.82	0.50	0.420	0.48	0.84	0.446	0.45	0.89	N/A	N/A	N/A
R5	0.250	0.100	2.50	0.20	0.237	1.06	0.47	0.186	1.34	0.37	0.312	0.80	0.62	0.450	0.55	0.90	N/A	N/A	N/A
R6	0.313	0.080	3.91	0.16	0.113	2.77	0.23	0.250	1.25	0.50	0.363	0.86	0.73	0.438	0.71	0.88	N/A	N/A	N/A
R7	0.500	0.050	10	0.10	0.248	2.02	0.50	0.247	2.02	0.49	0.365	1.37	0.73	0.412	1.21	0.82	N/A	N/A	N/A

[1] Depth from the external surface (D) (in)

[2]AR: aspect ratio which is equal to the ratio of defect diameter (d) to the defect depth (D) (AR=d/D)

[3] D/t: Ratio of the defect depth (D) to the wall thickness (t)

[4] it was impossible to measure the depth due to the small defect size

Table 7. Characters of the defects created on the west side of the laboratory 6000-gallon storage tank (t=0.75 in, t=19.1 mm)

Defects	Diameter (in)	C1			C2			C3			C4			C5			C6		
		Depth[1]	AR [2]	D/t [3]	Depth	AR	D/t	Depth	AR	D/t	Depth	AR	D/t	Depth	AR	D/t	Depth	AR	D/t
R1	0.063	N/A[4]	N/A	N/A	N/A	N/A	N/A	N/A	N/A	N/A	N/A	N/A	N/A	N/A	N/A	N/A	N/A	N/A	N/A
R2	0.172	0.409	0.42	0.55	0.373	0.46	0.50	0.493	0.35	0.66	0.574	0.30	0.77	0.683	0.25	0.91	0.719	0.24	0.96
R3	0.188	0.624	0.30	0.83	0.124	1.52	0.16	0.091	2.07	0.12	0.283	0.66	0.38	0.546	0.34	0.73	0.395	0.47	0.53
R4	0.203	0.078	2.61	0.10	0.257	0.79	0.34	0.311	0.65	0.41	0.484	0.42	0.65	0.635	0.32	0.85	0.693	0.29	0.92
R5	0.250	0.171	1.46	0.23	0.249	1.00	0.33	0.357	0.70	0.48	0.426	0.59	0.57	0.491	0.51	0.66	0.631	0.40	0.84
R6	0.313	0.285	1.10	0.38	0.167	1.88	0.22	0.246	1.27	0.33	0.413	0.76	0.55	0.516	0.61	0.69	0.654	0.48	0.87
R7	0.500	0.156	3.20	0.21	0.246	2.03	0.33	0.263	1.91	0.35	0.336	1.49	0.45	0.537	0.93	0.72	0.670	0.75	0.89

[1] Depth from the external surface (D) (in)

[2]AR: aspect ratio which is equal to the ratio of defect diameter (d) to the defect depth (D) (AR=d/D)

[3] D/t: Ratio of the defect depth (D) to the wall thickness (t)

[4] it was impossible to measure the depth due to the small defect size

Then, based on the results from the laboratory and full-scale experiments, field experiments were performed on two VDOT ASTs with details shown in Table 8. IRT and PAUT were used to evaluate these two ASTs.

Table 8. Information of the two high-density polyethylene above ground storage tanks tested in the field

Location	Tank capacity (gal)	Tank age (years)	Tank type	Wall thickness (in, (mm))	Tank Diameter (ft, (m))	Empty/full
Salem district, Virginia, USA	5000	12	Single wall	0.75 (19.1)	103.4 (2.60)	Empty
Salem district, Virginia, USA	5000	17	Single wall	0.75 (19.1)	103.4 (2.60)	Full

Development of Guidelines

Best practices were synthesized from the findings of previous tasks to establish the information needed to make policy decisions on how ASTs should be inspected and maintained. In addition, information not obtained from the previous tasks that would improve inspection procedure for ASTs was identified as a future research need.

RESULTS AND DISCUSSION

Literature Review

While an inspection of steel and other metal ASTs, such as for storing oil, have been investigated using NDE methods,[18-22] relatively few studies have been performed on HDPE ASTs.[23] Based on the literature, four primary NDE methods could be viable for inspecting HDPE ASTs: infrared thermography, UT, acoustic emission, and ground penetrating radar. These four methods are presented and discussed below for their relative appropriateness in investigating HDPE ASTs.

- Infrared thermography (IRT) is a popular NDE technique due to its portability, affordability, ease of use, large area of inspection, and ability to locate a range of surface and subsurface defects. IRT effectively detects any material with a different thermal conductivity, such as an air- or water-filled defect in a homogeneous solid. In the presence of a thermal gradient through the thickness of the investigated object, the IR image will identify these anomalies, provided that the thermal conductivity is different, as shown in Figure 9. The thermal gradient needed for IRT can be generated through passive or active methods. In passive IRT, the ambient environment and sunlight are used to generate this thermal gradient.[24] In active IRT, an external heat source provides the necessary energy to induce the thermal gradient.[24] The imposed thermal gradient can be generated from the same side as the measurement, known as the reflection method, and is used to locate superficial anomalies, or the opposite side of the measurement, known as the transmission method, and is used to identify deep

anomalies.[8] The transmission method is useful when both sides of the studied object are accessible. However, since ASTs are kept full or half-full all year, only the outside of the tank is accessible for imposing heat. Therefore, this research primarily focuses on the reflection method. Different heating sources can be considered when considering active thermography, such as laser heating, halogen lamps, flash lamps, ultrasonic excitation, microwaves, etc.[25] However, one of the challenges in using IRT on tanks constructed from HDPE is the material's low thermal diffusivity (≈1.80 × 10^{-7} m^2/s,[26] ≈19.4 × 10^{-7} ft^2/s). This means it takes a lot of energy to manipulate the HDPE material's temperature and initiate heat transfer over the object's thickness. Regardless, several studies have demonstrated the effectiveness of IRT for polyethylene components, such as pipes,[27-29] pipe joints, [30-32] and composites.[33] Since the thermal conductivity is different for solids compared to air- or water-filled defects or cracks, an infrared (IR) camera will detect evidence of these defects at a different temperature in the presence of a thermal gradient. For instance, IRT has proven to be useful in detecting delamination in pavements and bridge decks.[34-37] To detect defects or flaws, a thermal gradient must exist through the depth of the element, which can be generated through either passive or active methods. Emissivity – a measure of a given material's efficiency at radiating infrared light – is relatively high for HDPE at ~0.96, making it an excellent material to study by IRT.[24] Little IRT research has been performed on polyethylene (PE) in general or on HDPE specifically, but most of the studies have focused on the inspection of pipes,[27–29] pipe joints,[30-32] and composites.[33] For example, Zhu et al.[27] demonstrated that IRT could detect prefabricated flaws in a 0.394 in (10 mm) thick PE pipe.

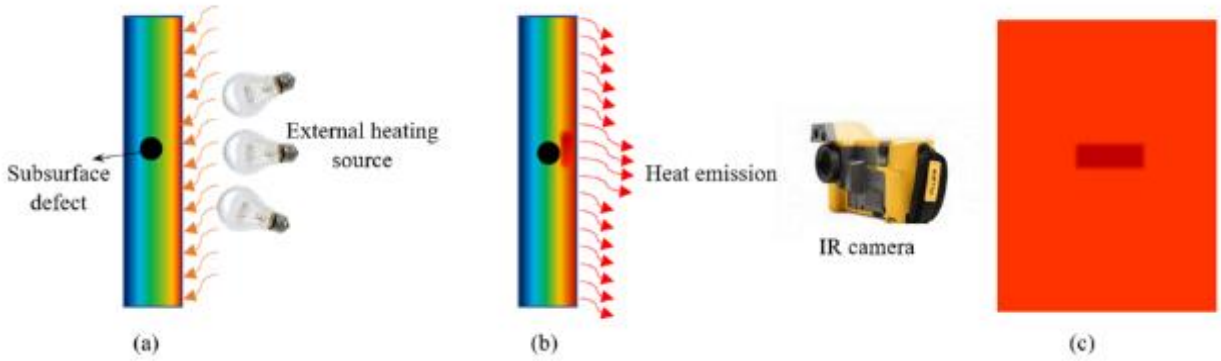

Figure 9(a). Schematic view of a plate cross-section during heating, (b) schematic view of the cross-section of a plate during Infrared thermography after removing the heating source, and (c) schematic view of a thermogram image with a contrast between the subsurface defect and surrounding area

- UT is commonly used to effectively locate and quantify defects in metal and steel structural components.[38] UT methods generally transmit and detect high-frequency sound waves through a material. Studies have demonstrated that ultrasonic methods can be effective for PE components;[39–43] although one critical issue is that PE will significantly diminish ultrasonic wave energy with energy losses reported at 18 dB/inch (7 dB/cm) and as large as 38 dB/inch (15 dB/cm).[10–12] However, conventional ultrasonic and phased array ultrasonic probes should be applicable based on the AST wall thickness. PEUT, also known as pulse reflection

ultrasound, is a conventional one-sided UT in which a single transducer generates an ultrasonic pulsed wave from one side of a specimen into the specimen. That same probe then receives a response signal reflected by an inhomogeneity, such as a defect or the back wall of the specimen.[44] PAUT uses probes composed of multiple ultrasonic elements that act as a synthetic aperture to "sweep" its focus without moving the probe,[45-46] thereby providing significantly more versatility and range than conventional methods. Since the probe's focus is "swept," even stacked defects can be detected, which would not be possible by conventional PEUT methods.[12] PAUT has shown excellent capabilities in detecting embedded defects in HDPE pipes and joints.[10,14–16,40,43,47–49] An examination of State DOT practices indicated that New York is the only one that discusses NDE for inspecting polymer ASTs. Specifically, the New York Department of Environmental Conservation lists UT as an inspection tool for plastic tanks[50] but no guidance on the procedure, testing frequency, or detection limits is discussed.

- Acoustic emission (AE) has been used with polyethylene systems, showing potential for leak detection in pipes.[51–53] However, leak detection is not necessarily within the purview of this study. Furthermore, multiple AE sensors would need to be affixed to each of the 400 brine tanks managed by VDOT, which makes this option costly, and the method would not provide information about ongoing degradation.

- Ground penetrating radar (GPR) is a powerful tool for inspecting pavements.[54] The typical GPR frequency range for pavement applications ranges from 16 MHz to 2.6 GHz.[55] However, these frequencies are too coarse for the resolution needed for ASTs, which needs to be on the order of ≥100 GHz to yield millimeter wavelengths, as has been demonstrated to locate defects in polymer components.[56,57] However, radar techniques with 100s GHz suffer from high attenuation and scattering,[58] which likely obviates their applicability in the field of ASTs.

State DOT Survey Results

Seventeen State DOTs responded to the questionnaire. Nearly 5,100 ASTs are in service in those 17 states. The tank capacities vary from 1,000 to 20,000 gal, but the most typical capacities range from 5,000 to 11,000 gal. More than 65% of all tanks in service have an age between 5 to 14 years. Of the states surveyed, 92% use polyethylene tanks to store their deicing salt solutions. The rest are using fiberglass and unspecified plastic tanks. The State DOTs reported that the thickness of their ASTs has been designed for 1.7 to 1.9 times the specific gravity of the solution and reported different values between 0.5 in (12.7 mm) to 0.75 in (19.1 mm) for the wall thickness. Seven states reported at least one tank failure experience, two of which were fitting failures. The remainder of the failures were due to an unexpected complete rupture of the tank. Maryland DOT reported two complete failures that were bomb-like explosions. These findings further indicate the importance of using NDT to evaluate the ASTs condition to prevent a catastrophic failure.

Results from the survey indicate that State DOTs currently do not have specific criteria to match the condition of the tanks under their control with criteria that would indicate a given tank needs to be removed from service. For this reason, they try to remove tanks from service before they reach the age of 12 to 15 years. Seven DOTs reported issues with fittings during their visual inspections. In most cases, the State DOTs keep their tanks full year-round. This common practice shows the importance of using NDT, which only needs access to the tank's outer side. Aside from Oregon DOT, who unsuccessfully attempted to patch one of their tanks, the respondents reported no other repairs (except fixing the leakage in fittings).

Laboratory-Scale Experiments

IRT results

Impact of Specimen Dimension on Heat Transfer

Two HDPE plates with different sizes were selected to study the impact of specimen size on the IRT measurements. The smaller plate with dimensions of 12 in × 12 in × 0.5 in (305 mm × 305 mm × 12.7 mm) was chosen to allow the whole area to be heated by the external heating source during the IRT. A larger sample with dimensions of 24 in × 24 in × 12 in (610 mm × 610 mm × 305 mm) was chosen to ensure the applied heat impacted only the center area. The results of the IRT technique on both HDPE plates are shown in Figure 10. The vertical axis shows the temperature difference between the center of the HDPE plates at different times and the initial temperature before starting the experiment. The results demonstrate that when the dimension of the specimen increases, the heat propagates toward the cold areas to induce a uniform temperature between the heated area and the surrounding area.

For this reason, the maximum temperature difference is lower in the plate with larger dimensions compared to the smaller plate with which the entire area is impacted by heating. These results show that when the specimen size increases, more energy (i.e., power and time of heating) is required to manipulate the temperature of the HDPE and induce the same thermal gradient over the thickness of the specimen. When the specimen size is small, the whole area is heated up, and the heat transfers only through the thickness of the sample. However, when the specimen size increases, the heat transfers in all directions of the HDPE plate and through the thickness of the sample. Therefore, it may reduce the efficiency of IRT in the field. Moreover, the conclusion on the impact of specimen size on IRT shows that, to apply IRT to the evaluation of HDPE ASTs in the field, a series of field tests are required to prove the efficacy of this technique.

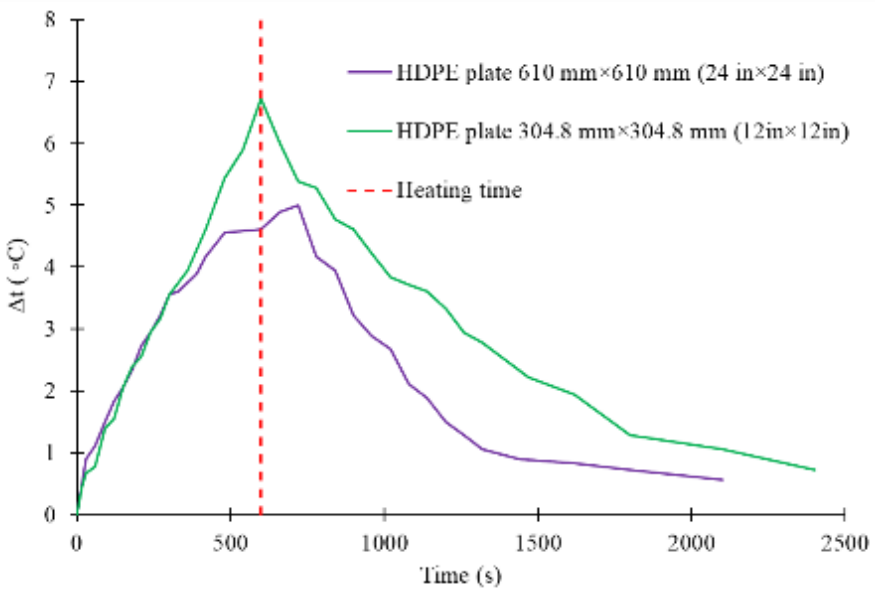

Figure 10. Impact of dimension on the heat transfer in HDPE plates (note: (1°C × 9/5) + 32 = 33.8°F)

Defect Detection with Active IRT on HDPE

At first, to investigate the capability of the IRT technique to detect abnormalities, the experiment was performed with an empty water tank. The empty tank was chosen because both sides of the HDPE plate had the same temperature, and there was no initial thermal gradient across the plate thickness. Figure 11 shows that IRT has the potential to detect some of the abnormalities that exist in HDPE. Figure 11 indicates that when there is no initial thermal gradient over the thickness (t), only shallow anomalies located less than 0.5 t, where t is the wall thickness, from the outer surface can be detected. For this reason, when there is no initial thermal gradient, S.H 1, S.H 2, S.H 4, R3, and R2 (defects introduced in Figure 7 and Table 7) were observed. This has happened due to the low heat diffusivity of HDPE and high heat attenuation.

For this reason, not enough heat is transferred to the other side of the plate over deep defects (like scratches and R1) to create a contrast on the thermograms. The minimum defect size detected for shallower defects (i.e., R3 defects) was circular with a diameter of 0.20 in (5 mm). This observation shows that under this circumstance, defects with a size of 0.11 in (2.8 mm) and smaller do not impact the heat transfer and, therefore, cannot be observed by IRT.

Moreover, in Figure 11, all of the defects that could be observed by IRT with no initial thermal gradient prior to heating will appear during the first 30 seconds after removing the heating source. When the tank is filled with water, the water temperature on the other side of the plate can induce an initial thermal gradient over the thickness, which may impact the observation. Therefore, the study was completed on the full tank under different circumstances, such as different initial thermal gradients or different water temperatures.

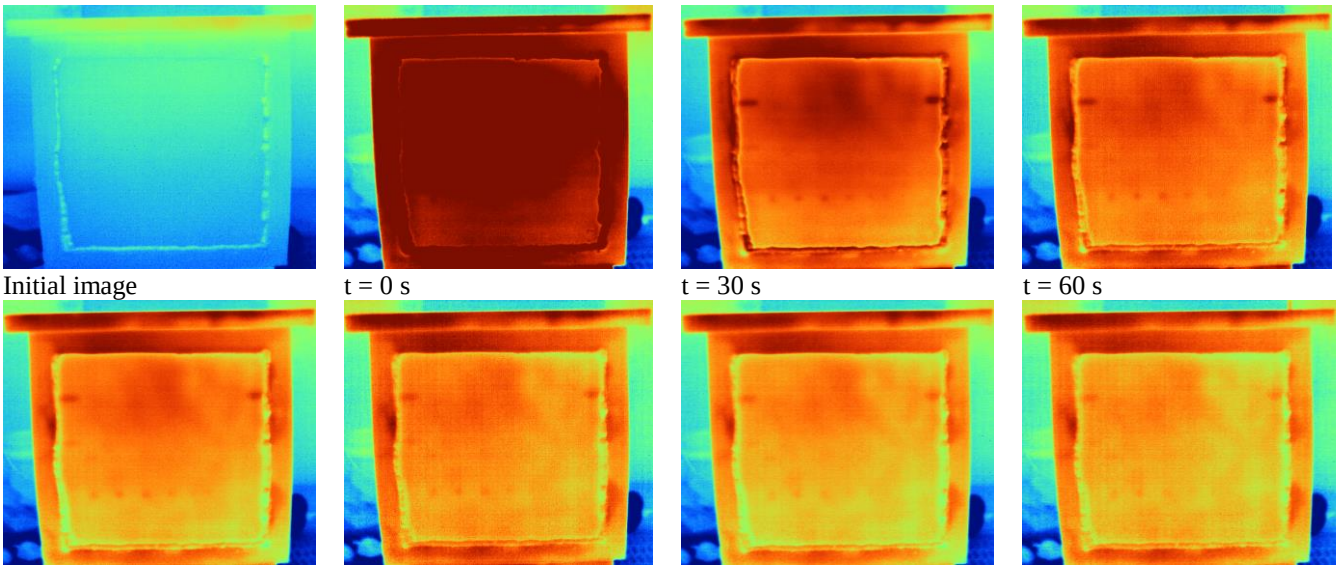

Figure 11. Anomaly detection by infrared thermography technique on the high-density polyethylene sample with a thickness of 0.75 in (19.05 mm) (note: the "initial image" is before applying the heating and starting the experiment, and "t" refers to the time after removing the heat source)

The quantitative results of IRT on all plates tested under different circumstances are shown in Figure 12 from the defects defined in Table 5. The S1 and S2 scratches were not detected in any of the measurements. S3 and S4 were detected only in measurements with a high initial thermal gradient ($|\Delta T| \geq 5.4°F$ (3°C)) on the plate with a 0.25 in (6.35 mm) thickness, where these two scratches had depths less than 0.5t from the exterior side (see Figure 13). The underneath defects S.H 1, S.H 2, and S.H 4 were detected in all measurements. Note that the defects detected underneath the surface were located less than 0.5t from the exterior surface of each plate. S.H 3 was only detected in the HDPE plate with a thickness of 0.25 in (6.35 mm), where S.H 3 and S.H 4 have the same characterization. The R1 backside defects with a depth of 0.75t from the exposed surface were not detected in all of the measurements. The measurements on R2 and R3 are summarized in Figure 13. For the case in which no defects were detected by this method, the bar representing the minimum detectable defect is set past the largest defect, at 1 in (25.4 mm). The previous study showed that the initial thermal gradient ($\Delta T = T_{surf} - T_{int}$) has an impact on the measurements gathered (i.e., smallest detectable defect and time required to detect).[59] T_{int} is equal to the water temperature when the tank is full. Negative values for ΔT imply that the water temperature inside the tank had a higher temperature than the outer tank's outer surface. If the tank was empty, it was assumed that the exterior and interior surfaces of the tank wall had the same temperature; therefore, the initial thermal gradient was equal to zero. For this reason, in this study, the right vertical axis in Figure 13 represents the initial ΔT over the thickness before starting the measurement. For the last measurement, where there is a high negative ΔT, no external heat was used because, as shown in the previous study, having a higher temperature on the backside of the plate. Applying external heat reduces the induced thermal gradient on the plate and reduces IRT's effectiveness. Looking at Figure 13a, ΔT considerably impacts the accuracy of defect identification. Where there was high $+\Delta T$, smaller defect sizes could be detected compared to when $\Delta T \approx 0$. When there is not considerable ΔT on the object, such as $\Delta T \approx 0$, R2 could not be detected in plates with t =1 in (25.4 mm) and t =2 in (50.8 mm).

The reason is the difficulty of temperature manipulation on these plates and consequently getting inadequate thermal gradient on the thickness of these plates, as discussed later in the "Impact of Thickness on the IRT Measurements" section. The results shown in Figure 13 indicate that as the thickness of the HDPE increases, the efficiency in defect detection is reduced. The smallest R2 defect size that could be detected in HDPE plates with $t \leq 0.75$ in (19.1 mm) was the defect with the size of 0.2 in (5 mm) in diameter. The smallest detectable R2 defect size for the HDPE plates with thicknesses of 1 in (25.4 mm) and 2 in (50.8 mm) was 0.3 in (7 mm) and 0.6 in (15 mm), respectively.

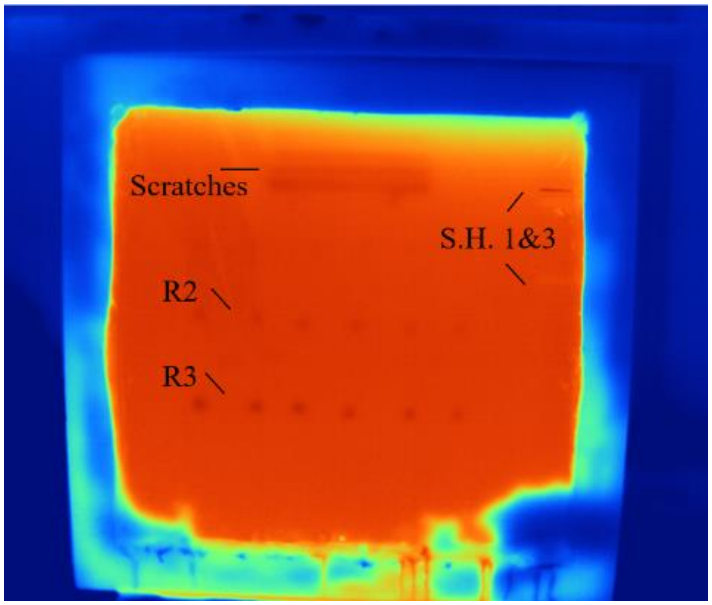

Figure 12. Detecting deep scratches on HDPE plate with t=0.25 in (6.35 mm) when ΔT = –5.76ºF (–3ºC)

By comparing Figure 13a and Figure 13b, it can be concluded that the accuracy of IRT increases as the defects are located closer to the exterior surface. The smallest detectable R3 defect size for both HDPE plates with thicknesses of 0.5 in (12.7 mm) and 0.75 in (19.1 mm) was 0.1 in (2.8 mm), and for the rest of the studied thicknesses, the smallest detectable defect size was 0.2 in (5 mm). Contrary to R2 defects, R3 defects could be detected even when there is not a high initial thermal gradient ($\Delta T \approx 0$) up until a thickness of t =2 in achieving a high enough thermal gradient across the thickness becomes more difficult. Note that the detected underneath defects, R2 and R3, were located less than 0.5t from the exterior surface of each plate. Since not all the defect sizes in each group could be detected, it can be concluded that the defect location is not the only parameter that defines the efficiency of IRT. Therefore, another parameter that describes the defect geometry should be considered.

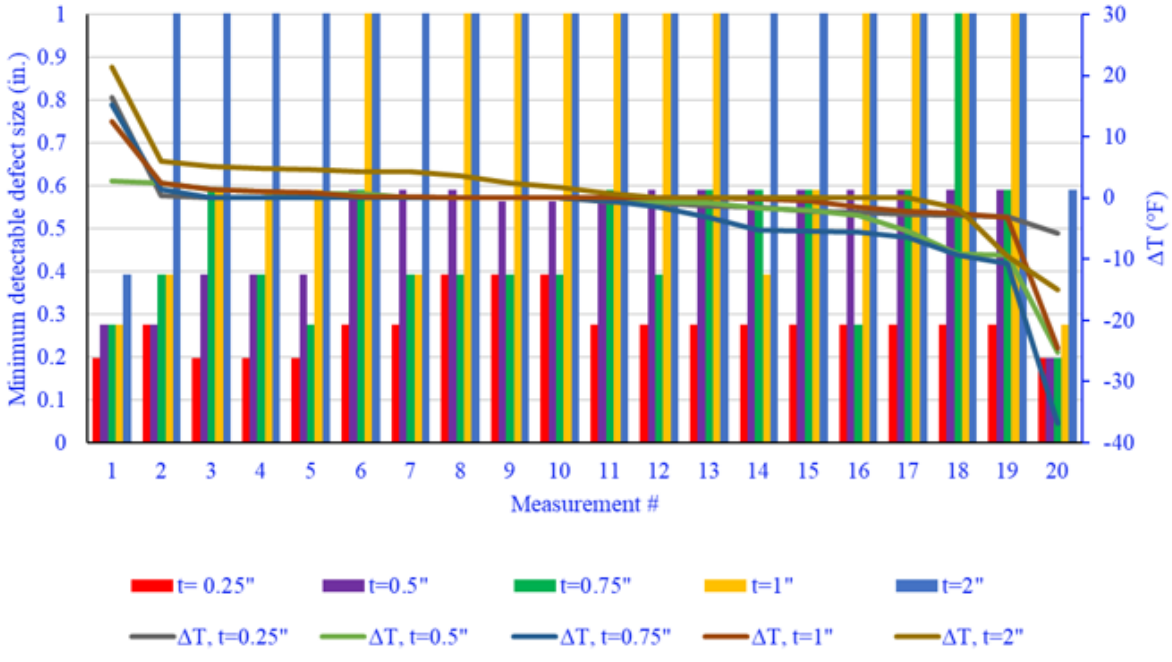

(a)

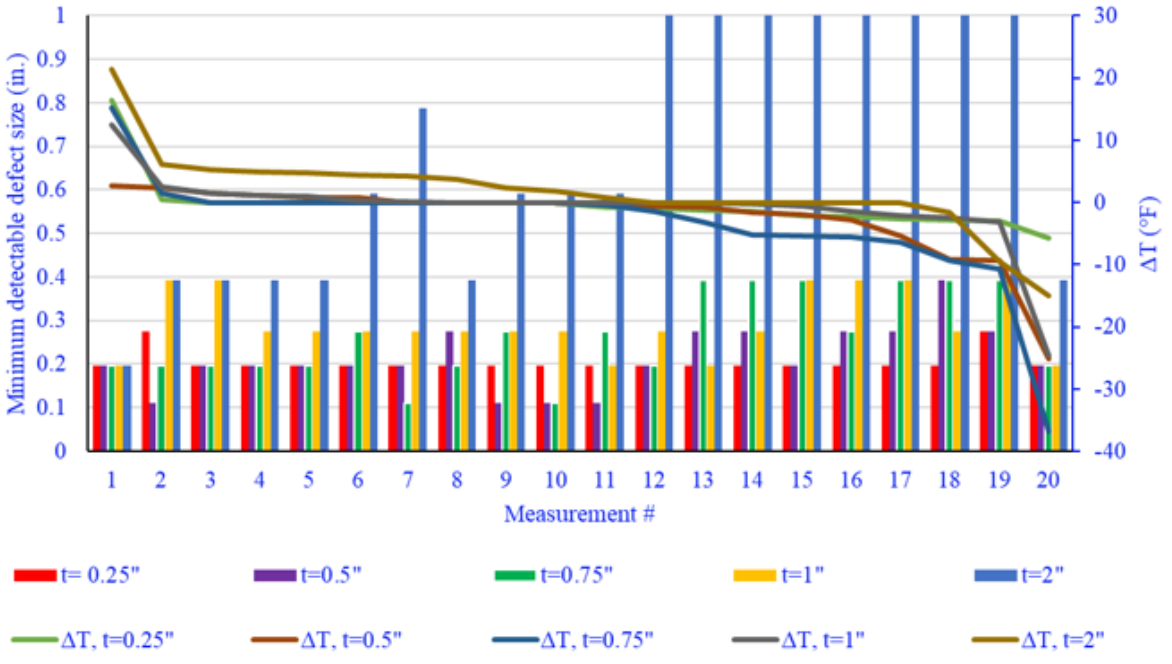

(b)

Figure 13. Measurements of backside defects in all 20 measurements (a) R2 defects (b) R3 defects

The discussion above signifies a direct correlation between the thermal diffusion length (i.e., the distance of the defect to the exterior surface) with the smallest detectable defect size. To summarize both the smallest detectable defect size and the thermal diffusion length in one term

and to account for the defect geometry, the aspect ratio (AR) can be considered. The AR values for both R2 and R3 defects are shown in Figure 14. By considering both graphs shown in Figure 14, it can be concluded that if a defect is located within the half thickness from the exterior and at

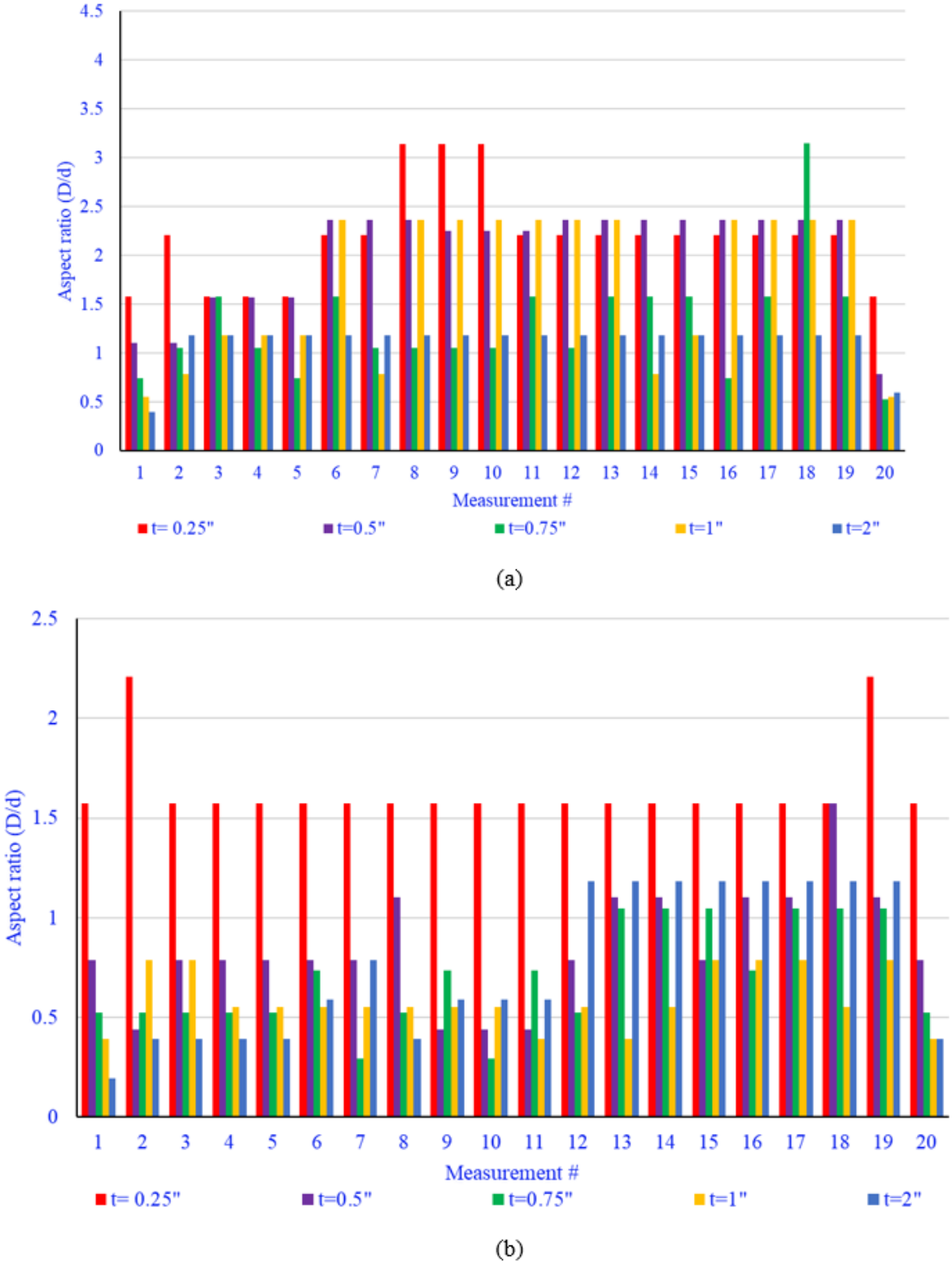

Figure 14. Aspect ratio (AR) of the detectable defects in (a) R2 defects and (b) R3 defects

the same time AR > 0.78, then the defect can be detected easily by IRT. Defects with AR < 0.78 can hardly be detected. Since there were no R1 defects in the experiments while some defects in some HDPE thicknesses had a high AR (e.g., the highest AR for the R1 defects when the thickness t=0.25 in (6.35 mm) was equal to AR = (D=1 in)/(d=0.75×0.25 in) = 5.33), the AR should not be considered as the only criteria for the defect detection threshold. To detect a defect, both criteria of d < 0.5t and AR > 0.78 should be satisfied. The last statement indicates that IRT may not detect cracks because they have narrow widths and very low AR. According to the authors' experiences during lab and field testing, cracks can be detected by IRT under two circumstances: 1) the crack is leaking fluid, and 2) the crack is not heated directly. The second circumstance refers to a situation where the crack is located in the conduction area (i.e., unheated but affected by heat transfer). The aforementioned circumstances are shown in Figure 20. The efficiency of uneven heating to detect cracks with different depths is still a question that requires additional study.

In summary, the explanations above indicate that the interaction of sample geometry, initial thermal gradient, defect location, and AR of the defect all impact the accuracy of IRT in detecting subsurface defects. The laboratory study showed that specimen size and distance of the camera to the object also impact the accuracy of IRT measurements.[59] The preliminary tests of this study revealed that the heating power influences inducing adequate thermal gradient on the thickness and therefore influences the effectiveness of IRT. Other studies have noted that the heating method (e.g., frequency-modulated heating, thermal wave heating, thermal compression heating, etc.) also impacts the efficiency of IRT in subsurface defect detection.[60–64]

Impact of Water Temperature on Defect Detection in Active IRT

Figure 15 indicates that the water inside the tank can impact the time of appearance of each defect in the thermograms and the minimum observable defect size. When the tank is empty, both sides of the tank wall have almost the same temperature ($\Delta T = 0$). Therefore, all the heating energy applied outside the wall will be transferred through the wall thickness and induce a thermal gradient.

In Figure 15b, when the tank is filled with water with almost the same temperature as the tank exterior ($\Delta T \approx 0$), the induced thermal gradient increases because the water has a high thermal capacity, and more energy is needed to increase the temperature. When the applied heat reaches the other side of the tank, the interaction between the water and the interior wall of the tank causes a smaller temperature change compared to the time in which the tank is empty. In Figure 15c, when the water has a lower temperature than the tank exterior, it creates the maximum thermal gradient across the thickness.

In Figure 15d, the water inside the tank has a higher temperature than the tank exterior. In this case, when heat is applied on the surface, the temperature of the tank exterior increases first to reach the temperature of the interior side and then increases past the internal temperature; this means that the thermal gradient induced on the thickness with the same amount of energy is negligible.

Another observation made was that the water temperature will impact the initial ΔT. A higher positive initial ΔT will result in a shorter time of defect appearance in the thermograms. In Figure 15, if the time t = 0 is to be used for comparison, it can be seen that when the ΔT increases from Figure 15a to Figure 15c, the time for observing the defects becomes shorter. Figure 25c shows the highest ΔT, which shows that most deep defects were observed immediately after removing the heating source. However, in Figure 15d, where ΔT is a negative value, even after 400 s, no defect was observed. In Figure 15a, the minimum defect size in R2 was an interior defect with a diameter of 0.28 in (7 mm). In the R3 defect series, the minimum observable defect size was 0.2 in (5 mm) in diameter. When the ΔT increased in Figure 15b, the minimum defect size in the R2 defect series was an interior defect with a diameter of 0.39 in (10 mm). In the R3 defect series, the minimum observable defect size was 0.2 in (5 mm) in diameter. Therefore, the water temperature will impact the minimum detectable defect size and the time for the appearance of defects on the thermograms.

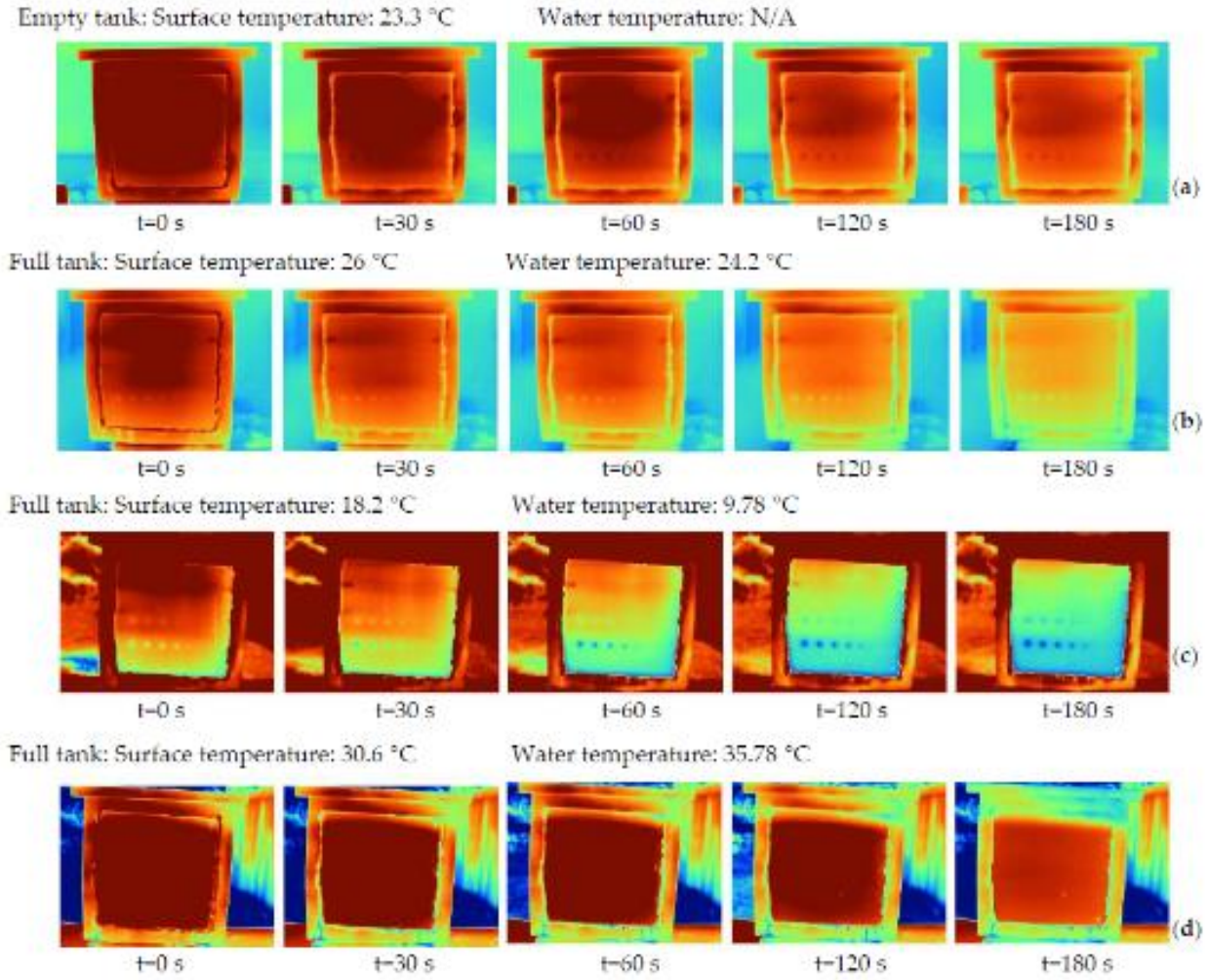

Figure 15. Impact of water temperature on defect detection: (a) when the tank is empty, (b) when the tank is filled with water at a temperature close to the tank temperature, (c) when the tank is filled with water with a lower temperature than the tank, and (d) when the tank is filled with water with a higher temperature than the tank

Indirect Transmission IRT

The initial images of Experiments #9, #15, and #20 were used to indirectly study transmission IRT. In these three experiments, the water inside the tank had a higher temperature than the tank's outer side; therefore, water could be used as a heating source on the opposite side of the wall, which is required for transmission IRT. For this reason, the initial images were used before applying an external heating source. Figure 16 shows that transmission IRT can help detect many anomalies quickly without applying external heating and spending additional time monitoring the defect appearance during the cooling phase. Those defects that were observable appeared at the same time on the first thermogram. The smallest interior defect that could be observed was the 0.2 in (5 mm) in diameter defect when the tank was filled with 45˚C (113°F) water and when the wall temperature did not reach equilibrium with the water (Figure 16a and Figure 16b). Figure 16a shows that when the water and the interior side of the tank wall did not reach a temperature equilibrium and had the highest absolute thermal gradient over the wall thickness, deep defects, like scratches, and R1 defects could be detected. For cases when the interior tank wall and water had reached a temperature equilibrium (Figure 16c and Figure 16d), the smallest observable defect size increases to 0.28 in (7 mm), and the deep defects like R1 and subsurface defects like S.H 4 could not be adequately detected.

Experiment #9 could not be extended for 24 hours to allow the water and interior side of the tank wall to reach equilibrium. This was because the water heater used to keep the water temperature constant could not maintain a 113°F (45˚C) temperature. In general, it can be concluded that transmission IRT helps to detect shallow anomalies with less energy in a shorter time. Transmission IRT can be applied in the field if the best time frame is found in which the brine in the tank is at a higher temperature than the outer side of the tank.

Figure 16d shows that if there is leakage (at the bottom of the tank in this figure), it can be detected immediately by using the IR camera without applying any heating. This helps to rapidly evaluate the ASTs for leakage and locate the origin of the leakage.

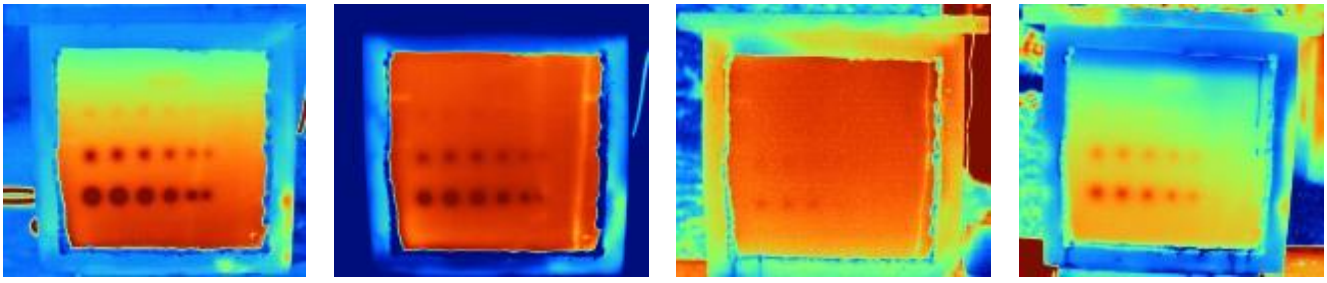

(a) (b) (c) (d)

Figure 16. Using warm water inside the tank as an indirect method of transmission infrared thermography: (a) during filling of the tank with 113˚F (45˚C) water, (b) three minutes after filling the tank with 113˚F (45˚C) water, (c) tank filled with 57.6˚F (14.2˚C) water after 24 hrs, and (d) tank filled with 96.4˚F (35.8˚C) water after 24 hrs

Passive IRT

Passive IRT, represented in Experiment #19 available from the authors, in which cold water with a temperature of 49.6˚F (9.8˚C) produced a positive ΔT due to the ambient temperature. The passive thermography worked in this measurement because the cold water inside the tank induced a very high positive initial thermal gradient (ΔT= 15.1˚F = 8.4˚C) over the thickness of the HDPE plate. Therefore, the ambient temperature could act as the external heating source, allowing shallow defects (R2 and R3) plus subsurface defects (S.H 1, S.H 2, and S.H 4) to be detected, as shown in Figure 17. The result provided in Figure 17 shows that passive IRT has the potential to detect these shallow defects; however, the optimum ΔT for passive thermography is still unknown.

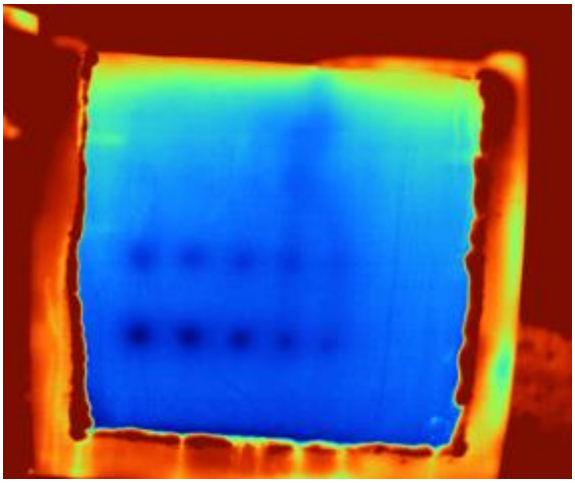

Figure 17. Passive infrared thermography testing on the small scale high-density polyethylene water tank

Impact of Thickness on the IRT Measurements

The cooling behavior at the center of HDPE plates of varying thicknesses was recorded during the cooling phase of the IRT experiment and is displayed in Figure 18. The starting point of the plot refers to the time immediately after removing the heating source, defined as the reference temperature in this study. By comparing the reference temperatures of different plates and the cooling behaviors, it can be concluded that, as the thickness increases, it becomes more difficult to manipulate the temperature of the HDPE and consequently induce higher thermal gradients across the thickness of the HDPE. On the other hand, when the plate is thin (e.g., 0.25 in (6.35 mm) in thickness), heat applied to one side from external sources diffuses quickly, resulting in both sides being heated to similar temperatures and thus a very low thermal gradient. As discussed earlier, the amplitude of the induced thermal gradient on the thickness of the tank wall considerably impacts the accuracy of measurements. To study the heat transfer mechanism across the thickness of the HDPE plate when both sides are exposed to the air, temperature changes during the cooling phase with regard to the reference temperature were calculated by subtracting the initial reference temperature from recorded temperatures (Figure 19). The results in Figure 19 indicate that when the thickness of the HDPE increases, the object starts to cool down faster because 1) heat diffuses through the material to colder regions via conduction, and 2) the heated surface loses heat to the colder air via convection. When the HDPE is thin enough that

the same temperature is measured on both sides of the plate after heating, there is no thermal gradient in the thickness; therefore, the HDPE plate cannot lose heat by conduction from both sides. For this reason, by increasing the thickness, conduction and convection helps the HDPE lose heat. When the thickness is too high (e.g., ≥ 2 in (50.8 mm)), the cooling rate reduces: 1) the heat from the heated side needs to travel a longer distance via conduction to reach the other cold side, and the heat remains in the material for a longer time; 2) the heat lost via convection happens only from the heated side, not both sides. The recent discussion shows that thickness impacts the cooling rate of the HDPE, consequently impacting the time necessary for detecting defects with different geometries. Therefore, more field testing on HDPE ASTs with different thicknesses under different environmental circumstances is required to study the efficiency of IRT in field investigations.

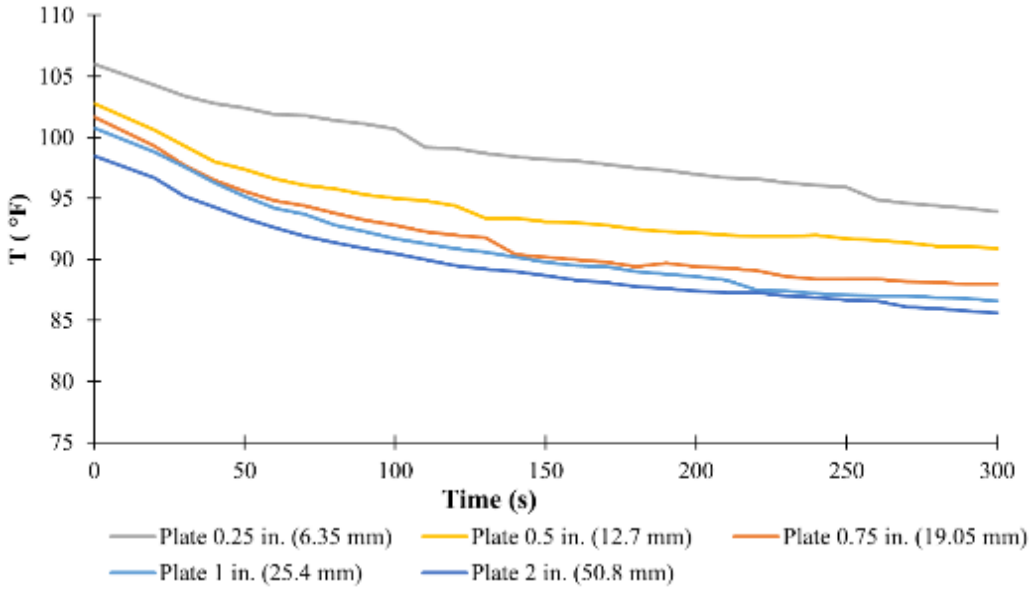

Figure 18. Temperature change on the center of high-density polyethylene plates with different thicknesses during the cooling phase

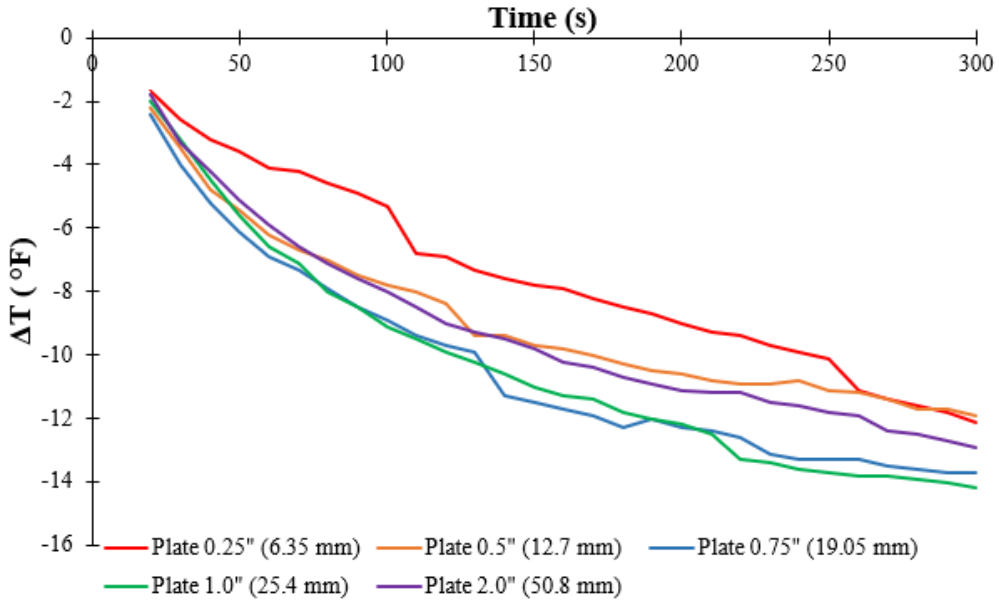

Figure 19. Temperature difference during the cooling phase compared to the reference temperature

UT Results

For viscoelastic materials, such as HDPE, at the temperatures studied here, the attenuation coefficient and phase velocity will vary with temperature.[65,66] Therefore, since the AST temperature changes seasonally, the effect of temperature on wave velocity was evaluated. For this purpose, Echo Pure low viscosity couplant from Echo Ultrasonics, LLC was used to investigate the wave velocity change vs. temperature on HDPE plates with thicknesses of 0.5 in (12.7 mm) and 0.75 in (19.1 mm). The results in Figure 20 show that the thickness of the specimen does not impact the sound wave velocity measurement. Results in Figure 20 show that when the temperature decreases, the sound wave velocity increases. The reason is that in colder temperatures HDPE becomes denser in structure due to crystallinity change and hydrocarbon chains' amorphousness because of the change in the degree of crosslinking and branching.[67–69] Therefore, the sound wave travels faster through the denser material at colder temperatures. These results demonstrate the importance of measuring the wave velocity in the field before inspecting ASTs.

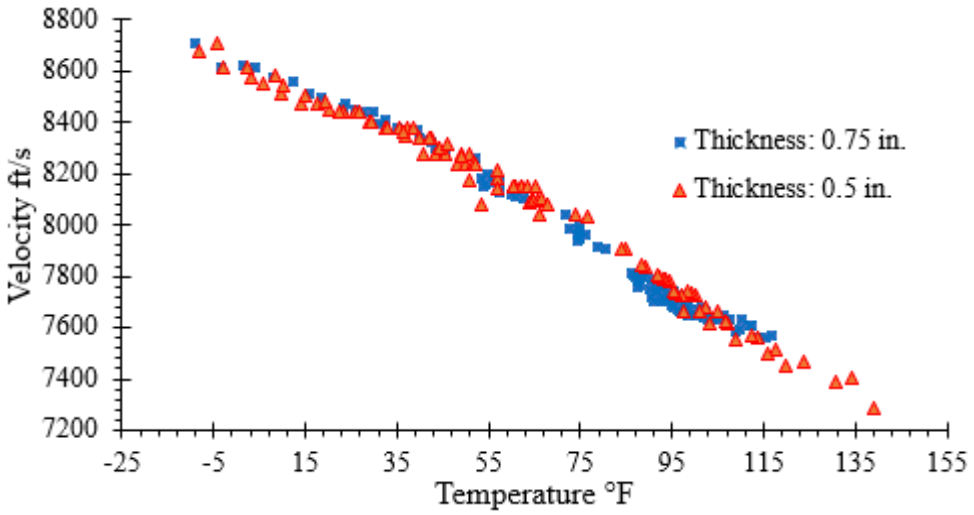

Figure 20. Sound wave velocity vs. temperature

To study the utilized couplant's impact on the measured sound wave velocity, the experiment was repeated with four variations of couplants while testing a 0.5 in (12.7 mm) thick HDPE. The couplants used for this preliminary investigation were water, petroleum jelly, Echo Pure low viscosity, and Echo Pure 414 FL. The results in Figure 21 show that there is little to no effect of couplant type on wave velocity, at least for the couplants examined here.

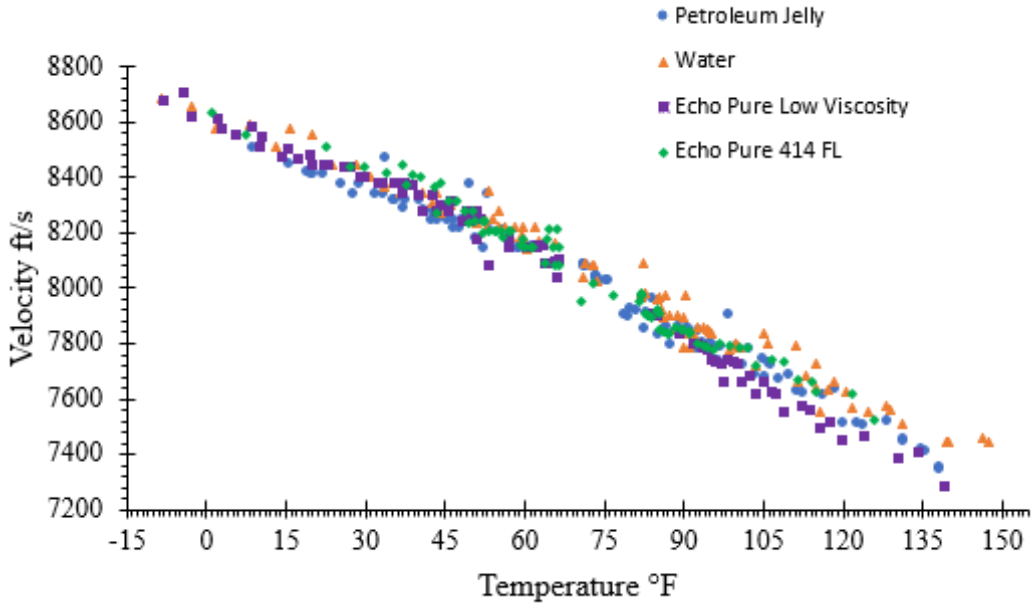

Figure 21. Sound wave velocity vs. temperature measured by using different couplants

The other concern about UT on the HDPE plate for the field tank evaluation is the impact of UV degradation. Since the HDPE tested in Figure 20 and Figure 21 was new, the temperature dependence was also evaluated for 15-year-old weathered HDPE collected from a failed AST to explore the potential field variability. The weathered HDPE, shown in Figure 22, exhibited

significant shallow cracking on the interior of the tank. Figure 23 compares the temperature difference between the new and weathered HDPE, demonstrating that most of the measured data was placed in the 95% prediction interval. These observations imply that weathering does not affect the sound wave velocity considerably.

Figure 22. Superficial cracks on the interior side of an old high-density polyethylene plate

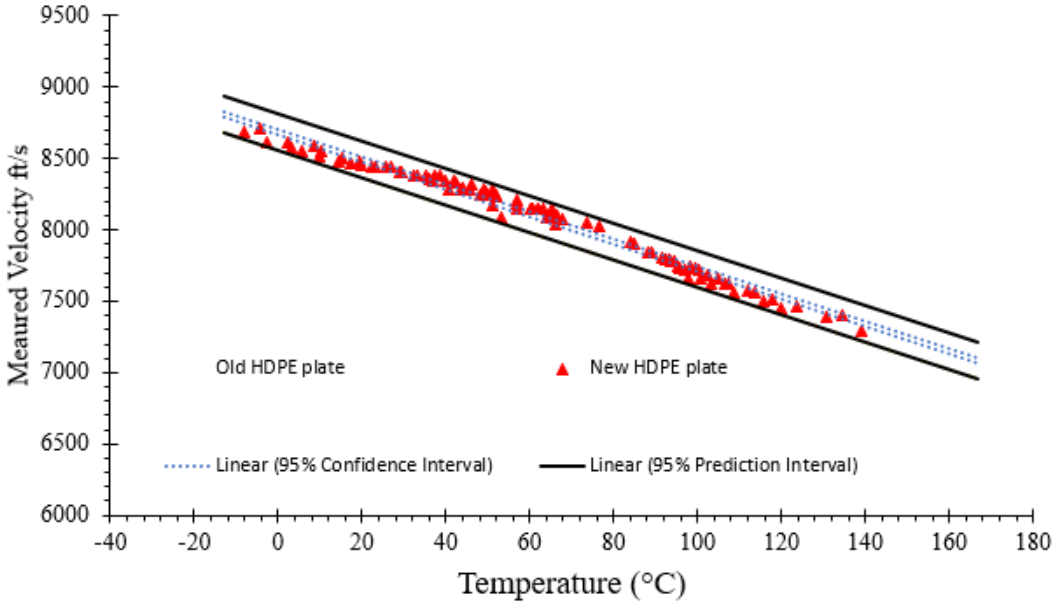

Figure 23. Sound wave velocity comparison in a 0.375 in (9.5 mm) weathered high-density polyethylene plate and a new 0.5 in (12.7 mm) HDPE plate

Pulse-Echo Ultrasonic Testing (PEUT)

UT could indicate subsurface defects and other useful information on the general location of these defects. Figure 24 shows the results of pulse-echo ultrasonic testing (PEUT) for detecting a single interior defect (i.e., the R2 defect on the HDPE plate with a thickness of 0.75 in (19.1 mm)). The depth of the defect from the surface can be measured by positioning the first cursor on the right peak. More specifically, by positioning the cursors on the right peaks and

subtracting "G2↓v" from "G1↓v," the location of the defect can be characterized. Additionally, the location of the defect can be visualized in the bottom window in Figure 24. The experiment was repeated on a subsurface defect (i.e., S.H 2 on the 0.75 in (19.1 mm) thick plate). As shown in Figure 25, there are three peaks. Two peaks are attributed to both sides of the plate, and the other peak (the first peak from the left) is attributed to the subsurface hole. Therefore, by positioning the cursors on the peak correlated to the hole and the plate's peak surface, the subsurface defect's location can be characterized, as shown in Figure 25. If the defect is smaller than the probe size, or the probe is located on the border of the defect and flawless area, more peaks will be observed in the response signals, as shown in Figure 26. This makes the interpretation of PEUT results difficult.

PEUT was also performed on a plate with two and four stacked side hole defects, shown in Figure 27 and Figure 28, respectively. By comparing the last two figures, it can be seen that the results resemble each other. These results indicate that PEUT is unable to characterize these stacked defects.

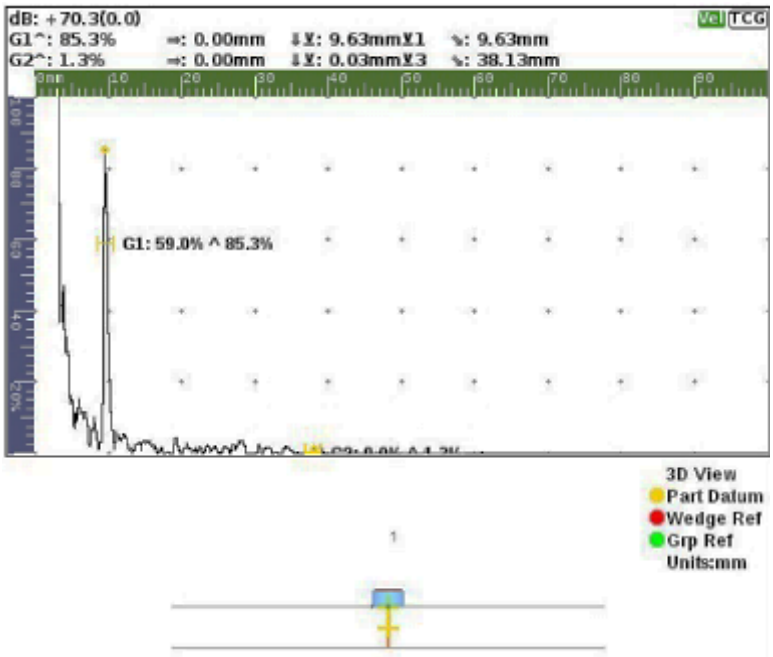

Figure 24. An interior defect (R2) detection on a 0.75 in (19.1 mm) thick high density polyethylene plate using pulse-echo ultrasonic testing (note: 1 mm = 0.039 in)

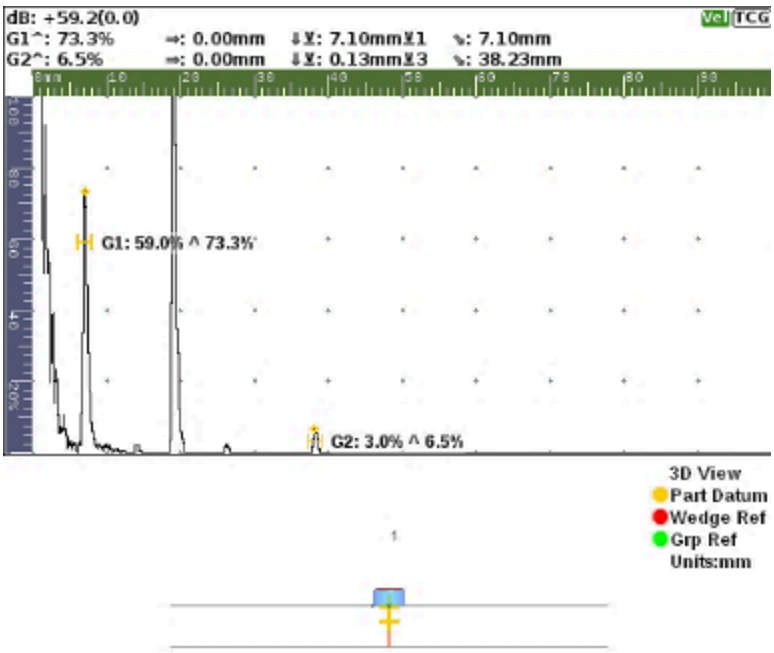

Figure 25. A subsurface defect (side hole) detection using pulse-echo ultrasonic testing (note: 1 mm = 0.039 in)

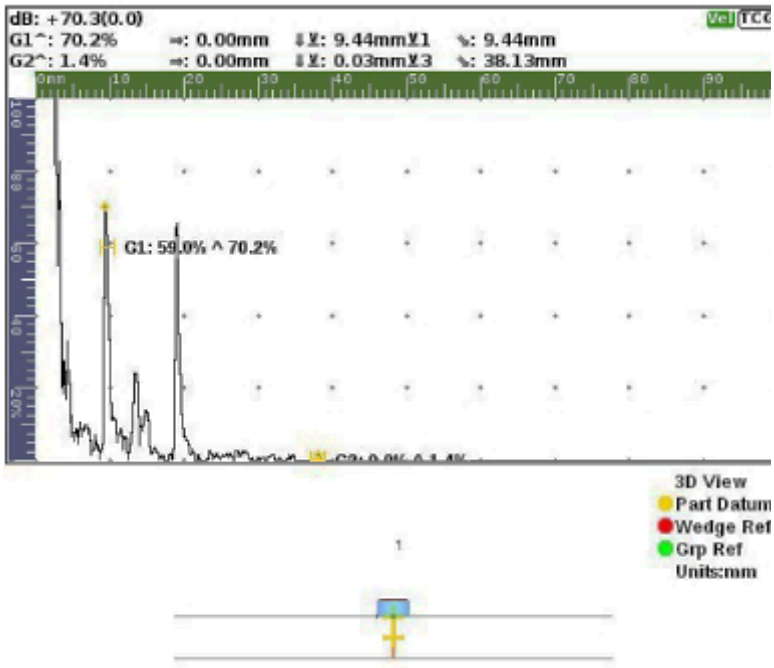

Figure 26. A subsurface defect detection when the ultrasonic probe is not completely on top of the defect (note: 1 mm = 0.039 in)

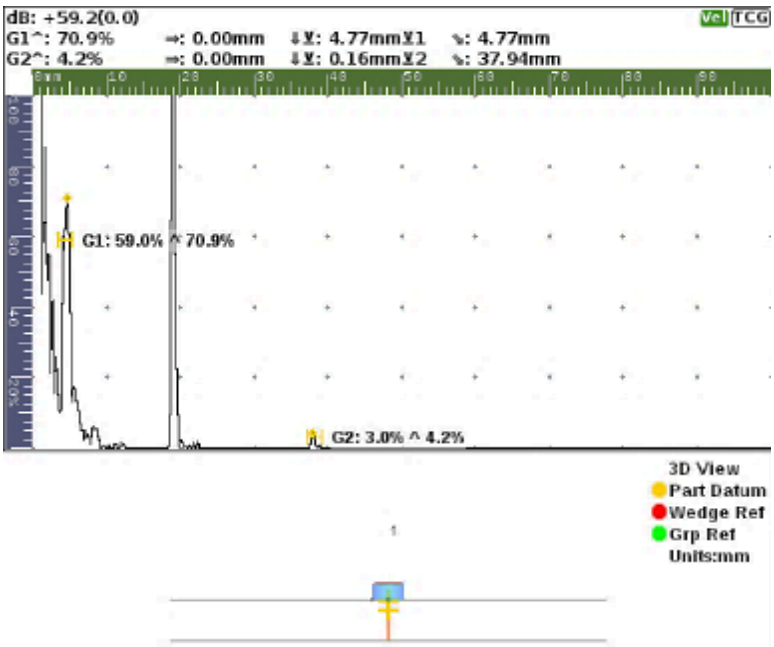

Figure 27. Pulse-echo ultrasonic testing on an area with two stacked defects (note: 1 mm = 0.039 in)

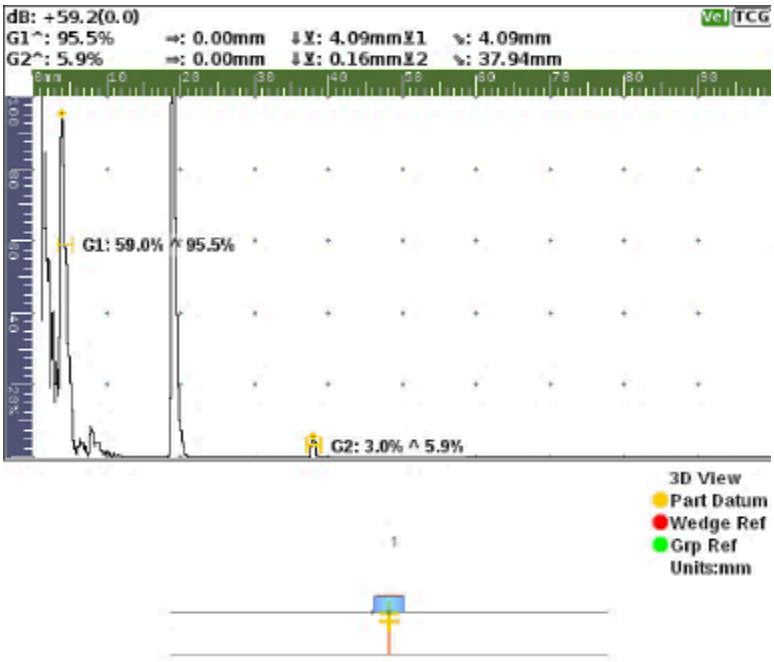

Figure 28. Pulse-echo ultrasonic testing on an area with four stacked defects (note: 1 mm = 0.039 in)

Phased Array Ultrasonic Testing (PAUT)

PAUT was used on a single interior defect (the largest defect in R3), two stacked defects, and four stacked defects. The results are shown in Figure 29 through Figure 31. When there was an interior defect with dimensions larger than the wedge, only a single defect was observable in the UT responses, as shown in Figure 29. However, if a defect with a smaller size than the wedge existed, more peaks and defects were observed in the UT responses, as shown in Figure 30.

The top window in Figure 30 shows two defects identified in the PAUT response. In addition, two peaks on the linear signals on the right side of the figure could be observed, further proving the two defects' existence. Depending on the positioning of the first and second cursors in the software, the depth of the defects from the surface or the distance between the defects can be measured. From the results shown in Figure 30, the distance between the stacked defects was measured in the top red box. Moreover, the width of the defects on the sectorial response shows the size of the defect. Figure 31 shows the results of PAUT on the 0.75 in (19.1 mm) thick HDPE plate with four stacked defects. There are four defects in the sectorial PAUT response. In addition, the four peaks on the signals on the right side of the figure further prove the existence of the four defects. As was performed for the two stacked defects, the distance between the defects or the depth of those defects can be estimated by positioning the first and second cursors on the right peaks. Figures 21 and 22 show that PAUT is a powerful technique that can characterize defects accurately. Moreover, while the results show that UT can be used as an effective technique to characterize defects, further work is needed to study its efficiency in evaluating ASTs in the field.

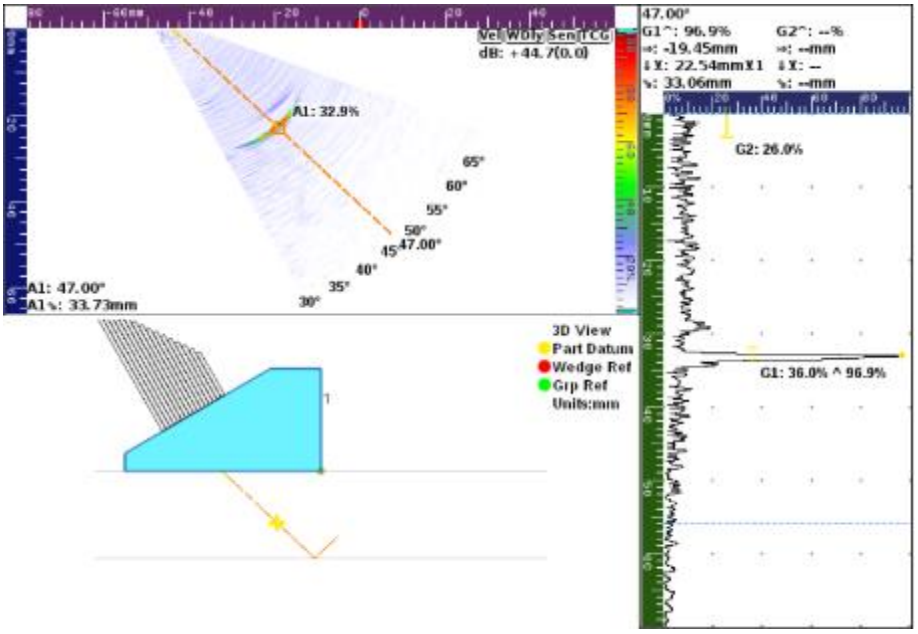

Figure 29. R3 defect detection on the 0.75 in (19.1 mm) thick plate (note: 1 mm = 0.039 in)

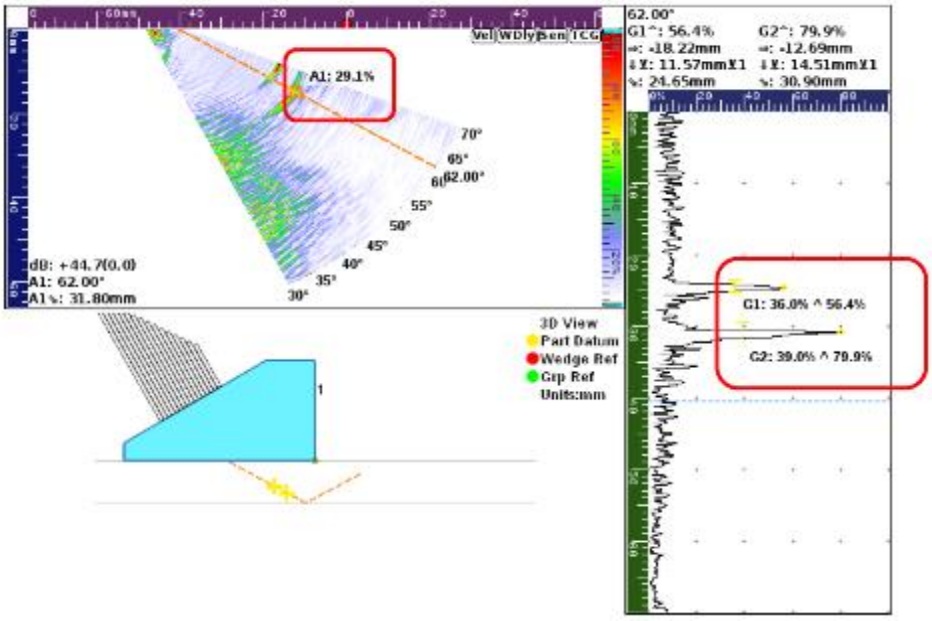

Figure 30. Phased array probe used for the detection of two stacked subsurface defects (note: 1 mm = 0.039 in)

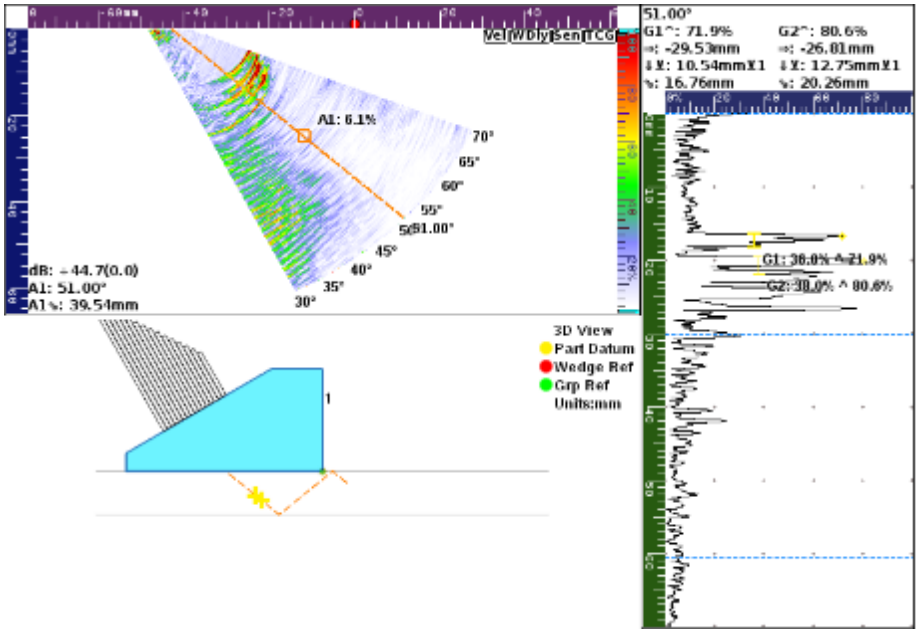

Figure 31. Phased array probe used for the detection of four stacked subsurface defects (note: 1 mm = 0.039 in)

Full-Scale Experiments

Temperature Measurements

It was determined from Task 2 that the initial temperature gradient through the tank wall ($\Delta T = T_{wall\_surface} - T_{water}$) affects the measurement and defect detection threshold. Therefore, it is

necessary to study the best time frame for conducting the IRT evaluation on HDPE AST in the field. During different times of the day, one-half of the tank is sun-facing, and the other half is shade-facing; therefore, uneven heating received from the sun can induce a nonuniform temperature on the tank, as proven by IRT and as shown in Figure 32. The tank wall temperatures recorded during 230 days are shown in Figure 33. The temperatures are recorded from three different elevations of top, middle, and bottom and two sides of the tank (east and west). East and west sides were selected for temperature monitoring because the east side is sun-facing in the morning while the west side is shade-facing in the afternoon. Figure 33a shows the temperatures recorded at 10:30 AM when the sun is on the east side, and Figure 33b shows the temperature at 4:30 PM when the sun is on the west side of the tank. As seen in Figure 33, the temperature of the tank wall varies from east to west depending on the sun's direction. In the morning, the east side of the tank has a higher temperature, and in the afternoon, the west and east sides of the tank have comparable temperatures. In the afternoon, the temperature of the tank wall, on both sides, has increased from heat accumulation that started at sunrise. Figure 34 shows the temperatures on the tank wall on two random cloudy days; the temperatures of east and west sides are similar and fall between the water and ambient temperatures. In other words, on cloudy days, there is a negative initial thermal gradient ($\Delta T < 0$) on the tank wall, which according to the previous studies, is not suitable for completing IRT evaluation. This was verified for all the data gathered, and the same pattern was seen on all cloudy days. Figure 35 shows examples of tank temperature changing behavior on sunny days during summer and winter. As seen, the peak temperature for the east and west sides shifted due to sunlight direction changes in the morning and the evening.

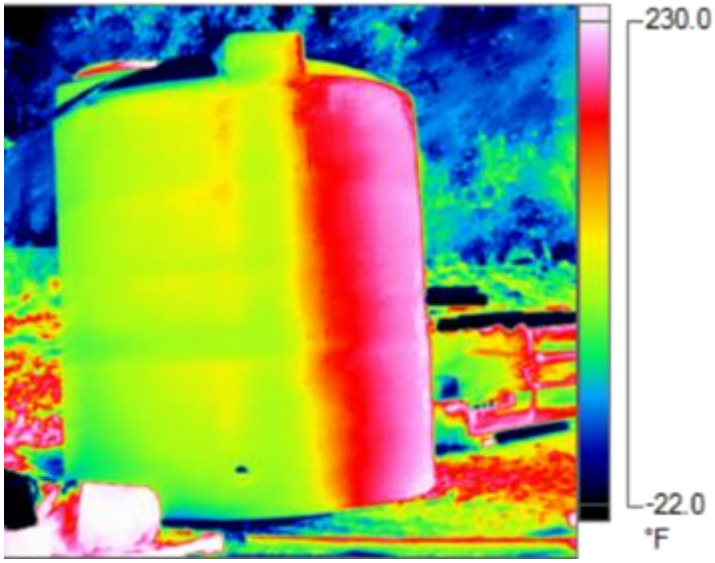

Figure 32. The non-uniform temperature on the tank

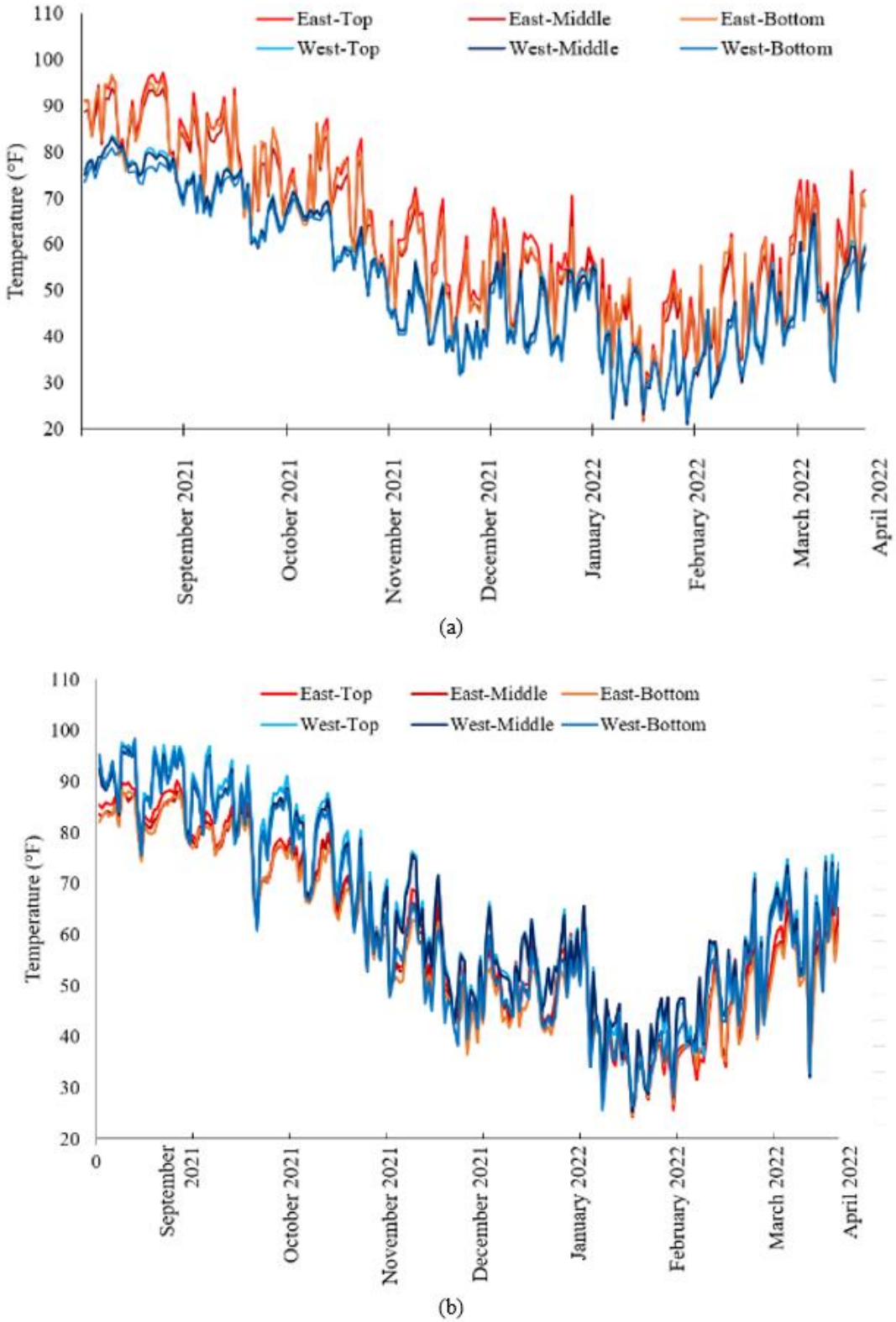

Figure 33. Temperature change on the tank wall at three different elevations of the top, middle, and bottom from two different sides of east and west (a) at 10:30 AM and (b) at 4:30 PM

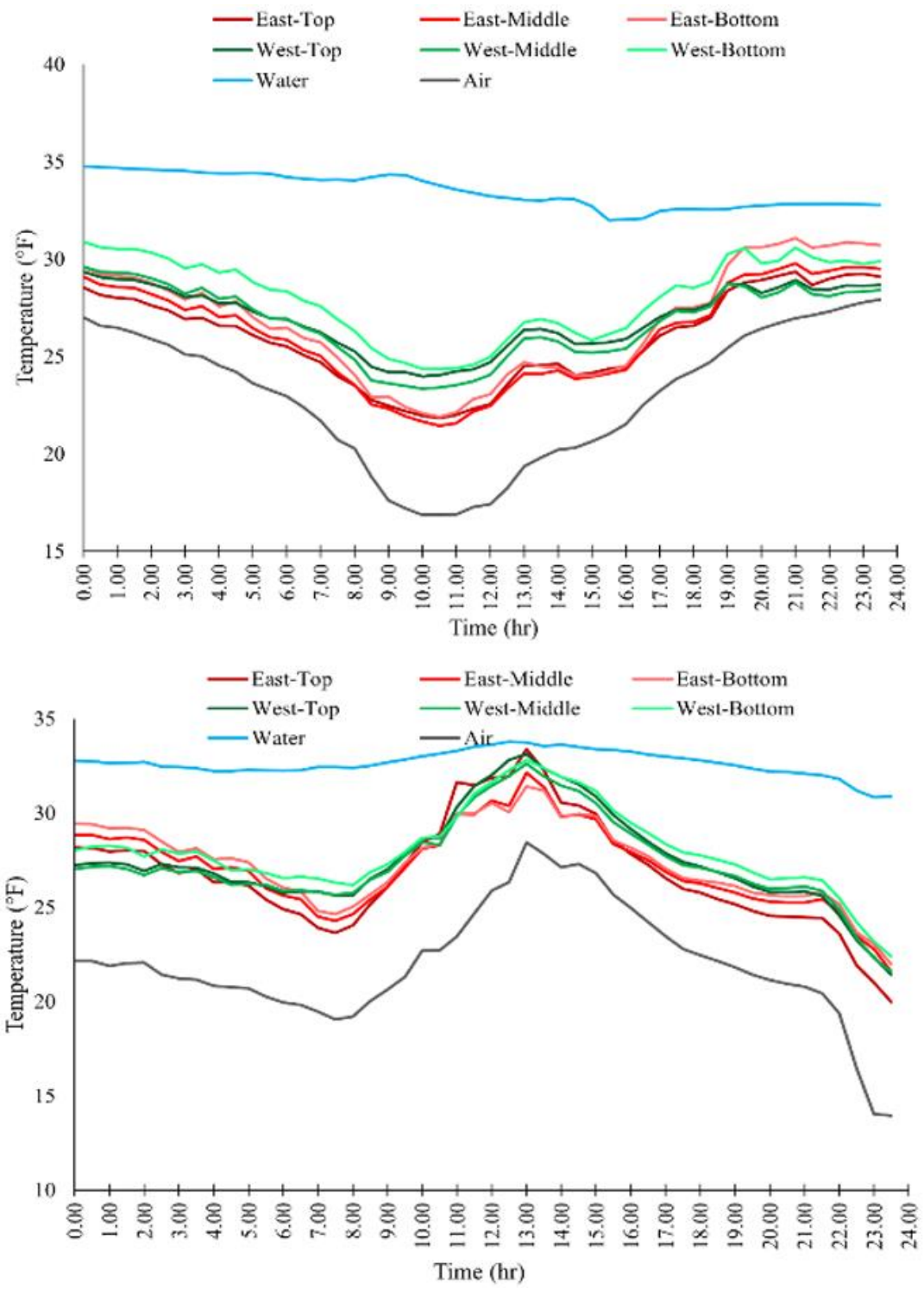

Figure 34. Temperatures of the high-density polyethylene tank, water, and ambient on two cloudy days during winter

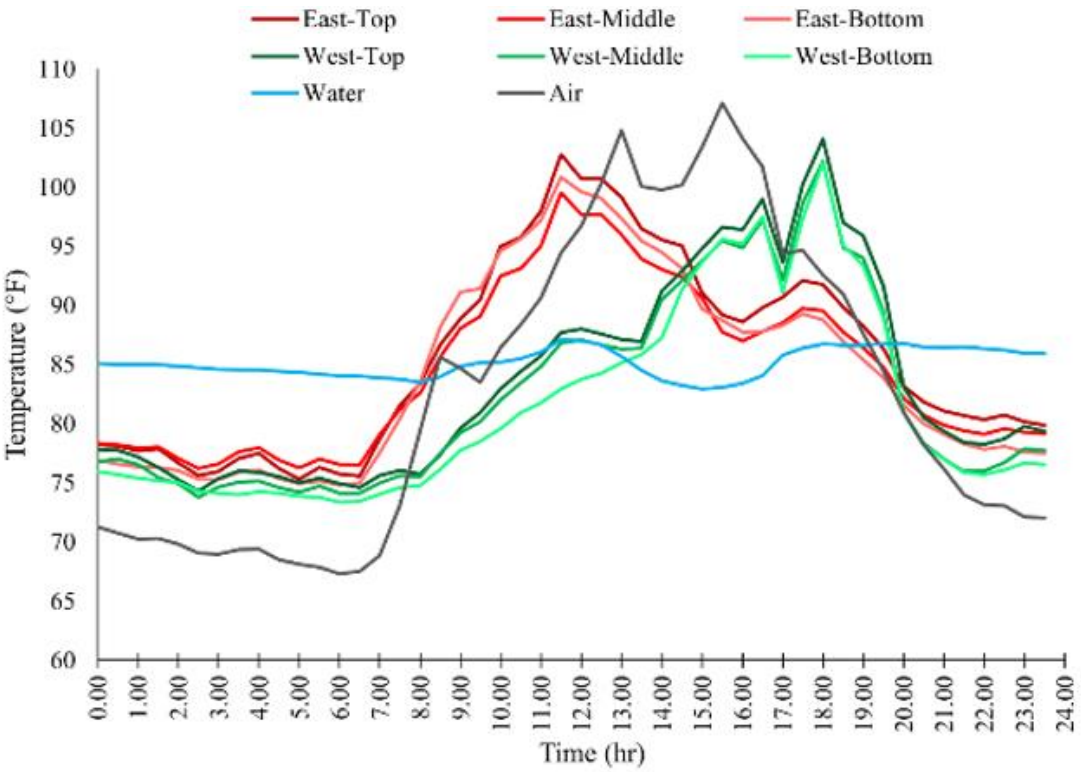

(a)

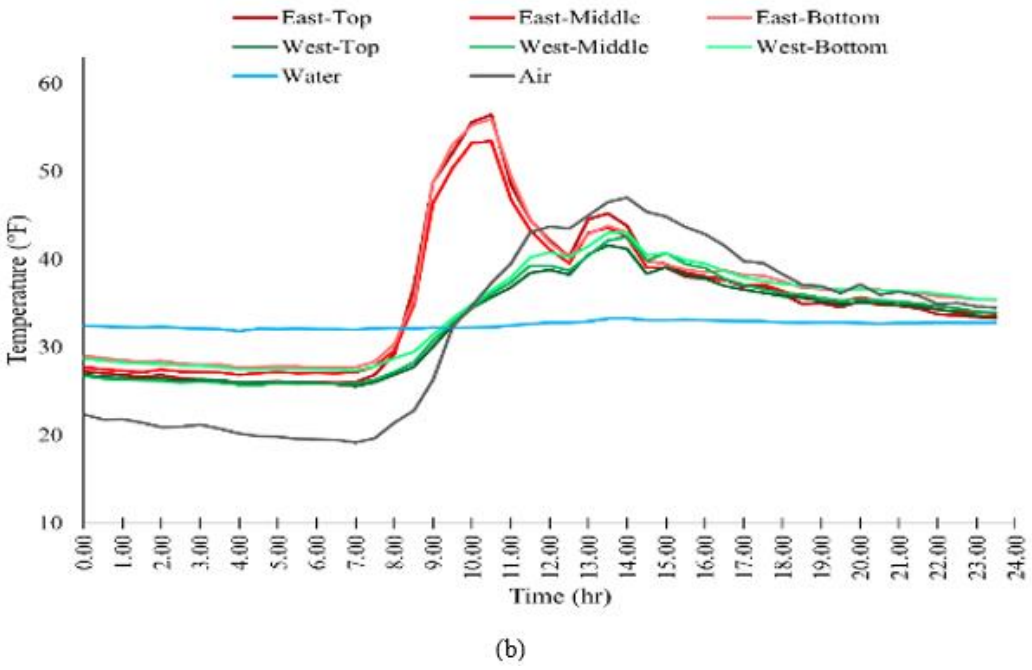

(b)

Figure 35. Temperatures of the high-density polyethylene tank, water, and ambient on two sunny days during (a) summer and (b) winter

Moreover, in most cases, there is a positive initial thermal gradient ($\Delta T > 0$) on the tank wall thickness between 9:00 AM to 6:00 PM, which is suitable for performing IRT. Therefore, it implies that the best time for conducting IRT is on sunny days between 9 AM to 6 PM, with a preferred time in the afternoon (2 PM to 6 PM) when both east and west sides have comparable temperatures. In addition, since the maximum ΔT for the east and west sides happen at different times during the day, it is hypothesized that it may be better to evaluate each tank twice a day, once in the morning and once in the afternoon. For this reason, the IRT was completed once in the morning and once in the afternoon for each heating-cooling combination to study the accuracy of the last hypothesis.

IRT Results

The results of IRT on the east and west sides in the morning (performed between 10:00 AM to 11:30 AM) and evening (performed between 2:00 PM to 3:30 PM) were summarized by the research team. Two examples of IR images are shown in Figure 36. For each combination of heating-cooling durations, the morning and afternoon tests have not been conducted on the same day. The reason was to get a wider range of the temperatures for a better decision on the suitable time frame for conducting IRT. For this reason, for most tests, there are considerable differences in the initial temperature between the morning and afternoon tests for a single heating-cooling combination. In each test, the IRT of the east and west sides was done at the same time (with an approximately 0.5 hours delay). The defects detected at each cycle for each heating-cooling combination are named according to the coordinates of the defect in row (R) and column (C). For example, R7C4 refers to the defect located at the 7^{th} row and the 4^{th} column. The list of defects were compiled by the research team to show the defect detection improvement as the cycles increased to figure out the optimum or minimum number of heating-cooling cycles. The results indicate that in most cases, the accuracy of completing five cycles is similar to six cycles. Therefore, five consequent heating-cooling cycles should be sufficient to detect the subsurface defects.

The optimum heating-cooling phase is the one that optimizes detection accuracy while minimizing the time taken to perform the test. The highest detection accuracy can be defined as the ability to detect the smallest aspect ratio (AR) and the largest ratio of defect depth (D) relative to the wall thickness (t) (D/t). For this reason, the plots of the smallest detected AR versus the maximum D/t for different heating-cooling combinations at the final cycle (cycle #6) have been shown in Figure 37 to Figure 40. The diameter of the bubbles in these figures stands for the AR, and values are printed next to each bubble. Therefore, comparing the diameter of the circles can help to visually compare the performance of different heating-cooling combinations in detecting the smaller defects. Results demonstrate that the maximum D/t highly depends on the initial thermal gradient (ΔT). As the ΔT increases regardless of being tested in the morning or afternoon, the maximum D/t increases. The reason is that by having a high initial ΔT and depositing additional external heat on the surface, the final thermal gradient on the thickness is higher than when the initial ΔT is negative. This finding agrees with the previous studies performed on the small-scaled tank in Task 2. Therefore, as was determined from the previous results, the best time for doing IRT should be when there is a high ΔT which can be achieved sometime between 9:00 AM to 6:00 PM on a sunny day. The results indicate that the maximum

D/t for the east side for all heating times is equal to 0.73, but when the heating time was 20 seconds, it needed a higher ΔT to reach this D/t. Therefore, reaching to D/t of 0.73 when the heating time is 20 seconds is not guaranteed, and special weather conditions are needed. The recent statement discloses that 20 seconds of heating alone is not enough for deep heat penetration into the AST wall, while heating times greater than 30 seconds provide enough heat to penetrate deep enough for subsurface defect detection. By comparing the results of various heating durations on the east side of the AST, it is evident that for any heating intervals larger than 30 seconds, there is little improvement in the heat penetration depth in terms of values of D/t. Therefore, for the east side, where the wall's thickness was 0.5 in (12.7 mm), 30 seconds of heating should be sufficient to allow the heat to penetrate sufficiently deep into the AST wall. The smallest AR that could be detected for the east side when the heating time was 20 seconds was equal to 0.86, and when the heating time was set to 30 seconds and 40 seconds, the smallest detectable AR was equal to 0.8, and this value for 60 seconds heating was equal to 0.73. The minimum detectable AR mentioned is not guaranteed for each heating duration because there is an interaction between the ΔT, D/t, and AR. In addition, the smallest detectable AR is controlled by the cooling duration in each cycle. If the cooling duration is long for that specific heating time, after completing all heating-cooling cycles, not enough heat will be accumulated in the AST wall thickness to induce the required thermal gradient.

Further, if the cooling duration is too short, the edges of the defects become saturated and do not have time to lose the extra heat needed to create good contrast between the defect and the solid area. Moreover, other environmental parameters like RH and wind speed may impact the accuracy of the results. For instance, as experienced by the authors, on a windy day, the surface of the AST cools faster during the cooling phase due to heat loss from the surface exposed to the wind, which results in less heat penetration and less contrast between the defect and the solid area. Results shown in Figure 37 to Figure 40 indicate that the heating-cooling combination of 30-90,30-120, 40-40,40-80, and 40-120 (in seconds) by having enough small AR and the same D/t of other combinations can be the best choices when the thickness of the AST is 0.5 in (12.7 mm) but the combination of 30-90 shortens the AST evaluation time. The combination of 30-90 allows the inspector to perform IRT heating on a first spot, and while the first spot is in its 90-second cooling phase, the inspector can then deposit heat on two other spots marked for inspection.

For the west side, where the defects were created on the wall thickness of 0.75 in (19.1 mm), heating times of 40 seconds and 60 seconds resulted in comparable heat penetration into the wall thickness. For the west side, the minimum AR detected for the heating time of 20 seconds was equal to 0.79, while for other heating times, it was equal to 0.3. The heating duration of 40 seconds or 60 seconds resulted in detecting the smallest AR on the west side. Therefore, 40 seconds should be selected as the shortest heating time to get the highest possible D/t and detect the smallest AR. Therefore, for a wall thickness of 0.75 in (19.1 mm), 40 seconds of heating should be sufficient for conducting IRT. When comparing the findings from the evaluation performed in the morning and the afternoon, it was found that the afternoon evaluation may provide greater accuracy by detecting smaller AR for the west side while maintaining the same accuracy in detecting defects for the east side. Completing the evaluation in the afternoon will give a higher possibility of detecting smaller defects for both east and west

sides. In addition, the smallest detectable AR depends highly on the cooling duration between two heating cycles. When the heating duration is 40 seconds, and by following 40, 80, or 120 seconds of cooling time (cycles of 40-40, 40-80, 40-120), the same AR can be detected that could be done by 60 seconds heating. Therefore, a heating-cooling combination of 40-40 or 40-80 can be applied in the field for five cycles as the shortest and most effective combination. The recommended heating-cooling combinations of 40-40 and 40-80 allow the inspector to heat 1 or 2 more spots and then return to the first spot to start the next cycle, which helps speed up the evaluation process.

Looking at the ΔT values reported for the 40-second heating duration, the highest D/t and the smallest AR can be detected at 7.2ºF (4ºC) < ΔT. If 0ºF (0ºC) < ΔT < 7.2ºF (4ºC), then the authors recommend increasing the heating duration to 60 seconds and following one of the heating-cooling combinations (in seconds) of 60-10, 60-20, or 60-60. This allows for greater surface heat deposit and compensates for the lower ΔT. The combination of 60-60 allows the inspector to heat the next spot while conducting thermography on the first spot, which is in the cooling phase. This will speed up the evaluation process in the field. If ΔT < 0ºC (0ºF), the accuracy of defect detection drops dramatically; therefore, it is recommended not to evaluate if this is the current AST condition.

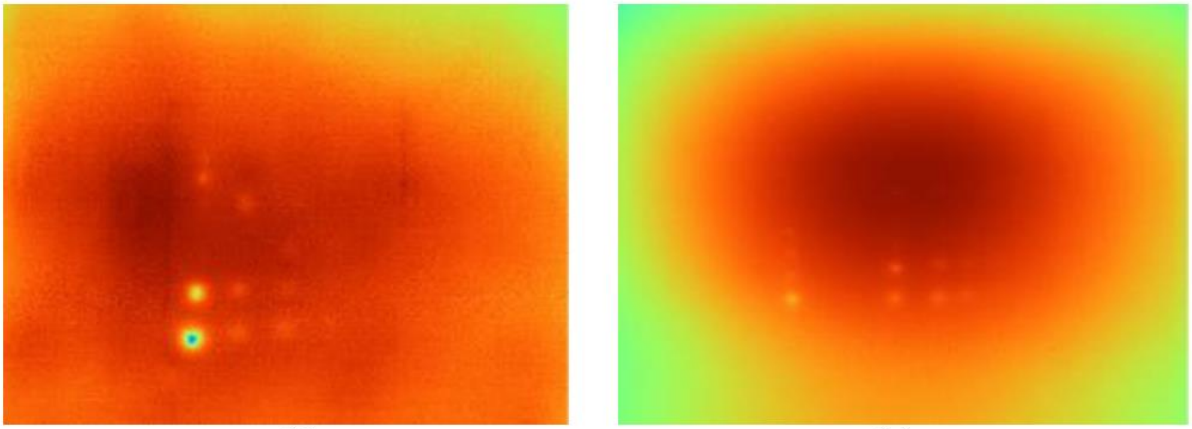

Figure 36. Two examples of the thermograms obtained from (a) cycle #6 of the heating-cooling combination of 40-80 performed on the east side and (b) cycle #6 of the heating-cooling combination of 60-60 performed on the west side

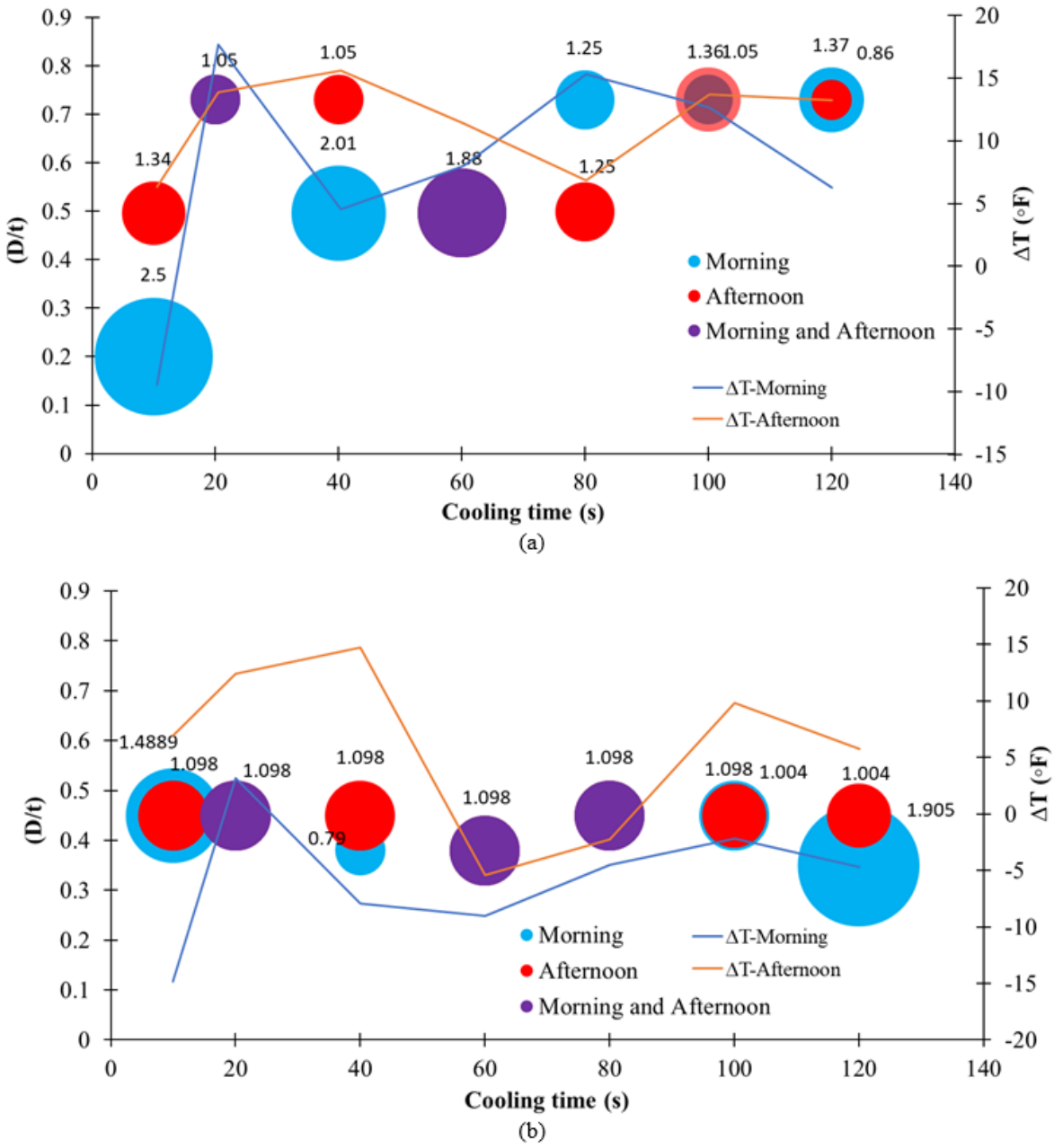

Figure 37. Characterization of the defects detected when the heating time was 20 seconds (a) east side and (b) west side (values next to each bubble represent the aspect ratio [AR]) (ideal case is when a smaller AR with a higher defect depth to wall thickness ratio [D/t] has been detected)

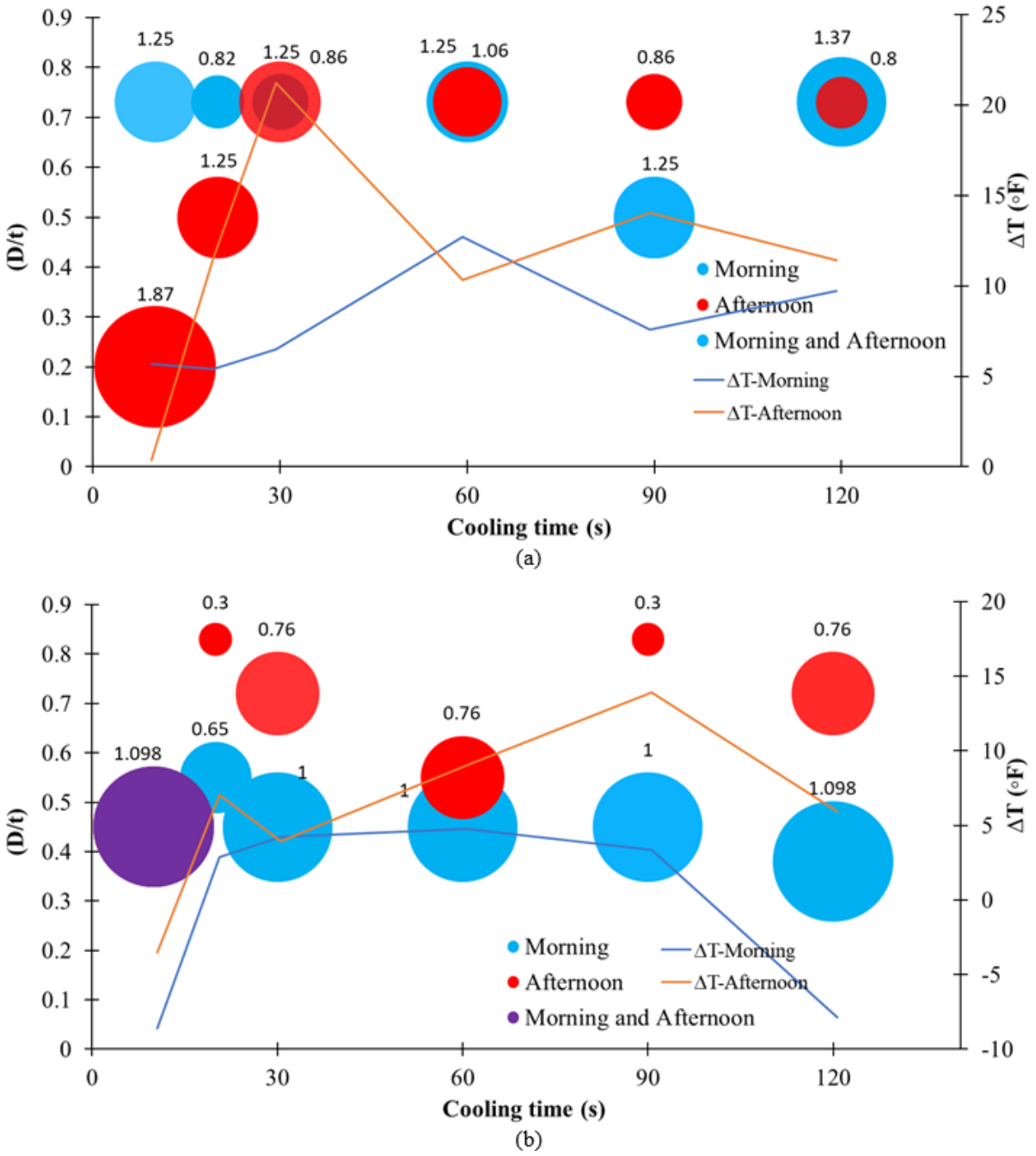

Figure 38. Characterization of the defects detected when the heating time was 30 seconds (a) east side and (b) west side (values next to each bubble represent the aspect ratio [AR]) (ideal case is when a smaller AR with a higher D/t has been detected)

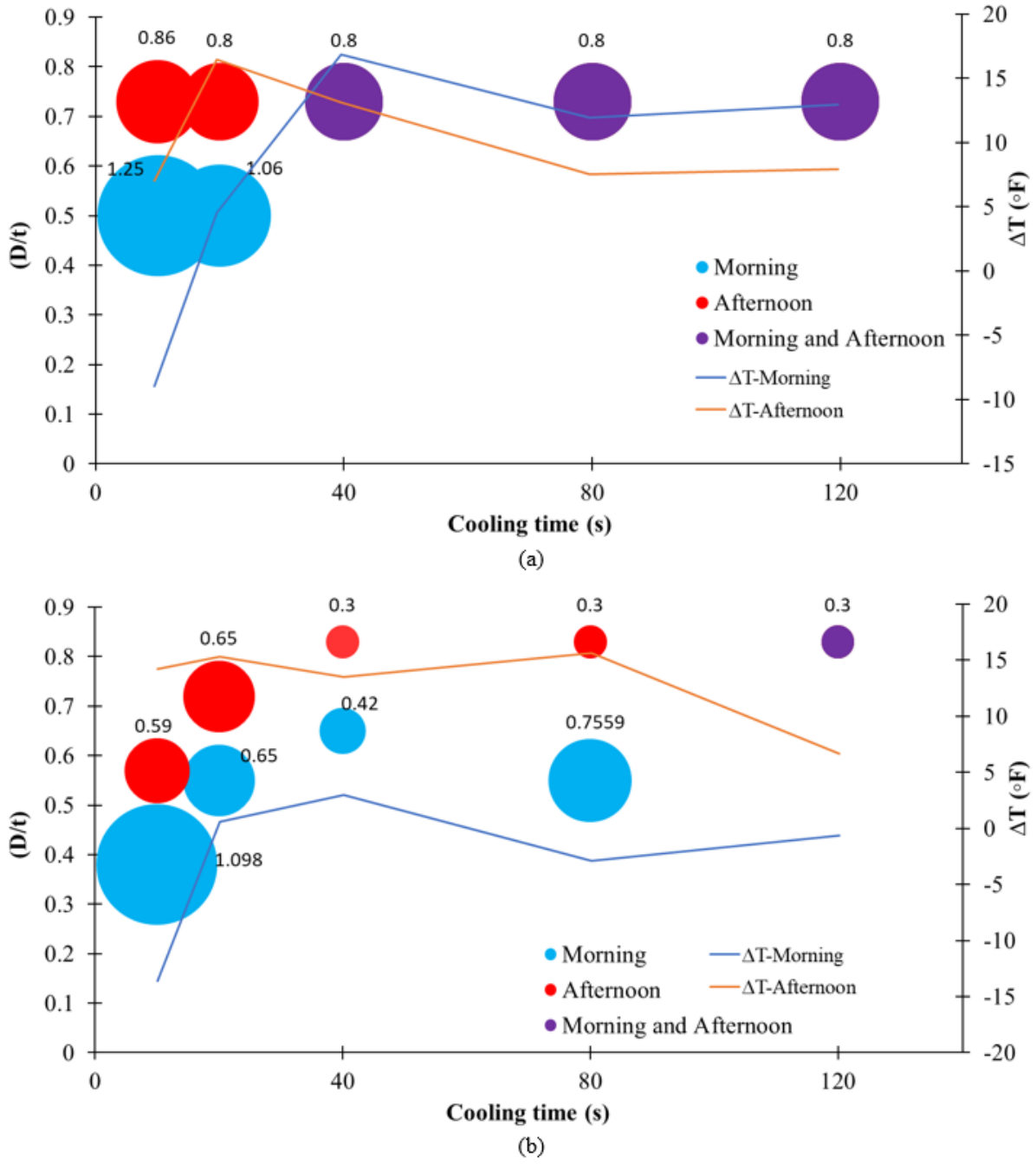

Figure 39. Characterization of the defects detected when the heating time was 40 seconds (a) east side and (b) west side (values next to each bubble represent the aspect ratio [AR]) (ideal case is when a smaller AR with a higher D/t has been detected).

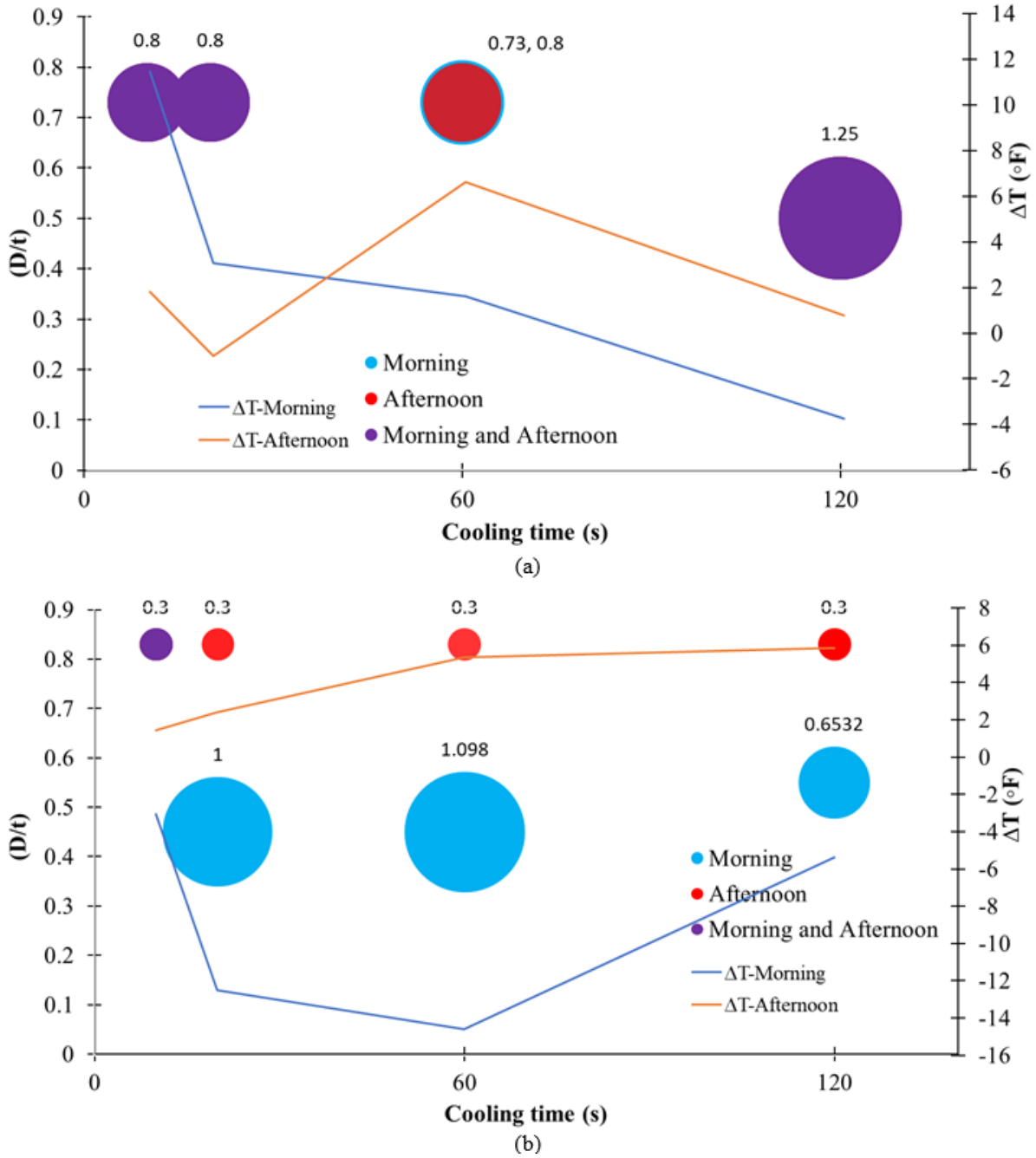

Figure 40. Characterization of the defects detected when the heating time was 60 seconds (a) east side and (b) west side (values next to each bubble represent the aspect ratio [AR]) (ideal case is when a smaller AR with a higher D/t has been detected)

Impact of Camera Distance on the Defect Detection

A concern about conducting the IRT in the field is the IR camera distance to the AST and its impact on the resolution and detection accuracy. In the field, there is no guarantee of enough space for evaluating the AST from the same distance chosen for this study. Completing the IRT in shorter distances is necessary when the ASTs are close to each other or the AST is located

next to a barrier. For this reason, a short study was performed on the impact of the thermography distance on the defect detection limits. Figure 41 shows the thermograms captured from different distances at cycle #6 of the heating-cooling combination of 30-30 performed on the east side. Quantitative results have been summarized in Table 9. The results imply that the thermography results conducted at a distance of 2.5 ft (0.75 m) to 4.3 ft (1.3 m) give similar accuracy. Previous studies performed in Task 2 showed that the accuracy of IRT remains constant at a distance of 1.6 ft (0.5 m) to 4.9 ft (1.5 m), which is in good agreement with the field results. At a distance of 1.6 ft (0.5 m) to 4.9 ft (1.5 m), the area under evaluation changes between 0.73 ft^2 (0.068 m^2) and 6.1 ft^2 (0.57 m^2), respectively. When the distance of the IR camera increases from 3.3 ft (1.0 m) to 6.6 ft (2.0 m), the smallest detectable AR and the maximum D/t drop by roughly 35%, but the area under study becomes 3.8 times larger. When the distance of the IR camera increases from 3.3 ft (1.0 m) to 9.8 ft (3.0 m), the accuracy of the smallest detectable AR drops by around 60%, and the area under the study increases by 8.6 times. Therefore, the authors recommend using the IR camera at the distance of 2.5 ft (0.75 m) to 4.9 ft (1.5 m), which the accuracy does not change. By setting the IR camera at the distance of close to 4.9 ft (1.5 m), a larger area can be evaluated while keeping the best possible accuracy, which speeds up the evaluation process.

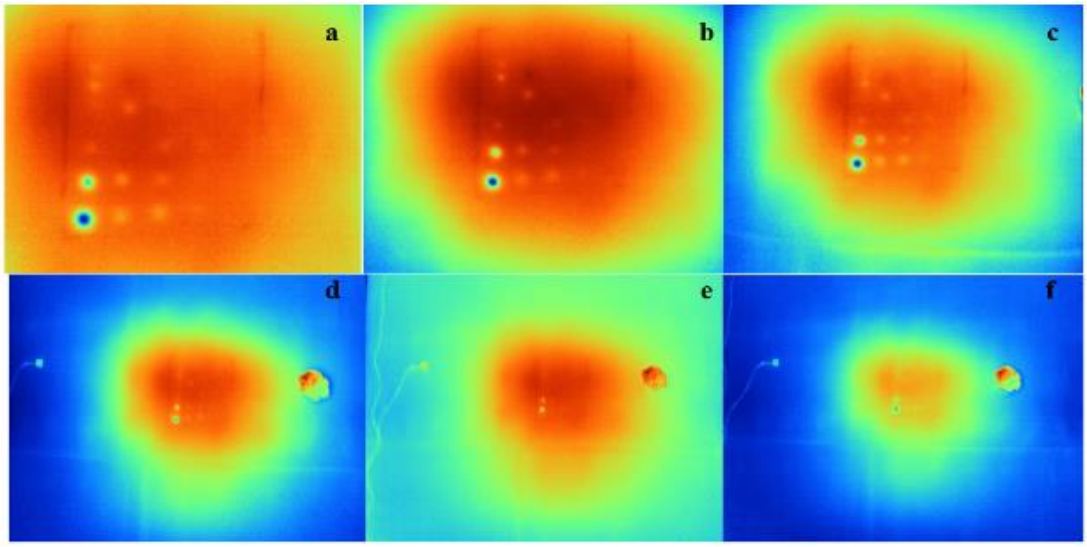

Figure 41. Thermograms captured at a single cycle but at different distances: (a) 2.5 ft (0.75 m), (b) 3.3 ft (1.0 m), (c) 4.3 ft (1.3 m), (d) 6.6 ft (2.0 m), (e) 7.5 ft (2.3 m), and (f) 9.8 ft (3.0 m)

Table 9. Accuracy of defect detection at different distances

Distance (ft (m))	Maximum D/t	Minimum AR	Area under evaluation (ft^2 (m^2)
2.5 (0.75)	0.73	0.80	1.58 (0.147)
3.3 (1.0)	0.73	0.80	2.78 (0.258)
4.3 (1.3)	0.73	0.80	4.74 (0.44)
6.6 (2.0)	0.50	1.25	10.5 (0.98)
7.5 (2.3)	0.50	1.25	17.9 (1.66)
9.8 (3.0)	0.50	2.01	23.9 (2.22)

Impact of Angle of View on Defect Detection

The other factor that may impact the accuracy of defect detection in IRT is the direction the IR camera is looking at the AST (angle of view). For this reason, a short study was performed on the impact of the view angle on defect detection accuracy. The results of these tests are shown in Figure 42. The direction perpendicular to the AST wall was considered the zero angle (0°), and other angles were measured compared to this direction. As it is clear from the thermograms shown in Figure 42, the defects detected in the directions 0˚ to 30˚ resemble, while in the greater angles, the accuracy decreased. Therefore, the authors recommend performing the IRT evaluation of the angles between 0˚ to 30˚.

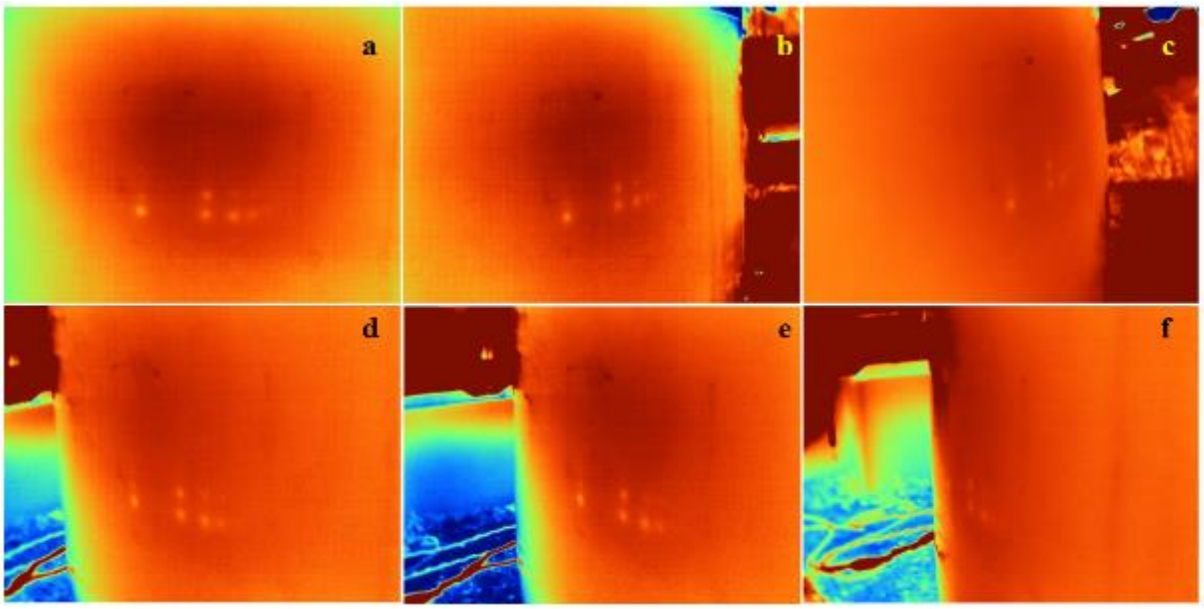

Figure 42. Thermograms captured from different angles: (a) 0˚, (b) 30˚, (c) 60˚, (d) 30˚, (e) 60˚, and (f) 75˚ relative to surface normal

Impact of Heating Source Distance to the AST on the Defect Detection

Similar to how the IR camera distance impacts the accuracy of defect detection, there is a concern about the distance of the external heating source to the AST wall. As shown in Figure 43, a close-distance heating causes a localized heating area, which saturates the heating in that area and reduces the deposited heat in the vicinity areas. Therefore, the induced thermal gradient in the area under study is not uniform, which interferes with defect detection. In the area heated up directly by close heating, the defects become saturated, reducing the contrast between the defect and the solid area. In areas away from direct heating, not enough heat is deposited on the surface, and therefore, a small thermal gradient will be induced due to heat transfer from the hot areas to the cold areas. Thus, the authors recommend stacking as many external heat sources to cover the entire area under the evaluation, which is correlated to the distance of the IR camera to the AST wall. Uniform heating helps to prevent heat diffusion on the surface and results in better heat penetration into the AST wall in the area under evaluation, which consequently results in better defect detection.

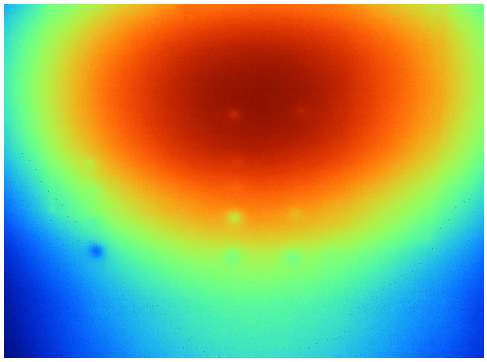

Figure 43. Impact of close heating on the defect detection

Ultrasonic Testing

Comparing the full-scale AST results with the laboratory-scale AST in Task 2, it is evident that the full-scale AST exhibits greater background noise during UT experiments, which is attributable to the waviness of the AST interior (Figure 44) and the liquid inside the AST. It was found that, generally, shallower defects (i.e., closer to the surface) were more easily detected by UT methods.

Using PAUT on the west side of the AST, all but one defect was detectable, and the depth of those defects could be successfully measured. The only defect that could not be measured was R1C6, which has a small depth that could not be measured with traditional tools. The defects surrounding R1C6, which are R1C5, R2C5, and R2C6, could all be identified using PAUT. As these three defects are the smallest in the set, the authors conclude that all other defects can also be measured using PAUT. Therefore, the smallest AR and the maximum D/t that PAUT could detect are equal to 0.24 and 0.95, respectively.

There were three types of results when using PAUT to find defects over locations where defects were known to exist. The first was a confident result, where the returned signal strength was strong enough to be easily distinguished from background noise. The second was a less confident result that returned weaker signal strength but still was distinguishable from background noise. The third and final possible test result was a returned signal strength indistinguishable from background noise. A skilled, trained operator can still distinguish a return signal from a defect in the third result type. When the phased array probe is moved back and forth over the location of a small defect, the return signal behaves differently from background noise, which is how it can be distinguished. Examples of confident and less confident results are shown in Figure 45 and Figure 46, respectively. An example of a signal indistinguishable from the background is shown in Figure 47.

Figure 44. The wavy wall inside a High-Density Polyethylene Above-Ground Storage Tank

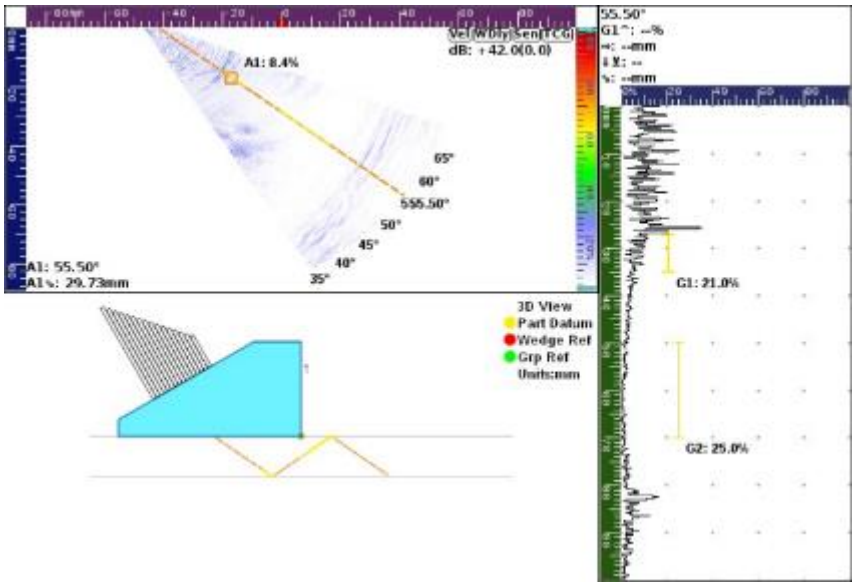

Figure 45. An example of a confident signal return (note: 1 mm = 0.039 in)

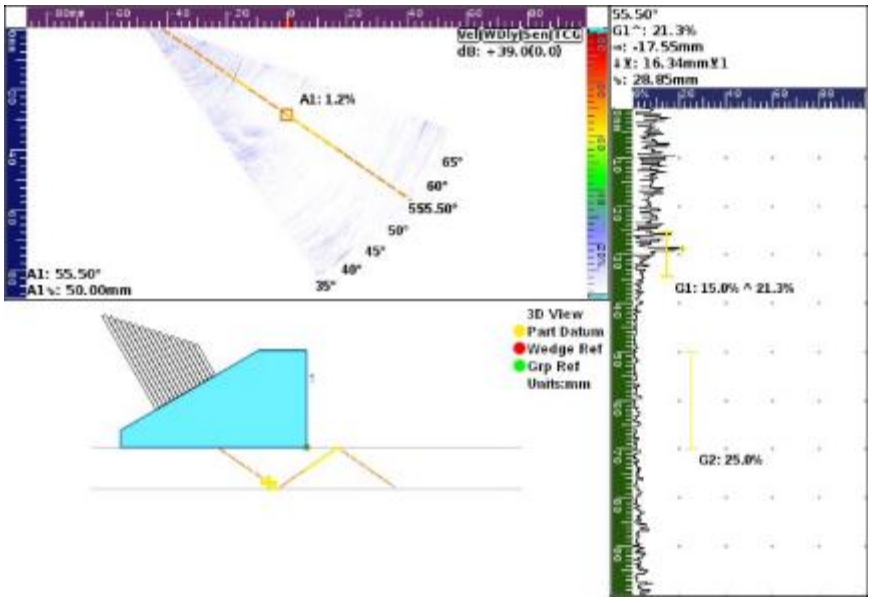

Figure 46. An example of less confident signal return (note: 1 mm = 0.039 in)

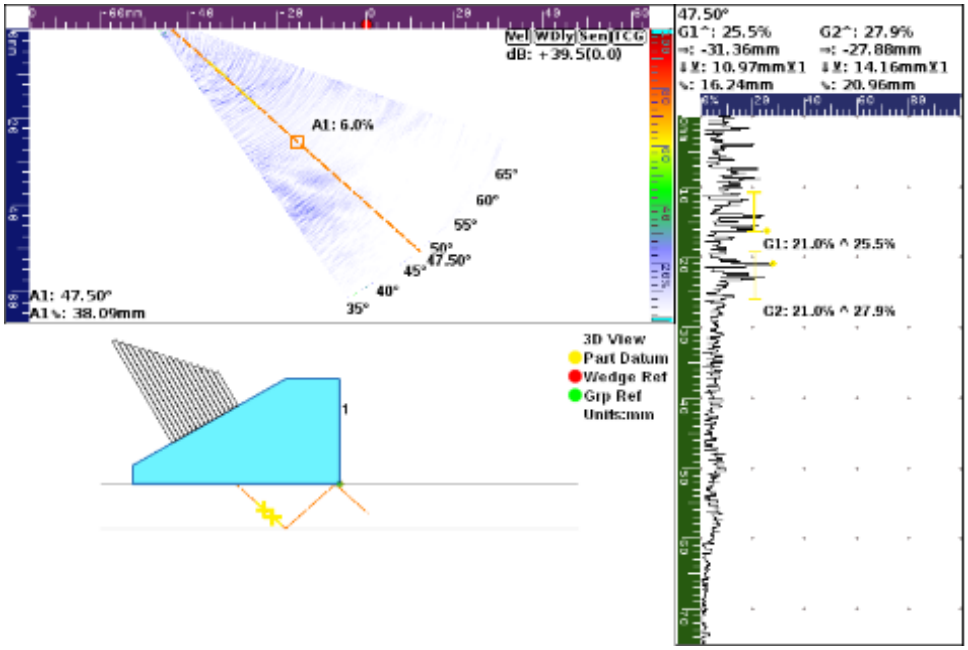

Figure 47. Return signal indistinguishable from background noise (note: 1 mm = 0.039 in)

Field Experiments

The goal of the field investigation was first to estimate the time needed to complete the evaluation of a single AST and, secondly, to identify the field testing challenges. The information on each AST is previously shown in Table 8. The wall thickness of the ASTs were measured using PEUT. It took around 2.5 minutes to measure the thickness. The first AST was empty, while the second one was full. Both ASTs were visibly in good condition and were in service. Since the first AST was empty, the ΔT was assumed to be $\Delta T = 0°C = 0°F$, and therefore, the heating-cooling cycle of 60-60 was chosen for this AST. For the second AST, the external wall

temperature was 86°F (30˚C), and the brine inside the AST had a temperature of 79.0°F (26.11˚C); therefore, the ΔT > 7.2°F (4˚C) and the heating-cooling cycle of 40-120 was chosen to do IRT. For both ASTs, the bottom 4.27 ft (1.3 m) all around the ASTs were examined. The battery life was about 100 minutes, so the investigation was performed for over 200 minutes by having two batteries. Due to the hoses connected to the fittings and outlets, it was impossible to heat up the fittings and evaluate them in one step. Therefore, fittings were heated up twice: once from the left side and once from the right side. In total, the circumference of the AST was divided into nine segments, as shown in Figure 48, with each segment consisting of four spots. While the first spot was in cooling, the second spot was heated for 60 seconds on the first AST to complete 60-60 cycles. On the second AST, when the first spot was cooling, the second, third, and fourth spots were heated for 40 seconds each to complete 40-120. Each segment had an average size of 13.5 ft^2 ± 2.4 ft^2 (1.25 m^2 ± 0.22 m^2).

Figure 48. The configuration of one segment consisted of four heated spots

For the first AST, each segment took 20 minutes to finish. Therefore, theoretically, 180 minutes were needed to investigate the first AST but in practice took 375 minutes. The reason for the longer time required in the field to evaluate the AST raised from the time needed to move the heating source, move the extension cables, switch the laborers and inspectors, and replace the battery. The longer time of evaluation in the field necessitates more batteries to evaluate only one AST, which can be one disadvantage of using IRT in the field.

For the second AST, each segment took around 13.3 minutes to finish. Therefore, theoretically, 120 minutes is needed to investigate the second AST, but in practice, it took 285 minutes. Comparing the time recorded for both ASTs shows that completing the IRT on a full AST reduces the time needed for evaluation by 24%. The long practical time required to finish

IRT on a single AST shows that it is better to start the evaluation from the east side in the morning and finish it on the west side in the afternoon.

Future Research Needs

According to the findings discussed above, the authors identified future research needs that would further improve the inspection procedure for ASTs. These research needs are listed below:

1. A follow-up implementation study geared toward improving both the methods and guidance documents associated with these inspection procedures based on user feedback. A select set of AST inspectors should be trained on the methods developed in this study and then allowed to put them into practice for at least one inspection cycle. Following the end of this cycle, feedback from these inspectors will be collected.
2. While it is believed that the inspection schedule for ASTs should be updated, additional data is needed to determine 1) if IRT and UT need to be performed on every tank yearly or biyearly; 2) if there is a tank age threshold for IRT and UT inspection (e.g., do new ASTs require yearly inspections); and 3) if ASTs always need to be inspected after an incident (e.g., impact from debris, minor abrasion from a vehicle, etc.)
3. To account for variability between the resolution of IR camera models/manufacturers and heating sources, an implementation study using the specific heating source and IR camera likely to be widely used by VDOT is needed. This would allow for fine-tuning aspects of the inspection procedure, like durations of heating-cooling cycles.
4. Currently, the only data collected regarding the service life of HDPE ASTs is the installation date of the tank. While this is important information, it is not sufficient to develop a threshold value for when a given tank should be decommissioned. To achieve this, further research and data collection is needed relating to the weather conditions, maintenance procedures experienced by these tanks, and better records of the number of filling-emptying cycles, etc.
5. While the primary focus of this research effort was on the inspection of single-walled ASTs, it is understood that these tanks are being phased out and replaced with double-walled tanks. Because of this, additional research is needed to determine how or if the methods developed during this study can be adapted for application on these tanks. For example, it is believed that the void space between the inner and out tanks could be filled with water to allow for passive IRT inspection. However, this theory has yet to be tested.

Guidelines for Field Implementation

Practical Guidelines for HDPE AST Integrity Evaluation

The performance of the HDPE AST depends on many parameters, such as the location and environment (e.g., weather conditions, the number of freezing cycles experienced during winters), the brine (e.g., solution concentration, salt type), the frequency of the filling-emptying cycles, maintenance program, etc. Therefore, the frequency and interval between inspections of an HDPE AST should be determined by its service history unless unique circumstances call for an earlier inspection. The service history of one tank can be estimated by reviewing the performance of a similar tank. Ideally, the tanks would store the same material at the same location, be made of the same material, and have the same capacity. The AST owner should develop detailed checklists that identify, record, and document all aspects of each inspection. To evaluate an HDPE AST, the authors recommend the following inspection procedures:

1. Review prior formal and periodic inspections, and identify the locations that need closer examination.
2. Visually inspect the AST and look for any abnormality or unusual signs, such as cracking, crazing, brittle appearance, holes, dents, and abrasions.
3. Visually check around the fittings, mainly focusing on the areas around the steel bolts. Check fittings, hoses, gaskets, and all connections for any signs of general corrosion (in steel bolts and gaskets), deterioration, or leaks. Note changes from the original design and installation information, if available.
4. Walk around the AST and look for any deformation, buckling, or distortion. Pay attention to where the upper section of the wall meets the lower section, which is usually waist height. This connection separates the thicker wall in the lower section from the thinner wall in the upper section. Compare changes from the current inspection with the last inspection report.
5. Look closely for signs of brittleness in the tank's dome. Chemicals that produce fumes can cause the dome to oxidize and embrittle without being in direct contact with the brine solution. To avoid walking or standing on the dome surface, the evaluation of the dome should be completed by safety-certified personnel using lift equipment.
6. Investigate the AST's base to ensure it rests on a firm and even base. Animals can burrow underneath the AST, causing the base to settle unevenly. Note changes from the original design and installation information if available.
7. Use the IR camera without the external heat source and walk around the AST to check for any anomalies that may interfere with the defect detection. If something is on the external wall, wipe off the AST wall to remove any moisture. Wait for at least 10 minutes until a uniform temperature forms in that area before starting the evaluation. In addition, pay attention to see if there is any leakage from the AST, especially close to fittings.
8. Power on the external heat source and allow it to reach maximum power. Record the ambient temperature, relative humidity, and wind speed. Measure the temperature of the liquid inside the AST, and measure the AST wall temperature at different spots to calculate a representative ΔT ($\Delta T = T_{wall\_surface} - T_{liquid}$).

a. If $\Delta T > 0$, then IRT can be conducted. If the AST is located outdoors, the best time frame for conducting the IRT evaluation is between 9:00 AM and 6:00 PM, preferably between 2:00 PM and 6:00 PM. ASTs located indoors can be inspected using IRT at any time of day.
b. If $\Delta T < 0$, then do not proceed with IRT investigations.

9. Start the IRT experiment by selecting the heating-cooling combination according to the recommendations provided in Table 10.
10. Heat the first area, and move to heat the next area. Heating successive areas limit downtime. While one area is in the cooling phase, perform IRT. When the cooling cycle is complete for the first area, return to it and begin heating it again. Repeat this procedure for five cycles in each area, and perform an IRT observation during each cooling phase. Mark areas that have potential subsurface defects based on the IRT inspection.
11. Use ultrasonic instrumentation over the marked areas for a more detailed investigation. Move the PAUT probe vertically and diagonally at 15º angles left and right along the surface of the AST to detect subsurface defects. Measure the defect size and depth from the external surface.
12. Based on the data collected on any present defects, develop an inspection report and schedule to re-inspect the tank and monitor the potential for degradation or failure.

Table 10. Guideline for selecting the heating-cooling durations

Wall thickness (in. (mm))	ΔT (˚F (˚C))	Heating-cooling durations (s)
0.5 (12.7)	$\Delta T > 10.8$ (6)	30-90
0.5 (12.7)	10.8 (6) $> \Delta T > 0$ (0)	60-20 or 60-60
0.5 (12.7)	$\Delta T < 0$ (0)	Do not do the evaluation
0.75 (19.1)	$\Delta T > 7.2$ (4)	40-40 or 40-80 or 40-120
0.75 (19.1)	7.2 (4) $> \Delta T > 0$ (0)	60-20 or 60-60
0.75 (19.1)	$\Delta T < 0$ (0)	Do not do the evaluation

IRT Challenges for the Field Evaluation of HDPE ASTs

Although IRT is an excellent technique for defect detection in many industries, it has some challenges, specifically regarding the inspection of HDPE ASTs. Some of the challenges found during this study are listed below:

- IRT can be used only as an indicator of the defect's existence and does not provide information about the location and depth of the defects. Supplementary evaluation with UT can further assess the location and depth of defects.
- Defect detection accuracy highly depends on the weather conditions.
- IRT cannot detect small defects ($AR < 0.3$) or very deep defects ($D/t > 0.83$).
- IRT cannot detect non-leaking cracks propagated from the internal side of the AST toward the surface.
- IRT is labor-intensive and requires personnel to heat areas in different cycles.
- IRT is time-consuming for HDPE ASTs due to the material's low thermal conductivity. The operator should be prepared with multiple charged batteries for the equipment.

- Using various IR cameras from various manufacturers or models produced by the same manufacturer could affect defect detection accuracy.
- Water droplets due to rain, fog, or other activities close to the AST can interfere with defect detection.
- Because many sites will contain several ASTs that need to be inspected, this task can become tedious. Therefore, to expedite the evaluation process, the inspection can be limited to the lower sections of the AST (i.e., waist-high and below), where failures are most frequently reported.
- IRT can be completed on the AST's lower (i.e., waist-high and below) sections without needing additional equipment. If there is an accident or a concern close to the top of the AST, the evaluation process may be challenging without hydraulic lifters or cranes.
- The IRT equipment needs to have access to electrical power. A portable generator is helpful in the field.
- Appropriate electrical access for IRT is challenging to obtain. The heaters recommended for IRT have a large current draw and will trip most conventional circuits. It is recommended to either use two separate electrical sources or to use a sufficiently capable portable generator.
- The heaters used for IRT can reach extremely high temperatures. Careful consideration must be taken to ensure that the operator is adequately insulated from the heat generated by the infrared heaters.
- To prevent fire or electrical hazards, it is recommended to turn off the heaters for 10 minutes every 20 minutes or for 15 minutes every 30 minutes. Aside from proper insulation, this is the best way to keep the heaters within a comfortable heat range for the operators. The authors recommend using stacked infrared heaters, like those used for paint curing, to reduce these hazards, keep the operator safe, and deposit a more uniform temperature on the area under study.
- Heating around the fittings is challenging and causes non-uniform heat deposits. Hoses connected to the outlets prevent heat application on the surface behind them. Moreover, heating these hoses may inadvertently cause damage to the hoses and gaskets.
- Since an operator is moving the heater, it is not guaranteed that the same area heated during one cycle will be heated in the next. Therefore, there is likely to be a gap between the heated spots, as shown in Figure 48. Therefore, some sections of the tank may be missed during inspection.
- Discolorations, stains, superficial scratches, and information tags interfere with defect detection, which may reduce the speed of evaluation by numerous false detection.

UT Challenges for the Field Evaluation of HDPE ASTs

While UT techniques are beneficial for steel infrastructure inspection, using PAUT in the field for evaluating HDPE ASTs has some challenges, as listed below:

- Due to the AST wall curvature, all sides of the probe cannot be in contact with the AST wall, and therefore, the water leaks from the water wedge probe. This can be solved by using a

more powerful water pump. Note that the pump used in this study had an uninhibited flow rate of 6 gallons per minute (gpm); however, when tubing was used to attach the pump to the water wedge probe, the flow rate fell to 0.25 gpm. To overcome this issue, a pump with a minimum uninhibited flow rate of 10 gpm is recommended to fill the water probe reservoir faster than the leakage discharge.

- Completing the PAUT on the upper section of the AST is difficult and requires a more powerful water pump to pump up the water to that elevation.
- The water pump requires electricity so that a portable generator may be required in the field.
- The water pump requires a consistent source of water, which can be accomplished by using a 5-gallon bucket, although larger volumes of water may be needed for longer inspections.
- Measure by moving the probe up and down or at an angle of 15º compared to the vertical line. This reduces the water leaks from the water probe and helps obtain better results. Moving the probe at angles greater than 15º from the vertical line will result in more leakage due to the AST wall curvature.
- Completing PAUT on the cone-shaped outlets is impossible. In such cases, using traditional pulse-echo ultrasonic testing (PEUT) is recommended.
- While manufacturing some HDPE ASTs, the interior of the AST can have a wavy texture, as shown in Figure 44. This texture will increase the background noise and can interfere with the results. High amounts of waviness inside the AST may reduce the effectiveness of UT techniques since the wavy texture will scatter the ultrasonic waves. If the investigator does not have enough experience evaluating the HDPE ASTs, the waviness could mistakenly be reported as a defect. In such cases, the UT is still beneficial since it can detect areas where the wall thickness is less than the thickness mentioned in the AST specifications.
- UT methods, PEUT and PAUT, depend on the temperature of the inspected element. If UT is performed after IRT, the UT equipment must be recalibrated to the new material temperature to generate accurate results. If it is desired to avoid recalibration, then UT can be performed either before IRT or after sufficient time has elapsed to allow the material to return to ambient temperature. Likewise, UT could be performed on a different day than IRT.
- The liquid inside the AST causes background noise in the returned signals, which may block some defect signal peaks. However, a skilled UT operator can read through the background noise to detect defects as small as 0.17 in (4.4 mm).

CONCLUSIONS

- *In general, it is concluded that IRT and UT methods can be employed for the NDE of HDPE ASTs. However, the inspector must understand the limitations of these techniques and how to perform the inspection to optimize data collection.*

- *The interaction of sample geometry, initial thermal gradient, defect location, and defect aspect ratio all impact the accuracy of IRT in detecting subsurface defects. The results*

showed that specimen size, the distance of the camera to the object, the angle of view, heating source power, and the distance of heating power to the object also impact the accuracy of IRT measurements.

- *The best time for conducting IRT inspections is on sunny days between 9:00 AM and 6:00 PM. Since the AST evaluation is time-consuming, it can be started on the east side of the AST in the morning and finished on the west side of the AST in the afternoon.*

- *If the temperature difference (ΔT) between the exterior surface of the tank and the liquid inside the tank is < 0ºF (0ºC), the accuracy of the defect detection provided by IRT decreases dramatically. Therefore, if this condition exists, it is not recommended to perform the evaluation.*

- *When the thickness of the AST is 0.5 in (12.7 mm) and $\Delta T > 10.8$ºF (6ºC), 30 seconds of heating for five consequential intervals should be sufficient to allow the applied heat to penetrate deep into the AST wall. Therefore, the combination of 30-90 (30 seconds heating, 90 seconds cooling) was the best choice when the thickness of the AST is 0.5 in (12.7 mm).*

- *When the thickness of the AST is 0.75 in (19.1 mm) and $\Delta T > 7.2$ºF (4ºC), a heating-cooling combination of 40-40, 40-80, or 40-120 was optimal.*

- *A distance between 1.6 ft (0.5 m) to 4.9 ft (1.5 m) and a viewing angle between 0˚ and 30˚ perpendicular to the AST wall were optimal for IRT analysis of HDPE ASTs.*

- *In addition to IRT, UT can be utilized to examine HDPE ASTs in greater detail. UT is accurate at locating flaws and estimating their size and shape. However, UT's detection limits depend on the condition of the tank under study and the experience of the UT operator. Using a Proceq Flaw Detector 100, the experienced users in this study were able to detect defects as small as 0.17 in (4.4 mm), but a less experienced user was only able to detect defects as small as 0.25 in (6.4 mm). The difference in performance between skilled UT operators and less-skilled UT operators is being able to read defects through background noise. To read defects through background noise, present in most field conditions, the UT probe cannot be static and must be carefully moved over the right spot to identify the peak corresponding to the defect.*

- *Both the liquid stored inside the AST and the waviness of the interior surface of the AST can increase the background noise, which may make UT interpretation difficult.*

- *The methods developed during this research, while applicable to single-walled tanks, cannot be directly applied to double-walled tanks.*

RECOMMENDATIONS

1. *VDOT's Environmental Division and Maintenance Division (in collaboration with VTRC scientists) should initiate an implementation study to identify and contract with a private sector tank inspection company to conduct inspections of HDPE AST in VDOT's inventory using the guidelines presented in the section of this report titled "Practical Guidelines for HDPE AST Integrity Evaluation."* The focus of these inspections should be to refine these guidelines further and to collect the information needed to develop threshold criteria that will inform when and what actions should be taken based on the number, size, and location of defects identified on a given HDPE AST when using these inspection procedures.

2. *VDOT's Environmental Division and Maintenance Division, in collaboration with VTRC scientists, should share the refined inspection methods referred to in Recommendation 1 with relevant technical standards organizations, such as ASTM International, and request their feedback.* Specifically, feedback should be requested regarding the identification of relevant technical committees within the organization and how these methods could be modified to ensure their applicability to a broader range of stakeholders.

IMPLEMENTATION AND BENEFITS

Researchers and the technical review panel (listed in the Acknowledgments) for the project work together to craft a plan to implement the study recommendations and to determine the benefits of doing so. This ensures that the implementation plan is developed and approved with the participation and support of those involved with VDOT operations. The implementation plan and the accompanying benefits are provided here.

Implementation

For Recommendation 1, contract language, including required equipment, inspection procedure, and number and location of inspections, will be advertised by VDOT's Environmental Division by June 30, 2024. Final contractor selection by the Environmental Division will be based on the company's familiarity with the basic concepts of IRT and UT testing, their application in other types of non-destructive testing scenarios (i.e., fiberglass and steel tanks), their familiarity with VDOT operations as they pertain to facilities inspections, and their access to or ability to procure the necessary equipment to conduct these inspections. Once selected, Environmental and/or Maintenance Division staff and VTRC scientists will coordinate with the contracted company to conduct these inspections.

The number and location of these inspections will be determined through a collaborative effort between VTRC and VVDOT Environmental Division and Maintenance Division staff based on the information available. This information includes age, geographic location, previous

inspection data (including incidences of accidental impact), degree of sun exposure, and the number of tanks at a given location. Particular attention will be placed on selecting tanks with a distribution of these characteristics so that correlations can be made between them and the defects identified using the IRT and UT methods developed during this study. These correlations would allow for the development of the aforementioned threshold values. Because these methods are currently limited to application on single-walled tanks, double-walled tanks will not be included in this effort. Assuming a sufficient number of tanks with a representative distribution of the selected characteristics are available, it is envisioned that these correlations can be made with one round of inspections. However, if not, follow-up inspections will be conducted annually until sufficient data is collected. Funding and documentation for this effort, including site identification, contractor costs, and development of updated methods and threshold values, will be allocated through the initiation of a VTRC implementation project. Staffing for this implementation project will consist of two scientists from VTRC from the Environmental, Planning, and Economics team and the Structures team.

For Recommendation 2, engagement with technical standards organizations will be initiated by VTRC scientists within six months of the completion of the implementation project noted in Recommendation 1. For instance, using ASTM International's guidance as an example, the Staff Manager of the most relevant ASTM Technical Committee will be contacted with the expressed interest of collecting feedback from the members of that committee and requesting aid in identifying other relevant stakeholders. These other stakeholders will then be contacted to request feedback regarding the need for this method and what modifications should be made.

If the responses from the given technical standards organizations and the other stakeholders indicate interest in these methods, then a formal request to consider the formation of a new task group or subcommittee will be made to the organization.

Benefits

Qualitative Benefits

Implementation of Recommendation 1 will allow these methods to be further refined to increase their accuracy and ease of use. Additionally, the development of threshold values will enable inspectors to make recommendations to VDOT on when a given tank should be taken out of service or is nearing that point based on the testing results. Not only will this allow better planning and budgeting decisions at the area headquarters level, but it will also reduce the chances of sudden tank failures and the associated risk to human life and adverse impacts on the environment.

Implementation of Recommendation 2 will benefit VDOT and the larger community of HDPE AST users by providing them with a standardized and fully vetted inspection method. While several other inspection methods were identified throughout this research, many of them either lacked the necessary level of detail, did not apply to this use case, or required the use of chemical dyes that, on their own, would require additional containment and cleanup. Using ASTM International's existing framework would not only allow the standardization of these

methods, but it would also function as the vehicle for distributing this knowledge to these other stakeholders.

Quantitative Benefits

Recommendations 1 and 2 are incremental steps that can lead to a nondestructive inspection program. To monetize the potential benefits of a non-destructive inspection program, there are two types of costs that such a program could potentially eliminate: cleanup costs (assuming no environmental damage) and tank replacement costs. Both costs are highly variable as they depend on site specific conditions and thus the costs presented here should only be viewed as an order of magnitude estimate.

Cleanup Costs (Assuming no Environmental Damage)

To estimate the costs of the cleanup, VTRC staff contacted by phone the Virginia Department of Environmental Quality, where a representative noted DEQ did not have costs available for cleanup but suggested that staff contact two firms that might provide this service. The representative at one firm noted that it did not perform brine cleanups. The representative at the other firm was able to provide a rough cost, explaining that costs depend on a variety of site-specific factors, such as the presence of groundwater or utilities, whether permitting is required, and whether sampling or testing is needed. Under a somewhat benign scenario (e.g., no groundwater is encountered, no permitting is required, no utilities are present, and no testing is needed), a rough cost for a 6,000-gallon tank spill might be, based on three hours for a project manager, 4 technicians present for an eight hour day, two drivers present for an eight hour day, and other costs such as trucks and equipment, around $8,000 for a single failure assuming no substantial environmental damage.

The above figure does not indicate the frequency of failures. One state DOT survey respondent, when later asked for additional information, noted that over the past two years their state DOT had had four fitting failures and three tank failures (two of those three failures were structural and one failure was due to an accident where the tank was hit by a piece of equipment). The total cost, not including the cost of replacing the tank nor the cost of disposal, was around $90,000. Treating these seven events as being equal in terms of cost, the mean failure cost is around $13,000 per tank event (and these are 10,000-gallon tanks rather than 6,000-gallon tanks used in the above paragraph). This figure includes the cost of product replacement.

Thus one way to estimate the benefits of a non-destructive inspection program is, in terms of elimination of cleanup costs, around $8,000 - $13,000 per tank failure avoided. This benefit does not include the cost of the tank replacement and it presumes no substantial environmental damage. If like the respondent, Virginia had two structural tank failures in two years, this would suggest a benefit of $8,000 - $13,000 per year in terms of cleanup costs, assuming the failures did not have environmental damage. One might select $10,000 per year as a middle figure.

(If environmental damage were sustained, then the cleanup costs would be higher than those shown above, however, staff do not have a good way of estimating those cleanup costs and thus they are not included here.)

Tank Replacement Costs

The aforementioned respondent noted that the cost of a 10,000-gallon tank is around $14,000. If the nondestructive inspection program did not yield any changes in the tank's service life beyond the use of age, then the monetized benefit based on tank replacement would be $0. Suppose, however, a nondestructive inspection program was able to extend the life of each tank by one year. With a 14-year service life, then the value of this benefit is very roughly $1,000. With about 400 above-ground storage tanks, an extra year of life for each tank is 400×$1,000 = $400,000.

Total Potential Benefits

A successful nondestructive inspection program thus could have the potential to yield an annual benefit in excess of $400,000. Implementation of Recommendations 1 and 2 does not necessarily mean this benefit will be realized, however. Instead, the implementation of Recommendations 1 and 2 would give VDOT sufficient information to determine the value of a non-destructive inspection program. If, for example, Recommendation 1 is successful, then VDOT would know how much service life is added by having an inspection and thus could determine whether the aforementioned estimate of one year is too high or too low.

In sum, the monetized benefits of Recommendations 1 and 2 are that VDOT can then determine whether an inspection program would yield substantial cost savings. Using the assumptions presented in this case study, such cost savings could be in the neighborhood of $400,000 annually. However, Recommendations 1 and 2 would give an opportunity to test the validity of those assumptions.

ACKNOWLEDGMENTS

The authors acknowledge the valuable feedback, continued support, and technical guidance of the technical review panel: David Wilson, Program Manager, Compliance and Hazmat, VDOT Environmental Division (Project Champion), James Martin, Environmental Compliance Manager, VDOT Environmental Division, and Stephen Sharp, Associate Principal Research Scientist, VTRC. The authors also acknowledge Martin Krebs, VDOT Maintenance Division, for his valuable feedback during the final stages of the project. The authors also thank David Mokarem and Brett Farmer at Virginia Tech for assistance with preparing specimens. The authors appreciate the support of Fred Whitford from Purdue University for providing a weathered piece of a failed HDPE AST that was used to contain a brine solution. Additionally, the authors thank Echo Ultrasonics LLC for providing ultrasonic couplants to the researchers. The authors thank Mike Bortner at Virginia Tech for helping to interpret the DSC results. The authors thank James Helvey for his assistance in moving the AST from VDOT facilities to

Virginia Tech and for filling the AST with water. The authors thank Tom Ott and Darrell Stanyard for their assistance with the Proceq Flaw Detector 100.

REFERENCES

1. F. Whitford, S. Salomon, D. Oltman, J. Obermeyer, S. Hawkins, M. Pearson, B. Overstreet, M. Titus, S. Lambert, M. Hawkins, Poly Tanks for Farms and Businesses: Preventing Catastrophic Failures, Report PPP-77, 2008.

2. F. Whitford, S. Hawkins, L. Holland, B. Carr, D. Meredith, K. Ileleji, D. Campbell, L. Gentry, L. Hamby, M. Roach, A. Blessing, Aboveground Petroleum Tanks: A Pictoral Guide, Report PPP-73, 2007.

3. P.E. Myers, Aboveground Storage Tanks, McGraw-Hill Education, New York, 1997.

4. W. Atherton, J.W. Ash, Review of failures, causes & consequences in the bulk storage industry, in: Proc. 2nd Annu. Liverpool Conf. in Built Environment and Natural Environment, Citeseer, 2007.

5. J.R. Cornell, M.A. Baker, Catastrophic tank failures: Highlights of past failures along with proactive tanks designs, in: US EPA Fourth Biennial Freshwater Spills Symposium, Cleveland, 2002.

6. U.S. Chemical Safety and Hazard Investigation Board, Allied Terminals, Inc. – Catastrophic Tank Collapse, Report 2009-03-I-VA, U.S. Chemical Safety Board, Washington D.C., 2009.

7. Office of Solid Waste and Emergency Response, Rupture Hazard from Liquid Storage Tanks, EPA 550-F-09-004, Washington D.C., 2009.

8. T. Lourenço, L. Matias, P. Faria, Anomalies detection in adhesive wall tiling systems by infrared thermography, Construction and Building Materials. 148 (2017) 419–428.

9. E. Barreira, V.P. de Freitas, Evaluation of building materials using infrared thermography, Construction and Building Materials. 21 (2007) 218–224.

10. Y. Qin, J. Shi, J. Zheng, D. Hou, W. Guo, An Improved Phased Array Ultrasonic Testing Technique for Thick-Wall Polyethylene Pipe Used in Nuclear Power Plant, Journal of Pressure Vessel Technology. 141 (2019).

11. L. Mažeika, R. Šliteris, A. Vladišauskas, Measurement of velocity and attenuation for ultrasonic longitudinal waves in the polyethylene samples, Ultragarsas. 65 (2010) 12–15.

12. C. Frederick, A. Porter, D. Zimmerman, High-density polyethylene piping butt-fusion joint examination using ultrasonic phased array, Journal of Pressure Vessel Technology. 132 (2010) 051501. https://doi.org/10.1115/1.4001212.

13. K. Adachi, G. Harrison, J. Lamb, A.M. North, R.A. Pethrick, High frequency ultrasonic studies of polyethylene, Polymer. 22 (1981) 1032–1039. https://doi.org/10.1016/0032-3861(81)90287-1.

14. C. Miao, Y. Qin, W. Guo, C. An, Z. Ling, Z. Chen, Ultrasonic phased array inspection with water wedge for butt fusion joints of polyethylene pipe, in: ASME 2019 Pressure Vessels and Piping Conference, 2019: pp. PVP2019-93500. https://doi.org/10.1115/PVP2019-93500.

15. F. Hagglund, M. Robson, M.J. Troughton, W. Spicer, I.R. Pinson, A novel phased array ultrasonic testing (PAUT) system for on-site inspection of welded joints in plastic pipes, in: 11th European Conference on Non-Destructive Testing, 2014.

16. N. Thorpe, M. Acebes, D. Wylie, M. Troughton, O. Gilmour, O. Roy, G. Benoist, R. Dweik, Ultrasonic phased array non-destructive testing and in-service inspection system for high integrity polyethylene pipe welds with automated analysis software, in: 12th European Conference on Non-Destructive Testing, 2018.

17. Amir Behravan; Thien Q. Tran; Alan Hernandez; Matthew M. deJong; Alexander S. Brand, Evaluating the integrity of high-density polyethylene (HDPE) storage tanks, Journal of Materials in Civil Engineering. (2022). https://doi.org/DOI: 10.1061/(ASCE)MT.1943-5533.0004744.

18. B.C. Mohan, M.C. Jeyasekhar, Combination of infrared thermography and computed radiography nondestructive methods detect oil and gas storage tank drainage pipe blockage, in: 3rd Singapore International Non-Destructive Testing Conference and Exhibition, Singapore, 2019: p. 8.

19. R.T. Nisbet, M.D. Pesce, NDT of welded steel tanks, NDT Technician. 10 (2011) 1–4.

20. L.P. Kalra, W. Shen, J. Gu, A wall climbing robotic system for non destructive inspection of above ground tanks, in: 2006 Canadian Conference on Electrical and Computer Engineering, Ottawa, 2006: p. 9376469. https://doi.org/10.1109/CCECE.2006.277523.

21. B. Blakeley, C. Emmanouilidis, K. Hrissagis, Above-ground storage tank inspection using the 'Robot Inspector,' Insight - Non-Destructive Testing and Condition Monitoring. 47 (2005) 705–708. https://doi.org/10.1784/insi.2005.47.11.705.

22. P.S. Lowe, W. Duan, J. Kanfoud, T.-H. Gan, Structural health monitoring of above-ground storage tank floors by ultrasonic guidedwave excitation on the tank wall, Sensors. 17 (2017) 2542. https://doi.org/10.3390/s17112542.

23. M. Spicer, F. Hagglund, M. Troughton, Development and validation of an automated ultrasonic system for the non-destructive evaluation of welded joints in thermoplastic storage tanks, in: 11th European Conference on Non-Destructive Testing, Prague, 2014.

24. S. Lagüela, L. Díaz-Vilariño, D. Roca, Infrared thermography: Fundamentals and applications, in: B. Riveiro, M. Solla (Eds.), Non-Destructive Techniques for the Evaluation of Structures and Infrastructure, CRC Press, 2016: pp. 113–138. https://doi.org/10.1201/b19024.

25. S. Verspeek, J. Peeters, B. Ribbens, G. Steenackers, Excitation Source Optimisation for Active Thermography, in: Multidisciplinary Digital Publishing Institute Proceedings, 2018: p. 439.

26. X. Li, L.G. Tabil, I.N. Oguocha, S. Panigrahi, Thermal diffusivity, thermal conductivity, and specific heat of flax fiber–HDPE biocomposites at processing temperatures, Composites Science and Technology. 68 (2008) 1753–1758.

27. Z. Zhu, X. Qiu, S. Zhong, X. Fu, X. Yang, Active infrared thermography for defect detection of polyethylene pipes, Advanced Materials Research. 1044–1045 (2014) 700–703. https://doi.org/10.4028/www.scientific.net/AMR.1044-1045.700.

28. A.C. Murariu, J.V. Lozanović Šajić, Temperature and heat effects on polyethylene behaviour in the presence of imperfections, Thermal Science. 20 (2016) 1703–1712. https://doi.org/10.2298/TSCI151110220M.

29. A.C. Murariu, A.-V. Bîrdeanu, R. Cojocaru, V.I. Safta, D. Dehelean, L. Boţilă, C. Ciucă, Application of Thermography in Materials Science and Engineering, in: R. V. Prakash (Ed.), Infrared Thermography, InTech, 2012: pp. 27–52.

30. M.A. Omar, Y. Zhou, R. Parvataneni, E. Planting, Calibrated pulse-thermography procedure for inspecting HDPE, Advances in Materials Science and Engineering. 2008 (2008) 186427. https://doi.org/10.1155/2008/186427.

31. M.J. Azad, M.S. Tavallali, A novel computational supplement to an IR-thermography based non-destructive test of electrofusion polyethylene joints, Infrared Physics and Technology. 96 (2019) 30–38. https://doi.org/10.1016/j.infrared.2018.10.031.

32. M. Doaei, M.S. Tavallali, Intelligent screening of electrofusion-polyethylene joints based on a thermal NDT method, Infrared Physics and Technology. 90 (2018) 1–7. https://doi.org/10.1016/j.infrared.2018.01.030.

33. M. Genest, S. Ouellet, K. Williams, Infrared thermography for inspection of aramid and ultra-high-molecular-weight polyethylene armor systems, in: Thermosense: Thermal Infrared Applications XL, 2018: p. 106610V. https://doi.org/10.1117/12.2303829.

34. T. Omar, M.L. Nehdi, T. Zayed, Infrared thermography model for automated detection of delamination in RC bridge decks, Construction and Building Materials. 168 (2018) 313–327. https://doi.org/10.1016/j.conbuildmat.2018.02.126.

35. G. Washer, R. Fenwick, N. Bolleni, J. Harper, Effects of environmental variables on infrared imaging of subsurface features of concrete bridges, Transportation Research Record. 2108 (2009) 107–114. https://doi.org/10.3141/2108-12.

36. G. Washer, R. Fenwick, S. Nelson, R. Rumbayan, Guidelines for thermographic inspection of concrete bridge components in shaded conditions, Transportation Research Record. 2360 (2013) 13–20. https://doi.org/10.3141/2360-02.

37. S.-H. Kee, T. Oh, J.S. Popovics, R.W. Arndt, J. Zhu, Nondestructive bridge deck testing with air-coupled impact-echo and infrared thermography, Journal of Bridge Engineering. 17 (2012) 928–939. https://doi.org/10.1061/(ASCE)BE.1943-5592.0000350.

38. H. Azari, R. Kok, Evaluating ultrasonic techniques to detect bridge weld flaws, Public Roads. 84 (2021) 32–38.

39. C. Frederick, A. Porter, D. Zimmerman, High-density polyethylene piping butt-fusion joint examination using ultrasonic phased array, in: Proceedings of the ASME 2009 Pressure Vessels and Piping Division Conference, 2009: pp. 1295–1299. https://doi.org/10.1115/PVP2009-77783.

40. J. Zheng, J. Shi, W. Guo, Development of nondestructive test and safety assessment of electrofusion joints for connecting polyethylene pipes, Journal of Pressure Vessel Technology. 134 (2012) 021406. https://doi.org/10.1115/1.4004869.

41. J. Zhu, R.P. Collins, J.B. Boxall, R.S. Mills, R. Dwyer-Joyce, Non-destructive in-situ condition assessment of plastic pipe using ultrasound, Procedia Engineering. 119 (2015) 148–157. https://doi.org/10.1016/j.proeng.2015.08.866.

42. Y. Zhang, P.-Y. Ben Jar, K.-C.T. Nguyen, L.H. Le, Characterization of ductile damage in polyethylene plate using ultrasonic testing, Polymer Testing. 62 (2017) 51–60. https://doi.org/10.1016/j.polymertesting.2017.06.010.

43. J.S. Egerton, M.J.S. Lowe, P. Huthwaite, H. V. Halai, Ultrasonic attenuation and phase velocity of high-density polyethylene pipe material, Journal of the Acoustical Society of America. 141 (2017) 1535–1545. https://doi.org/10.1121/1.4976689.

44. Š. Kočiš, Z. Figura, Ultrasonic Measurements and Technologies, Springer, Boston, 1996. https://doi.org/10.1007/978-1-4613-1199-7.

45. L.W. Schmerr Jr., Fundamentals of Ultrasonic Phased Arrays, Springer, Cham, 2015. https://doi.org/10.1007/978-3-319-07272-2.

46. B. Saleh, Introduction to Subsurface Imaging, Cambridge University Press, Cambridge, 2011. https://doi.org/10.1017/CBO9780511732577.

47. W. Guo, J. Shi, D. Hou, Research on phased array ultrasonic technique for testing butt fusion joint in polyethylene pipe, in: 2016 IEEE Far East NDT New Technology & Application Forum (FENDT), IEEE, 2016: pp. 1–5.

48. M. Troughton, M. Spicer, F. Hagglund, Development and assessment of a phased array ultrasonic inspection system for polyethylene pipe joints, in: ANTEC 2014 - Proceedings of the Technical Conference and Exhibition, Las Vegas, 2014: pp. 2016–2021.

49. M. Spicer, M. Troughton, F. Hagglund, Development and assessment of ultrasonic inspection system for polyethylene pipes, in: ASME 2013 Pressure Vessels and Piping Conference, Paris, 2013. https://doi.org/10.1115/PVP2013-97098.

50. New York State Department of Environmental Conservation, Five-Year Inspection of Plastic Tanks (DER-16), Bulk Storage Guidance Documents. (2007). https://www.dec.ny.gov/regulations/38102.html.

51. M. Pal, N. Dixon, J. Flint, Detecting and locating leaks in water distribution polyethylene pipes, in: Proceedings of the World Congress on Engineering 2010, London, 2010.

52. A. Martini, M. Troncossi, A. Rivola, Leak detection in water-filled small-diameter polyethylene pipes by means of acoustic emission measurements, Applied Sciences. 7 (2017) 2. https://doi.org/10.3390/app7010002.

53. K. Marmarokopos, D. Doukakis, G. Frantziskonis, M. Avlonitis, Leak detection in plastic water supply pipes with a high signal-to-noise ratio accelerometer, Measurement and Control. 51 (2018) 27–37. https://doi.org/10.1177/0020294018758526.

54. R. Salvi, A. Ramdasi, Y.A. Kolekar, L. V. Bhandarkar, Use of ground-penetrating radar (GPR) as an effective tool in assessing pavements—A review, in: R. Sundaram, J. Telangrao Shahu, V. Havanagi (Eds.), Geotechnics for Transportation Infrastructure, Springer, 2019: pp. 85–95. https://doi.org/10.1007/978-981-13-6713-7_7.

55. R. Korczak, A. Abd El Halim, Case studies and innovative uses of GPR for pavement engineering applications, in: 2017 Conference and Exhibition of the Transportation Association of Canada, St. John's, Newfoundland, 2017.

56. I. Ullmann, J. Adametz, D. Oppelt, M. Vossiek, Millimeter wave radar imaging for non-destructive detection of material defects, in: Proceedings Sensor 2017, 2017: pp. 467–472. https://doi.org/10.5162/sensor2017/D3.3.

57. R. Stakenborghs, J. Little, Microwave based NDE inspection of HDPE pipe welds, in: Proceedings of the 17th International Conference on Nuclear Engineering, Brussels, 2009: pp. ICONE17-75742.

58. G. Dobmann, I. Altpeter, C. Sklarczyk, R. Pinchuk, Non-destructive testing with micro- and mm-waves — Where we are — Where we go, Welding in the World. 56 (2012) 111–120. https://doi.org/10.1007/BF03321153.

59. A. Behravan, M.M. DeJong, A.S. Brand, Laboratory study on non-destructive evaluation of polyethylene liquid storage tanks by thermographic and ultrasonic methods, CivilEng. 2 (2021) 823–851. https://doi.org/10.3390/civileng2040045.

60. R. Mulaveesala, J.S. Vaddi, P. Singh, Pulse compression approach to infrared nondestructive characterization, Review of Scientific Instruments. 79 (2008) 94901.

61. N.W. Pech-May, A. Paul, M. Ziegler, Pulse-compression laser thermography using a modified Barker code: enhanced detection of subsurface defects, in: Thermosense: Thermal Infrared Applications XLIII, International Society for Optics and Photonics, 2021: p. 117430J.

62. G. Schober, S. Kremling, T. Hochrein, D. Hoffmann, A. Stöhr, Multiple flash thermography for non-destructive testing of lightweight components, in: Proceedings of the IRS^2, AMA Conferences, 2017.

63. R. Mulaveesala, S. Tuli, Theory of frequency modulated thermal wave imaging for nondestructive subsurface defect detection, Applied Physics Letters. 89 (2006) 191913.

64. N. Tabatabaei, A. Mandelis, Thermal-wave radar: A novel subsurface imaging modality with extended depth-resolution dynamic range, Review of Scientific Instruments. 80 (2009) 34902.

65. N.D. Arnold, A.H. Guenther, Experimental determination of ultrasonic wave velocities in plastics as functions of temperature. I. Common plastics and selected nose-cone materials, Journal of Applied Polymer Science. 10 (1966) 731–743. https://doi.org/10.1002/app.1966.070100506.

66. J.E. Carlson, J. van Deventer, A. Scolan, C. Carlander, Frequency and temperature dependence of acoustic properties of polymers used in pulse-echo systems, in: IEEE Symposium on Ultrasonics, 2003: pp. 885–888. https://doi.org/10.1109/ULTSYM.2003.1293541.

67. S. Alnaimi, B. Elouadi, I. Kamal, Structural, thermal and morphology characteristics of low density polyethylene produced by QAPCO, in: Proceedings of the 8th International Symposium on Inorganic Phosphate Materials, Agadir, Morocco, 2015: pp. 13–19.

68. E. Hunter, W.G. Oakes, The effect of temperature on the density of polythene, Transactions of the Faraday Society. 41 (1945) 49–56.

69. I.A. Maigel'dinov, K.I. Tsyur, The thermomechanical properties of crystalline polymers—I. Polyethylene, Polymer Science USSR. 4 (1963) 864–874.